EUROPEAN ORGANISATION FOR NUCLEAR RESEARCH (CERN)

arXiv:1302.1283v1 [hep-ex] 6 Feb 2013

Measurements of $W\gamma$ and $Z\gamma$ production in pp collisions at $\sqrt{s} = $ 7 TeV with the ATLAS detector at the LHC

The ATLAS Collaboration

Abstract

The integrated and differential fiducial cross sections for the production of a W or Z boson in association with a high-energy photon are measured using pp collisions at $\sqrt{s} = $ 7 TeV. The analyses use a data sample with an integrated luminosity of 4.6 fb^{-1} collected by the ATLAS detector during the 2011 LHC data-taking period. Events are selected using leptonic decays of the W and Z bosons ($W(e\nu, \mu\nu)$ and $Z(e^+e^-, \mu^+\mu^-, \nu\bar{\nu})$) with the requirement of an associated isolated photon. The data are used to test the electroweak sector of the Standard Model and search for evidence for new phenomena. The measurements are used to probe the anomalous $WW\gamma$, $ZZ\gamma$ and $Z\gamma\gamma$ triple-gauge-boson couplings and to search for the production of vector resonances decaying to $Z\gamma$ and $W\gamma$. No deviations from Standard Model predictions are observed and limits are placed on anomalous triple-gauge-boson couplings and on the production of new vector meson resonances.

Measurements of $W\gamma$ and $Z\gamma$ production in pp collisions at $\sqrt{s} = 7$ TeV with the ATLAS detector at the LHC

(ATLAS Collaboration)

The integrated and differential fiducial cross sections for the production of a W or Z boson in association with a high-energy photon are measured using pp collisions at $\sqrt{s} = 7$ TeV. The analyses use a data sample with an integrated luminosity of 4.6 fb^{-1} collected by the ATLAS detector during the 2011 LHC data-taking period. Events are selected using leptonic decays of the W and Z bosons ($W(e\nu, \mu\nu)$ and $Z(e^+e^-, \mu^+\mu^-, \nu\bar{\nu})$) with the requirement of an associated isolated photon. The data are used to test the electroweak sector of the Standard Model and search for evidence for new phenomena. The measurements are used to probe the anomalous $WW\gamma$, $ZZ\gamma$ and $Z\gamma\gamma$ triple-gauge-boson couplings and to search for the production of vector resonances decaying to $Z\gamma$ and $W\gamma$. No deviations from Standard Model predictions are observed and limits are placed on anomalous triple-gauge-boson couplings and on the production of new vector meson resonances.

I. INTRODUCTION

The Standard Model (SM) has proved to provide an accurate description of the production of elementary particles observed in high energy physics experiments. The interactions of W and Z bosons with photons are particularly interesting as they test the self-couplings of these bosons as predicted by the non-Abelian $SU(2)_L \times U(1)_Y$ gauge group of the electroweak sector. In particular, the high-energy proton–proton collisions provided by the LHC explore the production of $W\gamma$ and $Z\gamma$ pairs in a new energy domain. The high center-of-mass energy also allows searches for new particles, for example techni-mesons which are predicted in Technicolor models [1, 2], that decay to these final states.

The measurements presented here are improvements on previous studies of the hadroproduction of $W\gamma$ and $Z\gamma$ pairs, as more precise measurements are performed with a larger data sample. The events used for the measurements were recorded in 2011 by the ATLAS detector [3] from 4.6 fb^{-1} of pp collisions at a center-of-mass energy of 7 TeV. The diboson candidate events are selected from the production processes $pp \to \ell\nu\gamma + X$ ($\ell = e$, μ), $pp \to \ell^+\ell^-\gamma + X$ and $pp \to \nu\bar{\nu}\gamma + X$. These final states include the production of W and Z bosons with photon bremsstrahlung from the charged leptons from the W/Z boson decays in addition to the $W\gamma$ and $Z\gamma$ diboson events of primary interest. In the SM, the latter originate from W and Z boson production with photons radiated from initial-state quarks (prompt photons), photons from the fragmentation of secondary quarks and gluons into isolated photons, and from photons radiated directly by W bosons. The diagrams of these production mechanisms are shown in Fig. 1. Theories beyond the SM, such as Technicolor, predict the decay of narrow resonances to $W\gamma$ or $Z\gamma$ pairs. The data analyses presented here provide differential distributions of relevant kinematic variables, corrected for detector effects, allowing the search for deviations from the SM predictions to be made with high sensitivity.

Previous measurements of $W\gamma$ and $Z\gamma$ final states from $p\bar{p}$ and pp production have been made at the Tevatron, by the CDF [4] and DØ [5, 6] collaborations, and at the LHC by the ATLAS [7, 8] and CMS [9] collaborations. These experiments have set limits on anomalous triple gauge-boson couplings (aTGCs) that are improved on by the current analysis. The limits on new vector meson resonances that are presented in this paper improve on previous limits set at the Tevatron by the DØ [10] collaboration in the $Z\gamma$ final state, and they are the first reported in the $W\gamma$ final state.

Throughout this paper the notations "$\ell\nu\gamma$", "$\ell^+\ell^-\gamma$" and "$\nu\bar{\nu}\gamma$" specify the production channels "$pp \to \ell\nu\gamma + X$", "$pp \to \ell^+\ell^-\gamma + X$" and "$pp \to \nu\bar{\nu}\gamma + X$", respectively, and the label "Z" refers to $Z/\gamma*$. In addition, "inclusive" refers to production with no restriction on the recoil system and "exclusive" refers to production restricted to those events with no central jets with transverse energy greater than 30 GeV. Measurements of integrated cross sections and differential kinematic distributions are performed within a fiducial region of the detector. Events with high-transverse-energy photons are used to establish aTGC limits and to carry out the searches for narrow $W\gamma$ and $Z\gamma$ resonances.

This paper is organized as follows: an overview of the ATLAS detector and the data samples used is given in Sec. II. Sec. III describes the signal and background Monte Carlo samples. Sec. IV defines the selections of the physics objects such as photons, leptons and jets. Sec. V describes the event selection criteria for $W\gamma$ and $Z\gamma$ candidates. Sec. VI presents the background estimations. Sec. VII presents the measured $V\gamma$ ($V = W$ or Z) fiducial cross sections. Sec. VIII summarizes the comparisons between the measurements and SM predictions. The observed aTGC limits are presented in Sec. IX and the limits on masses of new vector meson resonances are given in Sec. X.

II. THE ATLAS DETECTOR AND THE DATA SAMPLE

The ATLAS detector is composed of an inner tracking system (ID) surrounded by a thin superconducting
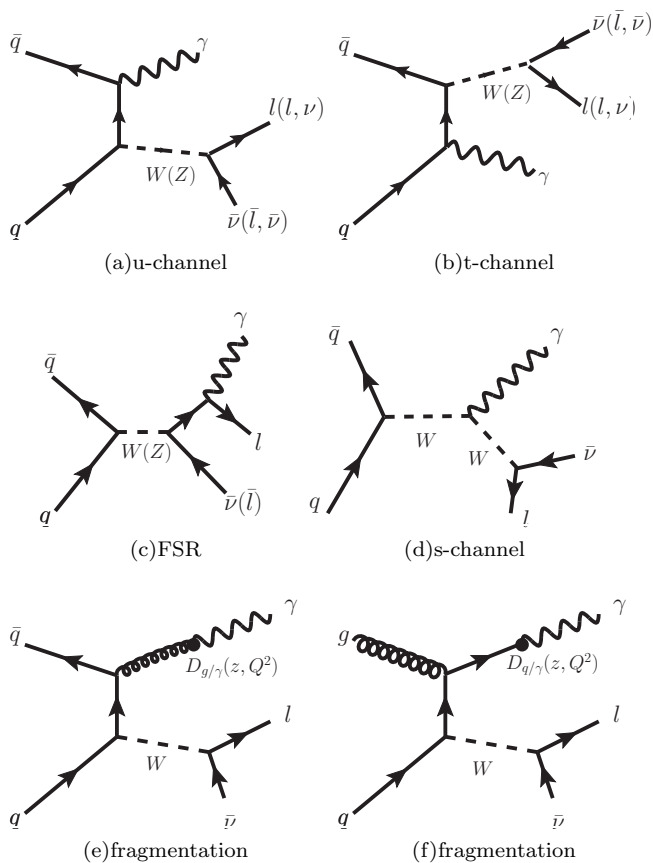
FIG. 1. Feynman diagrams of $W\gamma$ and $Z\gamma$ production in (a) u-channel (b) t-channel and (c) final state photon radiation (FSR) from the W and Z boson decay process. (d) Feynman diagram of $W\gamma$ production in the s-channel. Diagrams of the signal contributions from the $W + q(g)$ processes when a photon emerges from the fragmentation of (e) a gluon and (f) a quark in the final state.

solenoid providing a 2 T axial magnetic field, electromagnetic (EM) and hadronic calorimeters, and a muon spectrometer (MS). The ID consists of three subsystems: the pixel and silicon microstrip (SCT) detectors cover the pseudorapidity[1] range $|\eta| < 2.5$, while the Transition Radiation Tracker (TRT), which is made of straw tubes, has an acceptance range of $|\eta| < 2.0$. The calorimeter system covers the range $|\eta| < 4.9$. The highly segmented electromagnetic calorimeter, which plays a crucial role in electron and photon identification, comprises lead ab-

———————

[1] ATLAS uses a right-handed coordinate system with its origin at the nominal interaction point (IP) in the center of the detector and the z-axis along the beam pipe. The x-axis points from the IP to the center of the LHC ring, and the y-axis points upward. Cylindrical coordinates (r, ϕ) are used in the transverse (x,y) plane, ϕ being the azimuthal angle around the beam pipe. The pseudorapidity is defined in terms of the polar angle θ as $\eta = -\ln\tan(\theta/2)$. The distance ΔR in the $\eta - \phi$ space is defined as $\Delta R = \sqrt{(\Delta\eta)^2 + (\Delta\phi)^2}$.

sorbers with liquid argon (LAr) as the active material and covers the range $|\eta| < 3.2$. In the region $|\eta| < 1.8$, a pre-sampler detector using a thin layer of LAr is used to correct for the energy lost by electrons and photons upstream of the calorimeter. The hadronic tile calorimeter ($|\eta| < 1.7$) is a steel/scintillating-tile detector and is located directly outside the envelope of the barrel electromagnetic calorimeter. The two endcap hadronic calorimeters have LAr as the active material and copper absorbers. The calorimeter coverage is extended to $|\eta| = 4.9$ by a forward calorimeter with LAr as active material and copper (EM) and tungsten (hadronic) as absorber material. The MS is based on three large superconducting aircore toroid magnets, a system of three stations of chambers for precise tracking measurements in the range $|\eta| < 2.7$, and a muon trigger system which covers the range $|\eta| < 2.4$.

The data used for the analyses presented in this paper were collected in 2011 from pp collisions at a center-of-mass energy of 7 TeV. The total integrated luminosity is 4.6 fb^{-1} with an uncertainty of 3.9% [12, 13]. Events were selected by triggers requiring at least one identified electron, muon or photon. The transverse energy (E_T) threshold for the single-electron trigger was initially 20 GeV, and was raised to 22 GeV in the later part of 2011 to maintain a manageable trigger rate at higher instantaneous luminosity. The transverse momentum (p_T) threshold for the single-muon trigger was 18 GeV. Single-photon events were triggered with a transverse energy $E_T > 80$ GeV.

III. SIGNAL AND BACKGROUND MODELING

Monte Carlo (MC) event samples, including a full simulation [14] of the ATLAS detector with GEANT4 [15], are used to compare the data to the SM signal and background expectations. All MC samples are simulated with additional pp interactions (pile-up) in the same and neighboring bunch crossings. The number of pp interactions in the same bunch crossing averages 9 and extends up to about 20, as observed in the data.

The production of $pp \to \ell\nu\gamma$ and $pp \to \tau\nu\gamma$ is modeled with the ALPGEN (2.14) generator [16] interfaced to HERWIG (6.520) [17] for parton shower and fragmentation processes, and to JIMMY (4.30) [18] for underlying event simulation. The modeling of $pp \to \ell^+\ell^-\gamma$ and $pp \to \nu\bar{\nu}\gamma$ processes is performed with the SHERPA (1.4.0) generator [19] since the simulation of these processes is not available in ALPGEN. An invariant mass cut of $m(\ell^+\ell^-) > 40$ GeV is applied at the generator level when simulating the $pp \to \ell^+\ell^-\gamma$ process. The CTEQ6L1 [20] and CTEQ6.6M [21] parton distribution functions (PDFs) are used for samples generated with ALPGEN and SHERPA, respectively. The final-state radiation (FSR) photons from charged leptons are simulated by PHOTOS (2.15) [22] for the ALPGEN sample, and by the SHERPA generator [23] for the SHERPA sample. All the signal production processes,

including the quark/gluon fragmentation into photons, are simulated by these two generators. The ALPGEN sample is generated with leading-order (LO) matrix elements for final states with up to five additional partons, whereas the SHERPA sample is generated with LO matrix elements for final states with up to three additional partons. In the search for Technicolor, the signal processes are simulated using PYTHIA (6.425) [24] with a LO MRST2007 [25] PDF set.

The $Z(\ell^+\ell^-)$ and $Z(\tau^+\tau^-)$ backgrounds are modeled with PYTHIA. The radiation of photons from charged leptons is treated in PYTHIA using PHOTOS. TAUOLA (1.20) [26] is used to model τ lepton decays. The POWHEG (1.0) [27] generator is used to simulate $t\bar{t}$ production, and is interfaced to PYTHIA for parton showering and fragmentation. The WW and single top quark processes are modeled by MC@NLO (4.02) [28, 29], interfaced to HERWIG for parton showering and fragmentation. The LO MRST2007 PDF set is used to simulate the $Z(\ell^+\ell^-)$, $Z(\tau^+\tau^-)$ and $W(\tau\nu)$ backgrounds, and the CT10 [30] PDF set is used in simulating $t\bar{t}$, single top quark and WW production. The next-to-leading-order (NLO) cross-section predictions [31–34] are used to normalize the simulated background events. Backgrounds where a jet or an electron is misidentified as a photon are derived from data as described in Sec. VI.

IV. PHYSICS OBJECT RECONSTRUCTION

The W and Z bosons are reconstructed from their leptonic decays. The $\ell\nu\gamma$ final state consists of an isolated electron or muon, large missing transverse momentum due to the undetected neutrino, and an isolated photon. The $\ell^+\ell^-\gamma$ final state contains one e^+e^- or $\mu^+\mu^-$ pair and an isolated photon. The $\nu\bar{\nu}\gamma$ final state contains at least one isolated photon and large missing transverse momentum due to the undetected neutrinos. Collision events are selected by requiring at least one reconstructed vertex with at least three charged particle tracks with $p_T > 0.4$ GeV. If more than one vertex satisfies the vertex selection requirement, the vertex with the highest sum of the p_T^2 of the associated tracks is chosen as the primary vertex. Physics objects for the measurement are required to be associated with the primary vertex.

An electron candidate is obtained from an energy cluster in the EM calorimeter associated with a reconstructed track in the ID. The transverse energy of electrons is required to be greater than 25 GeV. The electron cluster must lie outside the transition region between the barrel and end-cap EM calorimeters and within the overall fiducial acceptance of the EM calorimeters and the ID, so it must satisfy $|\eta| < 1.37$ or $1.52 < |\eta| < 2.47$. At the electron track's closest approach to the primary vertex, the ratio of the transverse impact parameter d_0 to its uncertainty (the d_0 significance) must be smaller than ten, and the longitudinal impact parameter $|z_0|$ must be

less than 1 mm. Tight[2] electron identification [35] is used in the $W(e\nu)\gamma$ analysis, whereas medium identification [35] is used to select electrons in the $Z(e^+e^-)\gamma$ analysis. To reduce the background due to a jet misidentified as an electron, a calorimeter-based isolation requirement $E_T^{\mathrm{iso}} < 6$ GeV is applied to the electron candidate. E_T^{iso} is the total transverse energy recorded in the calorimeters within a cone of radius $\Delta R = 0.3$ around the electron position excluding the energy of the electron itself. E_T^{iso} is corrected for leakage from the electron energy cluster's core into the isolation cone and for contributions from the underlying event and pile-up [36, 37].

Muon candidates are identified by associating complete tracks or track segments in the MS to tracks in the ID [38]. Each selected muon candidate is a combined track originating from the primary vertex with transverse momentum $p_T > 25$ GeV and $|\eta| < 2.4$. It is required to be isolated by imposing $R^{\mathrm{iso}} < 0.15$, where R^{iso} is the sum of the p_T of the tracks in a $\Delta R = 0.3$ cone around the muon direction, excluding the track of the muon, divided by the muon p_T. The d_0 significance must be smaller than three, and $|z_0|$ must be less than 1 mm.

Photon candidates are based on clustered energy deposits in the EM calorimeter in the range $|\eta| < 2.37$ (excluding the calorimeter transition region $1.37 < |\eta| < 1.52$) with $E_T > 15$ GeV. Clusters without matching tracks are directly classified as unconverted photon candidates. Clusters that are matched to tracks which originate from reconstructed conversion vertices in the ID or to tracks consistent with coming from a conversion are considered as converted photon candidates. Tight requirements on the shower shapes [36] are applied to suppress the background from multiple showers produced in meson (e.g. π^0, η) decays. To further reduce this background, a photon isolation requirement $E_T^{\mathrm{iso}} < 6$ GeV is applied. The definition of photon isolation is the same as the electron isolation described above.

Jets are reconstructed from energy observed in the calorimeter cells using the anti-k_t jet clustering algorithm [39] with radius parameter $R = 0.4$. The selected jets are required to have $p_T > 30$ GeV with $|\eta| < 4.4$, and to be well separated from the lepton and photon candidates ($\Delta R(e/\mu/\gamma, \mathrm{jet}) > 0.3$).

The missing transverse momentum (E_T^{miss}) [40] magnitude and direction are measured from the vector sum of the transverse momentum vectors associated with clusters of energy reconstructed in the calorimeters with $|\eta| < 4.9$. A correction is applied to the energy of those clusters that are associated with a reconstructed physical object (jet, electron, τ-lepton, photon). Reconstructed muons are also included in the sum, and any calorime-

―――――

[2] The definitions of tight and medium identification [35] was reoptimized for 2011 data-taking conditions. They are based on information about calorimeter shower shapes, track quality, track–calorimeter-cluster matching, particle identification information from the TRT and a photon conversion veto.

ter energy deposits associated with them are excluded to avoid double counting.

V. $W\gamma$ AND $Z\gamma$ EVENT SELECTION

The $\ell\nu\gamma$ candidate events are selected by requiring exactly one lepton with $p_T > 25$ GeV, at least one isolated photon with $E_T^\gamma > 15$ GeV and E_T^{miss} above 35 GeV. In addition, the transverse mass[3] of the lepton–E_T^{miss} system (m_T) is required to be greater than 40 GeV. A Z-veto requirement is applied in the electron channel of the $W\gamma$ analysis by requiring that the electron–photon invariant mass ($m_{e\gamma}$) is not within 15 GeV of the Z boson mass. This is to suppress the background where one of the electrons from the Z boson decay is mis-identified as a photon. The events selected by the criteria above are used for the inclusive $W\gamma$ cross-section measurements.

The $\ell^+\ell^-\gamma$ candidates are selected by requiring exactly two oppositely charged same-flavor leptons with an invariant mass greater than 40 GeV, and one isolated photon with $E_T^\gamma > 15$ GeV.

The $\nu\bar{\nu}\gamma$ candidates are selected by requiring one isolated photon with $E_T^\gamma > 100$ GeV and $E_T^{miss} > 90$ GeV. The reconstructed photon, E_T^{miss} and jets (if jets are found) are required to be well separated in the transverse plane with $\Delta\phi(E_T^{miss}, \gamma) > 2.6$ and $\Delta\phi(E_T^{miss}, \text{jet}) > 0.4$, in order to reduce the γ+jet background. Events with identified electrons and muons are vetoed to reject W+jets and $W\gamma$ background. The selection criteria to identify the electrons and muons are the same as in the $Z(\ell^+\ell^-)\gamma$ analysis.

In both the $W\gamma$ and $Z\gamma$ analyses, a selection requirement $\Delta R(\ell, \gamma) > 0.7$ is applied to suppress the contributions from FSR photons in the W and Z boson decays. The events with no jets with $E_T > 30$ GeV are used to measure the exclusive $V\gamma$ cross sections. For $V\gamma$ production, events with a high-E_T photon tend to have more jet activity in the final state. Contributions from aTGCs also enhance $V\gamma$ production with high-E_T photons. Thus, the exclusive $V\gamma$ cross-section measurements are expected to be more sensitive to aTGC than the inclusive measurements. In the current analyses the sensitivity to aTGCs improves by $\sim 40\%$ when measurements are performed using exclusive channels compared to inclusive channels.

VI. BACKGROUND ESTIMATION

In the measurements of $\ell\nu\gamma$, $\ell^+\ell^-\gamma$ and $\nu\bar{\nu}\gamma$ production, the background contributions are estimated either

---

[3] $m_T = \sqrt{2p_T(\ell) \times E_T^{miss} \times (1 - \cos\Delta\phi)}$, and $\Delta\phi$ is the azimuthal separation between the directions of the lepton and the missing transverse momentum vector.

from simulation or from data. The backgrounds estimated from data include W+jets and γ+jets for the $\ell\nu\gamma$ final state, Z+jets for the $\ell^+\ell^-\gamma$ final state, and Z+jets, multi-jets, γ+jets and events with an electron faking a photon for the $\nu\bar{\nu}\gamma$ final state. The remaining backgrounds are estimated from simulation.

For the differential fiducial cross sections, the contributions from each background source are estimated in each bin used for the measurement. The sources of backgrounds and the methods of estimating them are described in the following sub-sections.

A. Background estimation for $pp \to \ell\nu\gamma$

The primary backgrounds to the $\ell\nu\gamma$ signal come from the W+jets, $Z(\ell^+\ell^-)$ and γ+jets processes.

- Events from W+jets production can be misidentified as signal candidates when photons come from the decays of mesons produced in jet fragmentation (mainly $\pi^0 \to \gamma\gamma$);

- $Z(\ell^+\ell^-)$ events mimic the $W\gamma$ signal when one of the leptons from the Z boson decay is misidentified as a photon (in the case of the electron channel), or is not identified and the photon originates from initial-state radiation from a quark or from photon bremsstrahlung from a charged lepton;

- Events from γ+jets production can mimic the $W\gamma$ signal when there are leptons from heavy quark decays (or, in the electron channel, when charged hadrons or electrons from photon conversions are misidentified as prompt electrons), and large apparent E_T^{miss} is created by a combination of real E_T^{miss} from neutrinos in heavy quark decays and of mis-measurement of jet energies;

- In addition, there are small background contributions from $t\bar{t}$, single top quark, WW, $W(\tau\nu)$ and $Z(\tau\tau)$ processes. The $pp \to \tau\nu\gamma + X$ source of events is considered as a background since measurements of cross sections for $pp \to \ell\nu\gamma + X$ production are quoted for a single lepton flavor.

The background contributions from W+jets and γ+jets events in the $W\gamma$ analysis are estimated from data.

W+jets background: A two-dimensional sideband method is used for measuring the W+jets background as in Refs. [8, 36, 41, 42] with the two discriminating variables being the photon isolation and the photon identification based on the shower shape (see Fig. 2). The non-signal regions are corrected for any contamination by signal events. A quantity f_γ is defined as the ratio of photon candidates passing the photon isolation criteria to the number of candidates failing the isolation requirement. The ratio f_γ is measured in $W(\ell\nu)$ events with one "low quality" photon candidate, which is defined as

one that fails the full photon shower-shape selection criteria, but passes a subset of them (C/D). Monte Carlo simulation is used to correct f_γ for signal contamination in the "low quality" photon sample. The estimated contribution from W+jets in the signal region is obtained by multiplying the measured f_γ by the number of events passing all $W\gamma$ selections, except the photon isolation requirement (region B).

The main contribution to the uncertainty in the W+jets background estimate comes from the potential bias in the $E_{\mathrm{T}}^{\mathrm{iso}}$ shape for the fake photons in background-enriched samples due to effects from the detector (e.g. measurement of shower shapes) and physics (e.g. simulation of the underlying event). This uncertainty is found to be less than 15% using a MC W+jets sample, by comparing the $E_{\mathrm{T}}^{\mathrm{iso}}$ shape between the "low quality" photon sample and the "high quality" photon sample. The difference is used to modify the ratio f_γ and a new W+jets background contribution in the signal region is estimated. The difference between the nominal estimate and the new estimate is taken to be the systematic uncertainty.

To estimate the uncertainty related to the selection of the background-enriched samples, two alternative selections, with tighter and looser background selection requirements based on the shower shapes are used.For the tighter selection, more shower shape variables are required to fail the selection cuts than for the looser background-enriched samples. The W+jets background estimates from the alternative background-enriched samples are consistent with those obtained from the nominal sample, and the differences (10%–15%) are assigned as a systematic uncertainty. The changes in the background estimates from varying the photon isolation requirements by ± 1 GeV for the sideband (2%–4%) are also assigned as a systematic uncertainty.

γ+jets background: Similarly, the γ+jets background is estimated from data using the two-dimensional sideband method, with lepton isolation (using the measured ratio f_l) and $E_{\mathrm{T}}^{\mathrm{miss}}$ as the independent variables. The ratio f_l is measured in a control sample, which requires the events to pass all the $W\gamma$ selection criteria, except the $E_{\mathrm{T}}^{\mathrm{miss}}$ requirement, which is inverted. The potential bias in the $E_{\mathrm{T}}^{\mathrm{iso}}$ shape for the fake lepton in the low-$E_{\mathrm{T}}^{\mathrm{miss}}$ background-enriched samples is found to be 10%–15% based on MC simulations. By varying the $E_{\mathrm{T}}^{\mathrm{miss}}$ threshold, alternative control samples are obtained to evaluate the systematic uncertainties on f_l. In addition, the impact parameter requirements for the muon-candidate tracks and the shower shape selection criteria for electron candidates are also varied to obtain alternative control samples enriched in γ+jets events. The differences between the γ+jets estimates (about 9%) from those control samples give one of the main systematic uncertainties. The change in the γ+jets estimates from varying the lepton isolation requirements (about 4%) is also assigned as a systematic uncertainty.

In the measurement of the differential fiducial cross section as a function of E_{T}^γ, the sideband method is used
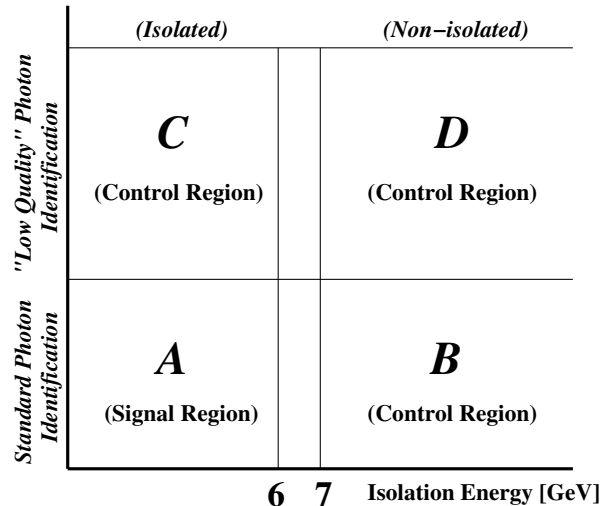

FIG. 2. Sketch of the two-dimensional plane defining the four regions used in the sideband method. Region A is the signal region. The non-isolated control regions (B and D) are defined for photons with $E_{\mathrm{T}}^{\mathrm{iso}} > 7$ GeV. The "low quality photon identification" control regions (C and D) include photon candidates that fail the full photon shower-shape selection criteria, but pass a subset of them. For the data driven W+jets background estimation to the inclusive $W\gamma$ measurement, about one thousand W+jets candidates are selected in the non-isolated control regions, and about two thousand W+jets candidates are selected in the "low quality photon identification" control regions.

to estimate the W/γ+jets backgrounds in each E_{T}^γ bin for the range $15 < E_{\mathrm{T}}^\gamma < 60$ GeV. Extrapolation methods are used to estimate the W/γ+jets background in the $E_{\mathrm{T}}^\gamma > 60$ GeV region, where few events are available. The statistical uncertainty on the background estimates become comparable to, or larger than, the systematic uncertainty at $E_{\mathrm{T}}^\gamma > 40$ GeV. The extrapolation from the low to the high E_{T}^γ regions is done using the E_{T}^γ distribution shape obtained from control samples ($W(\ell\nu)$ events with one "low quality" photon candidate to estimate the W+jets background, and $W(\ell\nu)$ events with a non-isolated lepton to estimate the γ+jets background). The difference between results (15%–30%) obtained from the sideband method and extrapolation methods is treated as an additional uncertainty for the high-E_{T}^γ bins.

To measure the differential fiducial cross sections as a function of jet multiplicity and the transverse mass of the $W\gamma$ system, the distributions of these kinematic variables for the W/γ+jets backgrounds are taken from the control samples described in the previous paragraph. The W/γ+jets distributions are then normalized to the predicted contributions to the measurements. The extracted jet multiplicity distribution for the W+jets background decreases with increasing jet multiplicity.

$Z(\ell^+\ell^-)$ background: To understand background contributions from the $Z(\ell^+\ell^-)$ process, MC simulation is needed to study the possibility of losing one lepton from

Z decay due to acceptance. Furthermore, two control regions are built to study the E_T^{miss} modeling in $Z + \gamma$ and Z+jets events. The events in the $Z + \gamma$ control regions are selected by imposing the nominal $\ell^+\ell^-\gamma$ event selection criteria, and the events in the $Z(e^+e^-)$+jets control regions are selected by imposing the nominal $e\nu\gamma$ selection criteria, except requiring that $m_{e\gamma}$ be within 15 GeV of the Z boson mass, assuming one of the electrons is mis-identified as a photon. It is found that the E_T^{miss} distributions of $Z+\gamma$ and $Z(e^+e^-)$+jets events are well modeled by MC simulations both in events with low pileup and in events with high pileup. Therefore their contributions are estimated from MC simulations. The uncertainties in E_T^{miss} modeling in the $Z(\ell^+\ell^-)$ process are studied by varying the energy scale and resolution of the leptons, photons, jets and unassociated energy clusters[4] in the calorimeter.

Other backgrounds: The background contributions from $t\bar{t}$, WW, single top quark, $Z(\tau^+\tau^-)$ and $W(\tau\nu)$ processes are estimated from MC simulations. The systematic uncertainties arise mainly from theoretical uncertainties on the production cross sections of these background processes and uncertainties on the lepton, photon, jet and E_T^{miss} modeling in the simulation.

A summary of background contributions and signal yields in the $W\gamma$ analysis is given in Table I. The estimated W+jets background is significantly smaller in the electron channel than in the muon channel due to the Z–veto requirement in the electron channel, described in Sec. V. The distributions of the photon transverse energy, E_T^{miss}, jet multiplicity, and three-body transverse mass (see Eq. (6)) from the selected $W\gamma$ events are shown in Fig. 3. The data are compared to the sum of the backgrounds and the SM signal predictions. The distributions for the expected $W\gamma$ signal are taken from signal MC simulation and normalized to the total extracted number of signal events shown in Table I ($N_{W\gamma}^{sig}$).

B. Background estimation for $pp \rightarrow \ell^+\ell^-\gamma$

The main background to the $\ell^+\ell^-\gamma$ signal (amounting to 98%–99% of the total background) originates from events with Z+jets where jets are misidentified as photons. The Z+jets contamination is estimated from data using a sideband method similar to the one described in Sec. VI A. The main uncertainty (20%) is due to the bias in the E_T^{iso} shape for the fake photons in background-enriched control samples defined by the "low quality" selection criteria. The small contribution from $t\bar{t} + X$ production (mainly from $t\bar{t} + \gamma$) is estimated from MC simulation. A summary of background contributions and

signal yields in the $\ell^+\ell^-\gamma$ analyses is given in Table II. The distributions of the photon transverse energy, jet multiplicity, and three-body mass from the selected $Z\gamma$ events are shown in Fig. 4. The data and simulation agree within the uncertainty of the background estimate.

C. Background estimation for $pp \rightarrow \nu\bar{\nu}\gamma$

Background to the $\nu\bar{\nu}\gamma$ signal originates mainly from the following processes:

- $W(e\nu)$ events, when the electron is misidentified as a photon;

- $Z(\nu\bar{\nu})$+jets and multi-jet events, when one of the jets in the event is misidentified as a photon;

- $\tau\nu\gamma$ and $\ell\nu\gamma$ events from $W\gamma$ production, when the τ decays into hadrons or when the electron or muon from τ or W decay is not reconstructed;

- γ+jets events, when large apparent E_T^{miss} is created by a combination of real E_T^{miss} from neutrinos in heavy quark decays and mis-measured jet energy.

$W(e\nu)$ *background:* To estimate the background contribution from $W(e\nu)$, the following dedicated studies are performed to determine the probability for an electron to be identified as a photon in the final state. A sample of $Z \rightarrow e^+e^-$ event candidates, with one of the e replaced by a photon, taken from data is used to estimate the fraction of electrons from the Z boson decay that are reconstructed as photons. The events are selected if the reconstructed invariant mass of the photon and the electron is close to the Z mass. This fraction ($f_{e\rightarrow\gamma}$) increases from 2% to 6% as $|\eta|$ increases. These fake rates are used to determine the $W(e\nu)$ background in the signal region, by weighting the electron candidates in the control region with the misidentification rate corresponding to their $|\eta|$. The events in the $W(e\nu)$ control region are selected by nominal $\nu\bar{\nu}\gamma$ selection criteria, except an electron is used instead of a photon in the final state. The data-driven estimates of the $W(e\nu)$ background are limited mainly by the accuracy of the measurement of the misidentification rate. The combined statistical and systematic uncertainties of the determination of $f_{e\rightarrow\gamma}$ are used to evaluate the systematic uncertainties of the $W(e\nu)$ background estimate.

$Z(\nu\bar{\nu})$+jets *and multi-jets backgrounds:* A data-driven method similar to the one described in Sec. VI A is used to determine the background contribution from $Z(\nu\bar{\nu})$+jets and multi-jets events. The main systematic uncertainty (20%) comes from the differences between f_γ values measured in various control samples obtained by varying the selection criteria for "low quality" photons.

$W\gamma$ *background:* Misidentified events from the $W\gamma$ process are one of the dominant background contributions to the $\nu\bar{\nu}\gamma$ signal. A large fraction (about 65%) of the $W\gamma$ contamination comes from $\tau\nu\gamma$ events. The

---

[4] Unassociated energy clusters in the calorimeter are the energy deposits that are not matched to any reconstructed high-p_T object (jet, electron, muon and photon).

	$e\nu\gamma$	$\mu\nu\gamma$	$e\nu\gamma$	$\mu\nu\gamma$
	$N_{\mathrm{jet}} \geq 0$		$N_{\mathrm{jet}} = 0$	
$N_{W\gamma}^{\mathrm{obs}}$	7399	10914	4449	6578
$W(\ell\nu)$+jets	$1240 \pm 160 \pm 210$	$2560 \pm 270 \pm 580$	$910 \pm 160 \pm 160$	$1690 \pm 210 \pm 270$
$Z(\ell^+\ell^-) + X$	$678 \pm 18 \pm 86$	$779 \pm 19 \pm 93$	$411 \pm 13 \pm 51$	$577 \pm 16 \pm 73$
γ+jets	$625 \pm 80 \pm 86$	$184 \pm 9 \pm 15$	$267 \pm 79 \pm 54$	$87 \pm 7 \pm 14$
$t\bar{t}$	$320 \pm 8 \pm 28$	$653 \pm 11 \pm 57$	$22 \pm 2 \pm 4$	$44 \pm 3 \pm 6$
other background	$141 \pm 16 \pm 13$	$291 \pm 29 \pm 26$	$52 \pm 5 \pm 6$	$140 \pm 22 \pm 18$
$N_{W\gamma}^{\mathrm{sig}}$	$4390 \pm 200 \pm 250$	$6440 \pm 300 \pm 590$	$2780 \pm 190 \pm 180$	$4040 \pm 230 \pm 280$

TABLE I. Total number of events passing the selection requirements in the data ($N_{W\gamma}^{\mathrm{obs}}$), expected number of background events and observed number of signal events ($N_{W\gamma}^{\mathrm{sig}}$) in the $e\nu\gamma$ and the $\mu\nu\gamma$ channels for inclusive ($N_{\mathrm{jet}} \geq 0$) and exclusive ($N_{\mathrm{jet}} = 0$) events. $N_{W\gamma}^{\mathrm{sig}}$ is defined as the difference between $N_{W\gamma}^{\mathrm{obs}}$ and the total number of expected background events. The first uncertainty is statistical and the second uncertainty represents an estimate of the systematic effects. The "other background" includes contributions from WW, single top quark, $W(\tau\nu)$ and $Z(\tau^+\tau^-)$ production.

	$e^+e^-\gamma$	$\mu^+\mu^-\gamma$	$e^+e^-\gamma$	$\mu^+\mu^-\gamma$
	$N_{\mathrm{jet}} \geq 0$		$N_{\mathrm{jet}} = 0$	
$N_{Z\gamma}^{\mathrm{obs}}$	1908	2756	1417	2032
$N_{Z\gamma}^{\mathrm{BG}}$	$311 \pm 57 \pm 68$	$366 \pm 83 \pm 73$	$156 \pm 43 \pm 32$	$244 \pm 41 \pm 49$
$N_{Z\gamma}^{\mathrm{sig}}$	$1600 \pm 71 \pm 68$	$2390 \pm 97 \pm 73$	$1260 \pm 56 \pm 32$	$1790 \pm 59 \pm 49$

TABLE II. Total number of events passing the selection requirements in the data ($N_{Z\gamma}^{\mathrm{obs}}$), expected number of background events ($N_{Z\gamma}^{\mathrm{BG}}$) and observed number of signal events ($N_{Z\gamma}^{\mathrm{sig}}$) in the $e^+e^-\gamma$ channel and the $\mu^+\mu^-\gamma$ channel with inclusive ($N_{\mathrm{jet}} \geq 0$) and exclusive ($N_{\mathrm{jet}} = 0$) selections. $N_{Z\gamma}^{\mathrm{sig}}$ is defined as the difference between $N_{Z\gamma}^{\mathrm{obs}}$ and the total number of expected background events. The first uncertainty is statistical and the second uncertainty represents an estimate of the systematic effects.

	$\nu\bar{\nu}\gamma$	$\nu\bar{\nu}\gamma$
	$N_{\mathrm{jet}} \geq 0$	$N_{\mathrm{jet}} = 0$
$N_{Z\gamma}^{\mathrm{obs}}$	1094	662
$W(e\nu)$	$171 \pm 2 \pm 17$	$132 \pm 2 \pm 13$
$Z(\nu\bar{\nu})$+jets, multi-jet	$70 \pm 13 \pm 14$	$29 \pm 5 \pm 3$
$W\gamma$	$238 \pm 12 \pm 37$	$104 \pm 9 \pm 24$
γ+jets	$168 \pm 20 \pm 42$	$26 \pm 7 \pm 11$
$Z(\tau^+\tau^-)\gamma$	$11.7 \pm 0.7 \pm 0.9$	$6.5 \pm 0.6 \pm 0.6$
$t\bar{t}$	$11 \pm 1.2 \pm 1.0$	$0.9 \pm 0.6 \pm 0.1$
$N_{Z\gamma}^{\mathrm{sig}}$	$420 \pm 42 \pm 60$	$360 \pm 29 \pm 30$

TABLE III. Total number of events in the data ($N_{Z\gamma}^{\mathrm{obs}}$), expected number of background events from various SM processes and observed signal yields ($N_{Z\gamma}^{\mathrm{sig}}$) after all $\nu\bar{\nu}\gamma$ selection criteria are applied for inclusive ($N_{\mathrm{jet}} \geq 0$) and exclusive ($N_{\mathrm{jet}} = 0$) events. $N_{Z\gamma}^{\mathrm{sig}}$ is defined as the difference between $N_{Z\gamma}^{\mathrm{obs}}$ and the total number of expected background events. The first uncertainty is statistical and the second uncertainty represents an estimate of the systematic effects.

branching fractions of the τ decay modes are well known and modeled by MC simulation. The main uncertainty on the $\tau\nu\gamma$ contamination is due to the uncertainty on the MC normalization factor. By assuming lepton universality for the W boson decays, the MC scale factor for $\tau\nu\gamma$ events and its uncertainty are taken from the measurement of $\ell\nu\gamma$ events. The scale factor is defined to correct the yield of $\ell\nu\gamma$ events estimated by MC simulation to match the $\ell\nu\gamma$ event yield measured in data as shown in Table I. About 35% of $W\gamma$ contamination comes from $\ell\nu\gamma$ events. Most of the $\ell\nu\gamma$ contamination consists of

events with a low-E_{T} lepton below 25GeV (70%) or with a high-E_{T} central lepton that failed to pass the identification or isolation criteria (20%). Less than 5% of $\ell\nu\gamma$ contamination comes from events with a forward lepton outside the detector's fiducial volume.

γ+jets background: Due to the high-$E_{\mathrm{T}}^{\mathrm{miss}}$ requirement in $\nu\bar{\nu}\gamma$ event selection, γ+jets contamination is suppressed, especially in the exclusive measurement with a jet veto cut. In order to measure this background from data, a sample is selected by applying all signal-region selection criteria except for requiring $\Delta\phi(E_{\mathrm{T}}^{\mathrm{miss}}, \mathrm{jet}) < 0.4$. By requiring the $E_{\mathrm{T}}^{\mathrm{miss}}$ direction to be close to the jet direction, the selected events in the control region are dominated by γ+jets background. The yield of γ+jets obtained in control regions is then scaled by an extrapolation factor to predict the γ+jets background yield in the signal region, where the extrapolation factor is taken from a γ+jets MC sample. By varying the $E_{\mathrm{T}}^{\mathrm{miss}}$ threshold from 60 GeV to 100 GeV and varying the jet multiplicity requirement for the events from $N_{jet} \geq 0$ to $N_{jet} \geq 1$, alternative control samples are obtained to evaluate the systematic uncertainties. The main systematic uncertainty in the γ+jets estimate comes from the different background yields in different control regions. The systematic uncertainty on the extrapolation factor is obtained by comparing the predictions from SHERPA and PYTHIA γ+jets MC samples and varying the energy scale and resolution for jets and $E_{\mathrm{T}}^{\mathrm{miss}}$ in MC samples.

Other backgrounds: Background contributions from other processes are determined from MC samples. The contributions from $Z(\tau^+\tau^-)\gamma$, and $t\bar{t}$ are found to be
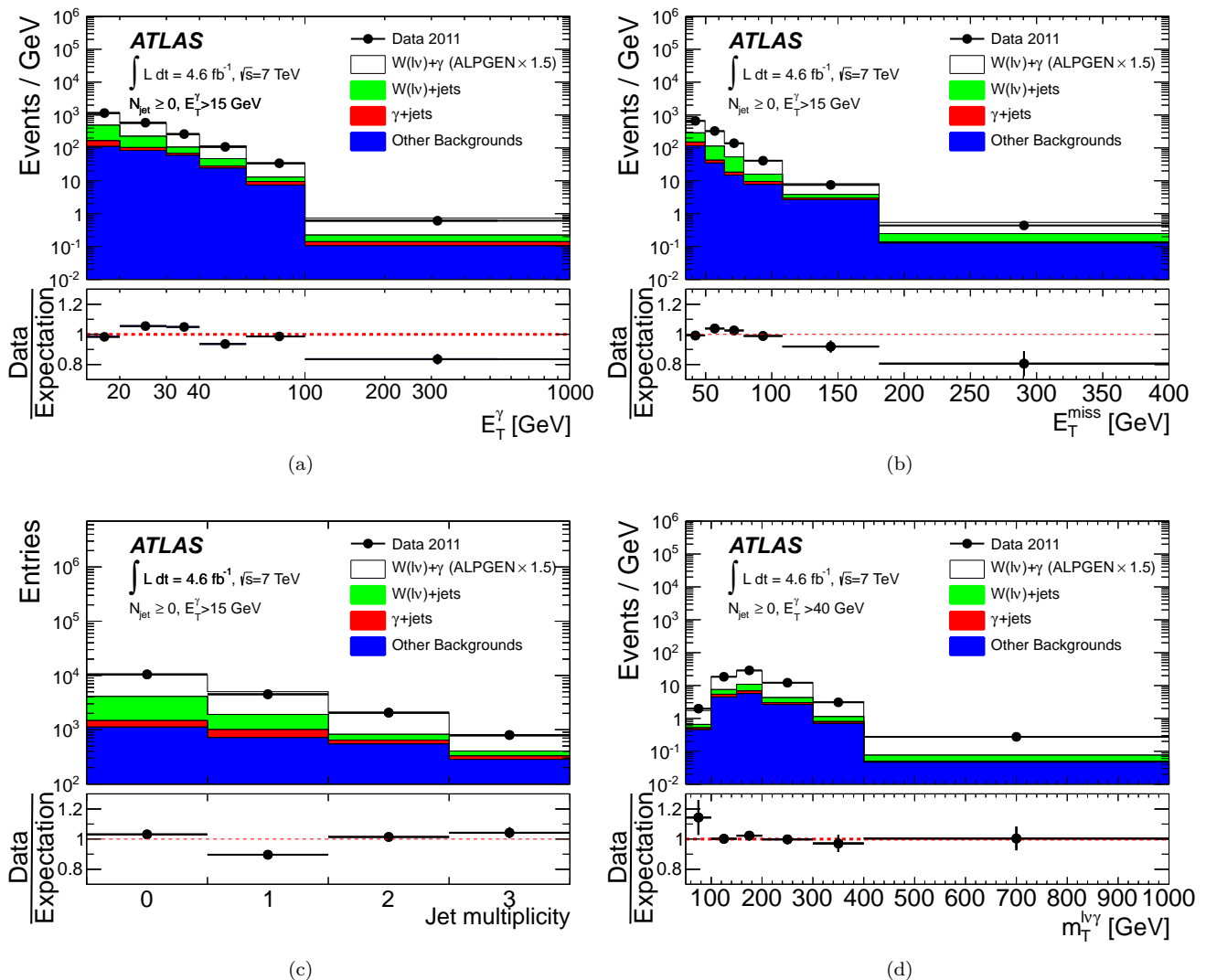
FIG. 3. Combined distributions for $\ell\nu\gamma$ candidate events in the electron and muon channels of (a) the photon transverse energy, (b) the missing transverse energy, (c) the jet multiplicity, and (d) the three-body transverse mass distribution as defined in Eq. (6). The selection criteria are defined in Sec. V, in particular the photon transverse energy is required to be $E_T^\gamma > 15$ GeV, except for panel (d) where it is required to be $E_T^\gamma > 40$ GeV. The distributions for the expected signals are taken from the ALPGEN MC simulation and scaled by a global factor (1.5) to match the extracted number of signal events shown in Table I. The ratio of the number of candidates observed in the data to the number of expected candidates from signal and background processes is also shown. Only the statistical uncertainties on the data are shown for these ratios. As the expected signal is normalized to match the extracted number of signal events, the ratio provides a comparison only between the observed and predicted shapes of the distributions. The histograms are normalized by their bin width.

small (about 1% of the total background). The contributions from the other processes such as $Z(\ell^+\ell^-)\gamma$, $\gamma\gamma$, and diboson production, are found to be negligible due to the strict cuts applied to the E_T^{miss} and the photon transverse energy.

To investigate the possibility of non-collision backgrounds, the distributions of the direction of flight as well as quality criteria (e.g. shower shapes) of the photon candidates in data are compared to those expected from the signal simulation to search for discrepancies. The direction of flight, which is determined by using the

depth segmentation of the EM calorimeter, can show if the photon appears to be coming from a vertex other than the primary vertex. The spectra of the direction of flight as well as the quality criteria are found to be completely consistent with those photons produced in events with real photons (e.g. $W(\ell\nu) + \gamma$ and $Z(\ell^+\ell^-) + \gamma$) leading to the conclusion that if there are non-collision background events, they are negligible.

A summary of background contributions and signal yields in the $\nu\bar{\nu}\gamma$ analysis is given in Table III. The photon transverse energy, the jet multiplicity and the miss-
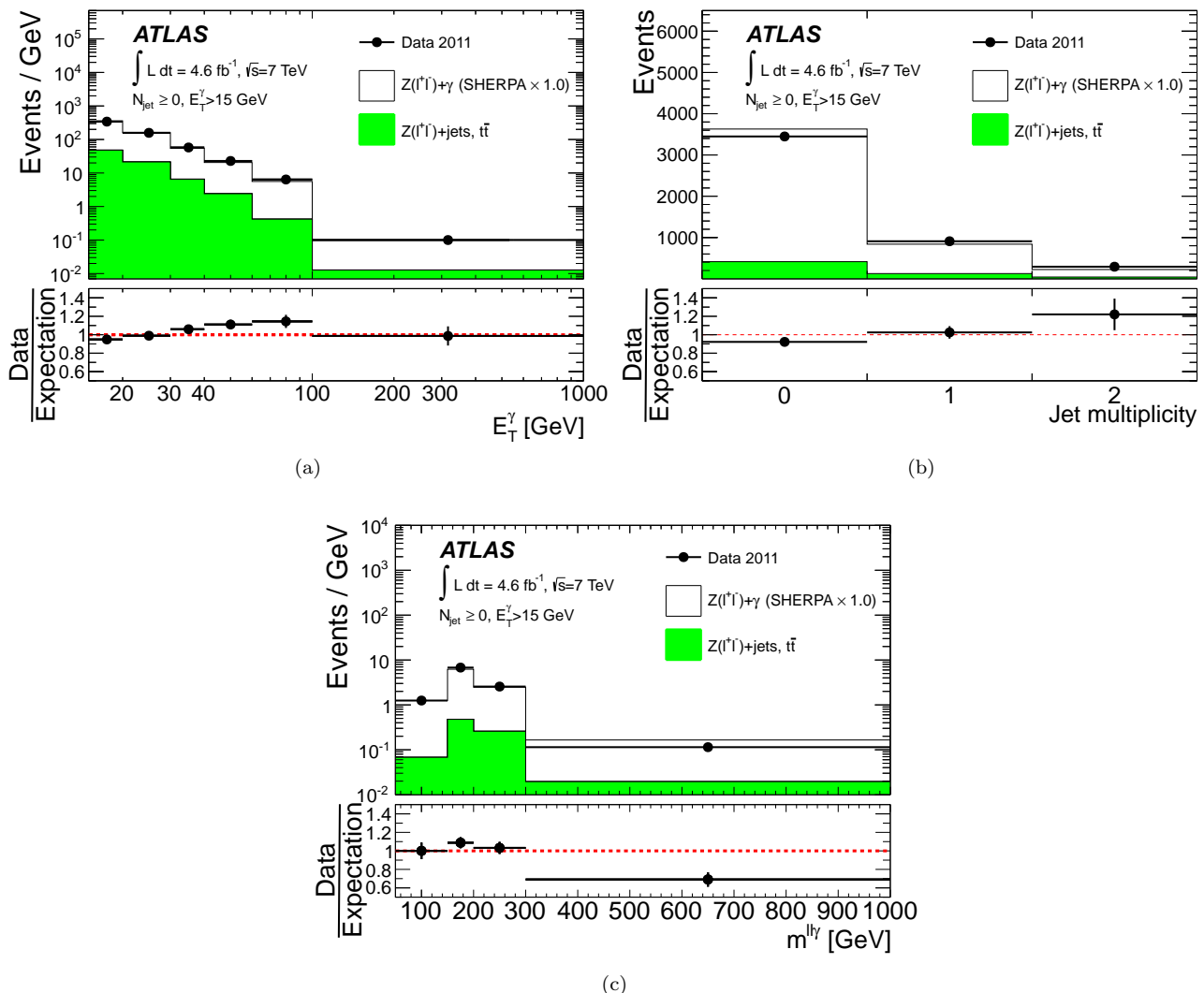
(a)

(b)

(c)

FIG. 4. Distribution for $\ell^+\ell^-\gamma$ candidate events combining the electron and muon channels of (a) the photon transverse energy, (b) the jet multiplicity, and (c) the three-body mass distribution. The selection criteria are defined in Sec. V, in particular the photon transverse energy is required to be $E_T^\gamma > 15$ GeV, except for panel (c) where it is required to be $E_T^\gamma > 40$ GeV. The distributions for the expected signals are taken from the SHERPA MC simulation and scaled by a global factor (which is 1.0) to match the extracted number of signal events shown in Table II. The ratio of the number of candidates observed in the data to the number of expected candidates from signal and background processes is also shown. Only the statistical uncertainties on the data are shown for these ratios. The histograms are normalized by their bin width.

ing transverse energy distributions from the selected $\nu\bar{\nu}\gamma$ events are shown in Fig. 5.

VII. CROSS-SECTION MEASUREMENTS

The cross-section measurements for the $W\gamma$ and $Z\gamma$ processes are performed in the fiducial region, defined at particle level using the object and event kinematic selection criteria described in Sec. V. They are then extrapolated to an extended fiducial region (defined in Table IV) common to the electron and muon final states. In this analysis, particle level refers to stable particles, defined as

having lifetimes exceeding 10 ps, that are produced from the hard scattering or after the hadronization but before their interaction with the detector. The extrapolation corrects for the signal acceptance losses in the calorimeter transition region ($1.37 < |\eta| < 1.52$) for electrons and photons, and in the high-η region ($2.4 < |\eta| < 2.47$) for muons. It also corrects for the Z-veto requirement in the $W\gamma$ electron channel, for the transverse mass selection criteria in both channels in the $W\gamma$ analysis, and for the acceptance loss due to the selection requirements on $\Delta\phi(E_T^{\mathrm{miss}}, \gamma)$ and $\Delta\phi(E_T^{\mathrm{miss}}, \mathrm{jet})$ in the $\nu\bar{\nu}\gamma$ analysis. Jets at particle level are reconstructed in MC-generated events by applying the anti-k_t jet reconstruction algo-
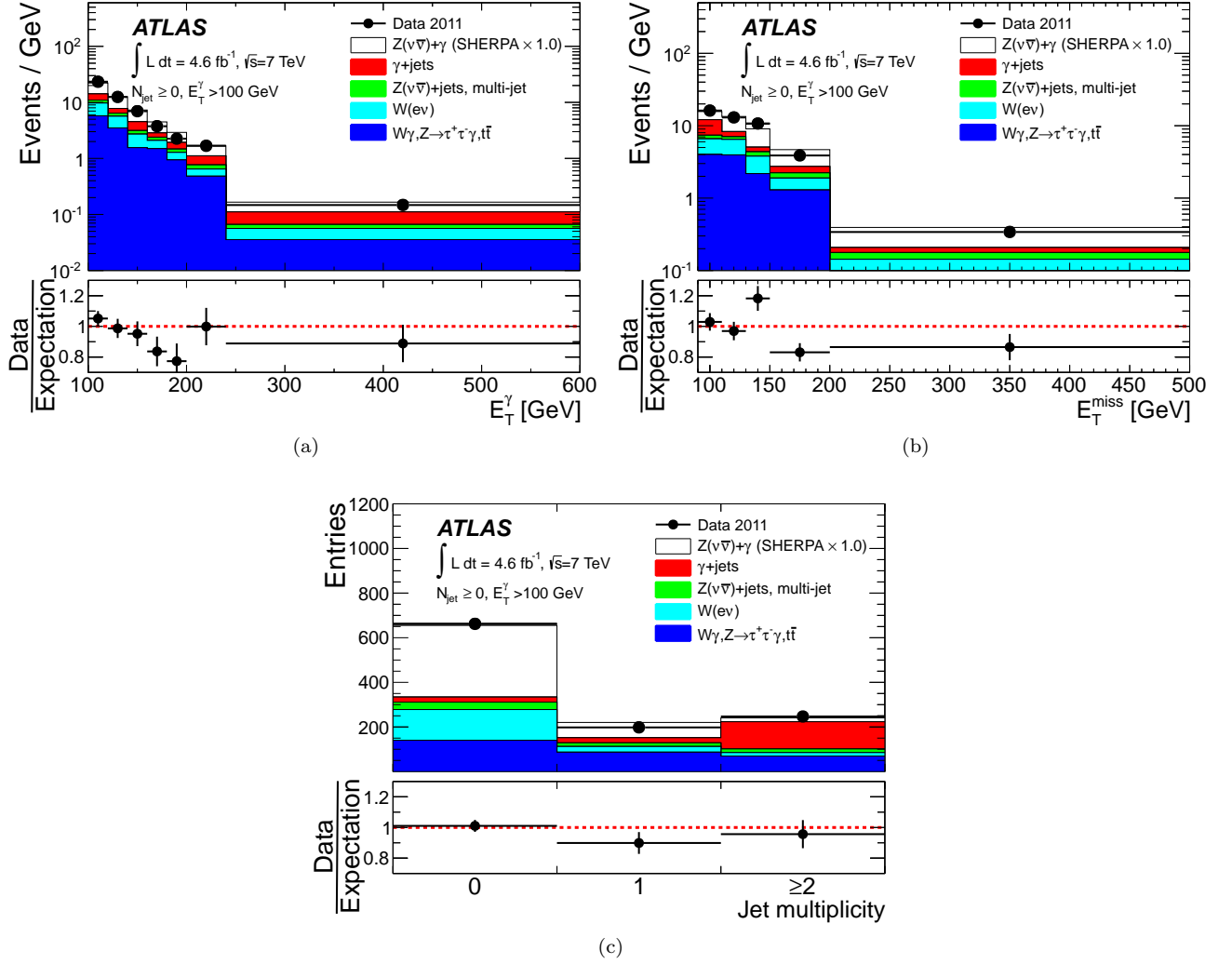
FIG. 5. Distributions of inclusive $\nu\bar{\nu}\gamma$ candidate events of (a) the photon transverse energy, (b) the missing transverse energy E_T^{miss}, and (c) the jet multiplicity. The selection criteria are defined in Sec. V. The distributions for the expected signal are taken from the SHERPA MC simulation and scaled by a global factor (which is 1.0) to match the extracted number of signal events shown in Table III. The ratio of the number of candidates observed in the data to the number of expected candidates from signal and background processes is also shown. Only the statistical uncertainties on the data are shown for these ratios. The histograms are normalized by their bin width.

rithm with a radius parameter $R = 0.4$ to all final-state stable particles. To account for the effect of final-state QED radiation, the energy of the generated lepton at particle level is defined as the energy of the lepton after radiation plus the energy of all radiated photons within a $\Delta R < 0.1$ cone around the lepton direction. Isolated photons with $\epsilon_h^p < 0.5$ [43, 44] are considered as signal, where ϵ_h^p is defined at particle level as the sum of the energy carried by final state particles in a $\Delta R < 0.4$ cone around the photon direction (not including the photon) divided by the energy carried by the photon.

A. Integrated fiducial cross-section

The cross-section measurements for the processes $pp \rightarrow \ell\nu\gamma + X$ and $pp \rightarrow (\ell^+\ell^-\gamma/\nu\bar{\nu}\gamma) + X$ are calculated as

$$\sigma_{pp\rightarrow\ell\nu\gamma(\ell^+\ell^-\gamma/\nu\bar{\nu}\gamma)}^{\text{ext-fid}} = \frac{N_{W\gamma(Z\gamma)}^{\text{sig}}}{A_{W\gamma(Z\gamma)} \cdot C_{W\gamma(Z\gamma)} \cdot \int \mathcal{L}dt}. \quad (1)$$

where

- $N_{W\gamma}^{\text{sig}}$ and $N_{Z\gamma}^{\text{sig}}$ denote the number of background-subtracted signal events passing the selection criteria of the $W\gamma$ and $Z\gamma$ analyses. These numbers are listed in Tables I, II and III.

Cuts	$pp \to \ell\nu\gamma$	$pp \to \ell^+\ell^-\gamma$	$pp \to \nu\bar{\nu}\gamma$
Lepton	$p_T^\ell > 25$ GeV	$p_T^\ell > 25$ GeV	—
	$|\eta_\ell| < 2.47$	$|\eta_\ell| < 2.47$	—
	$N_\ell = 1$	$N_{\ell^+} = 1, N_{\ell^-} = 1$	$N_\ell = 0$
	$p_T^\nu > 35$ GeV	—	—
Boson	—	$m_{\ell^+\ell^-} > 40$ GeV	$p_T^{\nu\bar{\nu}} > 90$ GeV
Photon	$E_T^\gamma > 15$ GeV	$E_T^\gamma > 15$ GeV	$E_T^\gamma > 100$ GeV
	$|\eta^\gamma| < 2.37, \Delta R(\ell, \gamma) > 0.7$		
	$\epsilon_h^p < 0.5$		
Jet	$E_T^{jet} > 30$ GeV, $|\eta^{jet}| < 4.4$		
	$\Delta R(e/\mu/\gamma, jet) > 0.3$		
	Inclusive : $N_{jet} \geq 0$, Exclusive : $N_{jet} = 0$		

TABLE IV. Definition of the extended fiducial region where the cross sections are evaluated; p_T^ν is the transverse momentum of the neutrino from W decays; $p_T^{\nu\bar{\nu}}$ is the transverse momentum of the Z boson that decays into two neutrinos; N_ℓ is the number of leptons in one event; ϵ_h^p is the photon isolation fraction.

- $\int \mathcal{L}dt$ is the integrated luminosity for the channels of interest (4.6 fb^{-1}).

- $C_{W\gamma}$ and $C_{Z\gamma}$ are defined as the number of reconstructed MC events passing all selection requirements divided by the number of generated events at particle level within the fiducial region. These ratios are shown in Table V.

- $A_{W\gamma}$ and $A_{Z\gamma}$ are the acceptances, defined at particle level as the number of generated events found within the fiducial region divided by the number of generated events within the extended fiducial region. These acceptances are listed in Table V.

The correction factors $C_{W\gamma}$ and $C_{Z\gamma}$ are determined by using $W/Z+\gamma$ signal MC events, corrected with scale factors to account for small discrepancies between data and simulation. These discrepancies include the differences in the lepton and photon reconstruction, identification and isolation efficiencies, as well as trigger efficiencies.

Table VI summarizes the systematic uncertainties on $C_{V\gamma}$ from different sources, on the signal acceptance $A_{V\gamma}$, and on the background estimates. The dominant uncertainties on $C_{V\gamma}$ come from photon identification and isolation efficiency. The photon identification efficiency is determined from the signal MC samples where the shower shape distributions of the photon are corrected to account for the observed small discrepancies between data and simulation. The systematic uncertainty is determined by comparing the corrected nominal value from MC simulation with the efficiency measurement using a pure photon sample from radiative Z decays in data. The uncertainty on the photon identification efficiency is found to be about 6% for all $V\gamma$ measurements. By doing a similar study, the uncertainty on the photon isolation efficiency is found to be less than 3%.

The uncertainties coming from the jet energy scale (JES) and resolution (JER) are important for all exclusive $V\gamma$ measurements. Uncertainties associated with the JES and JER affect the efficiency of the jet veto criteria and have an impact on E_T^{miss}. By separately varying the JES and JER within one standard deviation and propagating them to the E_T^{miss}, the uncertainties on $C_{V\gamma}$ due to these effects are found to be less than 4% for exclusive $\ell\nu\gamma$, and 3% for exclusive $\ell^+\ell^-\gamma$ and $\nu\bar{\nu}\gamma$ measurements.

The uncertainties on energy scale and resolution for unassociated energy clusters in the calorimeter and for additional pp collisions are propagated to E_T^{miss}, with an impact on $C_{V\gamma}$ of less than 2% for the $\ell\nu\gamma$ and $\nu\bar{\nu}\gamma$ measurements.

The muon momentum scale and resolution are studied by comparing the invariant mass distribution of $Z \to \mu^+\mu^-$ events in data and MC simulation [38]. The impact on $\ell\nu\gamma$ and $\ell^+\ell^-\gamma$ signal events due to the muon momentum scale and resolution uncertainty is smaller than 1%. The uncertainties due to the EM energy scale and resolution, which affect both the electron and photon, are found to be 2%–3%.

The efficiencies of the lepton selections, and the lepton triggers, are first estimated from the signal MC events and then corrected with scale factors derived using high-purity lepton data samples from W and Z boson decays to account for small discrepancies between the data and the MC simulation [35, 36, 38, 45]. In the $\ell\nu\gamma$ and $\ell^+\ell^-\gamma$ measurement, the uncertainty due to lepton identification and reconstruction is found to be about 2% in the electron channel, and less than 1% in the muon channel, and the uncertainty due to lepton isolation is found to be less than 2% in the electron channel and less than 0.5% in the muon channel.

The uncertainty due to single-muon trigger efficiencies is 2% for $\ell\nu\gamma$ and 0.6% for $\ell^+\ell^-\gamma$, while the uncertainty from single-electron trigger efficiencies is 0.7% for $\ell\nu\gamma$ and 0.1% for $\ell^+\ell^-\gamma$. The uncertainty from photon trigger efficiencies for $\nu\bar{\nu}\gamma$ is 1%.

The systematic uncertainties for $A_{W\gamma}$ and $A_{Z\gamma}$ are dominated by PDF uncertainties ($<0.8\%$), by the renormalization and factorization scale uncertainties ($<0.5\%$) and by the uncertainties on the size of the contributions from fragmentation photons ($<0.3\%$). The PDF uncertainty is estimated using the CT10 error eigenvectors at their 90% confidence-level (CL) limits and rescaled appropriately to 68% CL, with variations of α_s in the range 0.116–0.120. The renormalisation and factorisation scales are varied by factors of two around the nominal scales to evaluate the scale-related uncertainties.

The cross-section measurements of each leptonic decay channel and the combined (electron, muon) channels are extracted using a likelihood method. A negative log-likelihood function is defined as

	$pp \to e\nu\gamma$	$pp \to \mu\nu\gamma$	$pp \to e^+e^-\gamma$	$pp \to \mu^+\mu^-\gamma$	$pp \to \nu\bar{\nu}\gamma$
			$N_{\mathrm{jet}} \geq 0$		
$C_{V\gamma}$	0.51 ± 0.04	0.58 ± 0.04	0.33 ± 0.02	0.43 ± 0.03	0.71 ± 0.05
$A_{V\gamma}$	0.68 ± 0.01	0.86 ± 0.01	0.83 ± 0.01	0.91 ± 0.01	0.97 ± 0.01
			$N_{\mathrm{jet}} = 0$		
$C_{V\gamma}$	0.46 ± 0.04	0.55 ± 0.04	0.31 ± 0.02	0.40 ± 0.03	0.69 ± 0.05
$A_{V\gamma}$	0.73 ± 0.01	0.91 ± 0.01	0.83 ± 0.01	0.91 ± 0.01	0.98 ± 0.01

TABLE V. Summary of correction factors $C_{W\gamma}$ ($C_{Z\gamma}$) and acceptance $A_{W\gamma}$ ($A_{Z\gamma}$) for the calculation of the $W\gamma$ ($Z\gamma$) production cross sections. The combined statistical and systematic uncertainties are also shown.

$$-\ln L(\sigma, \mathbf{x}) = \sum_{i=1}^{n} -\ln\left(\frac{e^{-(N_s^i(\sigma,\mathbf{x})+N_b^i(\mathbf{x}))} \times (N_s^i(\sigma,\mathbf{x}) + N_b^i(\mathbf{x}))^{N_{\mathrm{obs}}^i}}{(N_{\mathrm{obs}}^i)!} \right) + \frac{\mathbf{x} \cdot \mathbf{x}}{2}. \qquad (2)$$

The expression inside the natural logarithm in Eq. (2) is the Poisson probability of observing N_{obs}^i events in channel i when N_s^i signal and N_b^i background events are expected. The nuisance parameters $\mathbf{x}$, whose distribution is assumed to be Gaussian, affect N_s^i and N_b^i as

$$N_s^i(\sigma, \mathbf{x}) = N_s^i(\sigma, 0)(1 + \sum_k x_k S_k^i), \qquad (3)$$

$$N_b^i(\mathbf{x}) = N_b^i(0)(1 + \sum_k x_k B_k^i), \qquad (4)$$

where S_k^i and B_k^i are, respectively, the relative systematic uncertainties on the signal and background due to the k-th source of systematic uncertainty. The quantity n in Eq. (2) is the number of channels to combine. By varying the nuisance parameters $\mathbf{x}$, the negative log-likelihood in Eq. (2) is minimized to obtain the most probable value of the measured cross section.

For the combination, it is assumed that the uncertainties on the lepton trigger and identification efficiencies are uncorrelated between different leptonic decay channels. All other uncertainties, such as the ones on the photon efficiency, background estimation, and jet energy scale, are assumed to be fully correlated. The measured production cross sections in the extended fiducial region defined in Table IV for the $\ell\nu\gamma$, $\ell^+\ell^-\gamma$ and $\nu\bar{\nu}\gamma$ processes are summarized in Table VII. These cross section measurements are the most extensive made to date for the study of V+γ production at the LHC.

B. Differential fiducial cross-section

Differential cross sections provide a more detailed comparison of the theoretical predictions to measurements, allowing a generic comparison of the kinematic distributions both in shape and normalization of the spectrum. For this purpose, the measured distributions are corrected to the underlying particle-level distributions by unfolding the effects of the experimental acceptance and resolution. A Bayesian iterative unfolding technique [46] is used. In the unfolding of binned data, effects of the experimental resolution are expressed by a response matrix, each element of which is the probability of an event in the i-th bin at the particle level being reconstructed in the j-th measured bin. In the iterative Bayesian unfolding, the initial prior for the underlying particle-level distribution is chosen to be the particle-level spectrum from the signal Monte Carlo sample. The posterior probability is obtained by Bayesian theory given the prior distribution, the measured distribution and the response matrix. The posterior is then used by the unfolding algorithm as a prior for the next iteration. Two iterations are used in the unfolding procedure because tests have shown that the unfolded spectrum becomes insensitive to the initial prior probability after two iterations. The unfolding techniques were tested using a data-driven closure test. In this test the particle-level spectrum in the MC simulation is reweighted and convolved through the folding matrix such that significantly improved agreement between the data and the reconstructed spectrum from the MC simulation is attained. The reweighted, reconstructed spectrum in the MC simulation is then unfolded using the same procedure as for the data. The comparison of the result with the reweighted particle-level spectrum from the Monte Carlo simulation provides the estimate of the bias. The typical size of the bias is less than 0.5%.

The E_{T}^γ bins are chosen to be large compared to the the detector resolution to minimize migration effects and to maintain a sufficient number of events in each bin.

The differential fiducial cross section is then defined in Eq. (5), where x is the variable of the measurement, dx is the width of the i-th bin of x, and N_i^{unfold} is the unfolded number of events in the i-th bin.

$$\frac{d\sigma_i}{dx} = \frac{N_i^{\mathrm{unfold}}}{\int \mathcal{L}dt \cdot dx}. \qquad (5)$$

Fig. 6 shows the differential fiducial cross sections as a function of E_{T}^γ in $V\gamma$ processes with the inclusive selection and with the exclusive zero-jet selection, as well as a comparison to the SM prediction. The corresponding

Source	$pp \to e\nu\gamma$	$pp \to \mu\nu\gamma$	$pp \to e^+e^-\gamma$	$pp \to \mu^+\mu^-\gamma$	$pp \to \nu\bar{\nu}\gamma$
Relative systematic uncertainties on the signal correction factor $C_{V\gamma}$ [%]					
γ identification efficiency	6.0 (6.0)	6.0 (6.0)	6.0 (6.0)	6.0 (6.0)	5.3 (5.3)
γ isolation efficiency	1.9 (1.8)	1.9 (1.7)	1.4 (1.4)	1.4 (1.4)	2.8 (2.8)
Jet energy scale	0.4 (2.9)	0.4 (3.2)	- (2.2)	- (2.4)	0.6 (2.0)
Jet energy resolution	0.4 (1.5)	0.6 (1.7)	- (1.7)	- (1.8)	0.1 (0.5)
unassociated energy cluster in $E_{\mathrm{T}}^{\mathrm{miss}}$	1.5 (1.6)	0.5 (1.0)	- (-)	- (-)	0.3 (0.2)
μ momentum scale and resolution	- (-)	0.5 (0.4)	- (-)	1.0 (0.8)	- (-)
EM scale and resolution	2.3 (3.0)	1.3 (1.6)	2.8 (2.8)	1.5 (1.5)	2.6 (2.7)
Lepton identification efficiency	1.5 (1.6)	0.4 (0.4)	2.9 (2.5)	0.8 (0.8)	- (-)
Lepton isolation efficiency	0.8 (0.8)	0.3 (0.2)	2.0 (1.6)	0.5 (0.4)	- (-)
Trigger efficiency	0.8 (0.1)	2.2 (2.1)	0.1 (0.1)	0.6 (0.6)	1.0 (1.0)
Total	7.1 (8.0)	6.8 (7.8)	7.6 (7.9)	6.5 (7.1)	6.6 (7.0)

TABLE VI. Relative systematic uncertainties on the signal correction factor $C_{V\gamma}$ for each channel in the inclusive $N_{\mathrm{jet}} >= 0$ (exclusive $N_{\mathrm{jet}} = 0$) $V\gamma$ measurement.

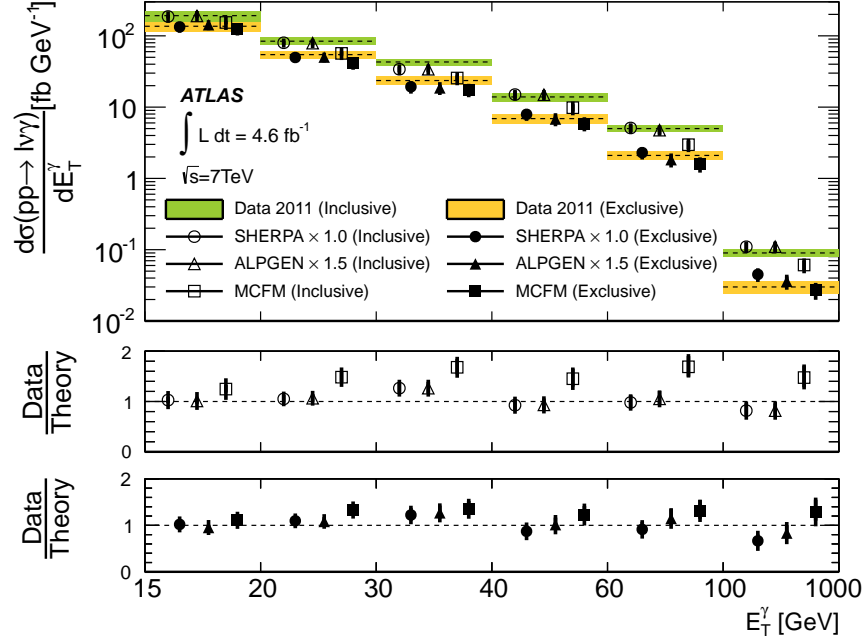|	$\sigma^{\mathrm{ext-fid}}$[pb] Measurement	$\sigma^{\mathrm{ext-fid}}$[pb] MCFM Prediction
	$N_{\mathrm{jet}} \geq 0$	
$e\nu\gamma$	2.74 ± 0.05 (stat) ± 0.32 (syst) ± 0.14 (lumi)	1.96 ± 0.17
$\mu\nu\gamma$	2.80 ± 0.05 (stat) ± 0.37 (syst) ± 0.14 (lumi)	1.96 ± 0.17
$\ell\nu\gamma$	2.77 ± 0.03 (stat) ± 0.33 (syst) ± 0.14 (lumi)	1.96 ± 0.17
$e^+e^-\gamma$	1.30 ± 0.03 (stat) ± 0.13 (syst) ± 0.05 (lumi)	1.18 ± 0.05
$\mu^+\mu^-\gamma$	1.32 ± 0.03 (stat) ± 0.11 (syst) ± 0.05 (lumi)	1.18 ± 0.05
$\ell^+\ell^-\gamma$	1.31 ± 0.02 (stat) ± 0.11 (syst) ± 0.05 (lumi)	1.18 ± 0.05
$\nu\bar{\nu}\gamma$	0.133 ± 0.013 (stat) ± 0.020 (syst) ± 0.005 (lumi)	0.156 ± 0.012
	$N_{\mathrm{jet}} = 0$	
$e\nu\gamma$	1.77 ± 0.04 (stat) ± 0.24 (syst) ± 0.08 (lumi)	1.39 ± 0.13
$\mu\nu\gamma$	1.74 ± 0.04 (stat) ± 0.22 (syst) ± 0.08 (lumi)	1.39 ± 0.13
$\ell\nu\gamma$	1.76 ± 0.03 (stat) ± 0.21 (syst) ± 0.08 (lumi)	1.39 ± 0.13
$e^+e^-\gamma$	1.07 ± 0.03 (stat) ± 0.12 (syst) ± 0.04 (lumi)	1.06 ± 0.05
$\mu^+\mu^-\gamma$	1.04 ± 0.03 (stat) ± 0.10 (syst) ± 0.04 (lumi)	1.06 ± 0.05
$\ell^+\ell^-\gamma$	1.05 ± 0.02 (stat) ± 0.10 (syst) ± 0.04 (lumi)	1.06 ± 0.05
$\nu\bar{\nu}\gamma$	0.116 ± 0.010 (stat) ± 0.013 (syst) ± 0.004 (lumi)	0.115 ± 0.009

TABLE VII. Measured cross sections for the $\ell\nu\gamma$, $\ell^+\ell^-\gamma$ and $\nu\bar{\nu}\gamma$ processes at $\sqrt{s} = 7$ TeV in the extended fiducial region defined in Table IV. The statistical uncertainty of each measurement corresponds to the statistical uncertainty of the data sample used by the measurement. The SM predictions from MCFM [47], calculated at NLO, are also shown in the table with systematic uncertainties. All MCFM predictions are corrected to particle level using parton-to-particle scale factors as described in Sec. VIII.

numerical values $\left(\frac{d\sigma_i}{dE_{\mathrm{T}}^{\gamma}}\right)$ are summarized in Table VIII. The systematic uncertainties on the differential fiducial cross sections are dominated by the uncertainties on the W+jet, γ+jet, $Z(\ell^+\ell^-)$ background normalization, on the photon identification, and on the EM and jet energy scales. The statistical uncertainties on the spectrum are propagated through the unfolding procedure by performing pseudo-experiments. Pseudo-experiments are generated by fluctuating the content of each bin in the data spectrum and the content of the response matrix according to their statistical uncertainties. The unfolding procedure is then applied to each pseudo-experiment, and the standard deviation of the unfolded results is taken as
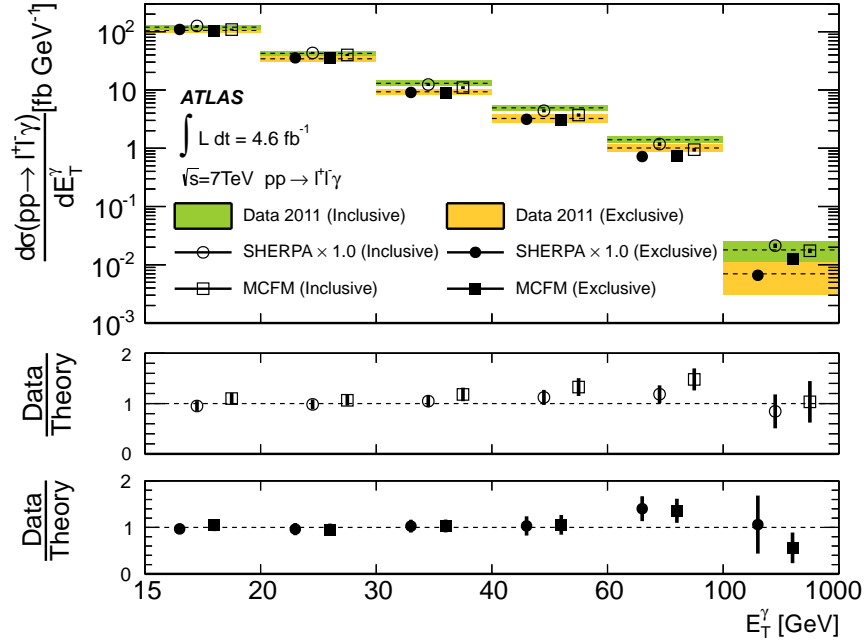
the statistical uncertainty. The systematic uncertainties on the spectrum are evaluated by varying the response matrix for each source of uncertainty and by combining the resulting changes in the unfolded spectrum.

The normalized differential fiducial cross section $\left(\frac{1}{\sigma} \times \frac{d\sigma_i}{dx}\right.$ and $\frac{1}{\sigma} \times d\sigma_i(x)$, where $\sigma = \sum \sigma_i(x) = \int \frac{d\sigma_i}{dx} dx$ and x is the variable under consideration such as E_{T}^{γ}) is also provided for shape comparisons. Some generators (SHERPA and ALPGEN) the kinematic variable shapes but are less accurate for the normalization. Table VIII shows the normalized differential fiducial cross sections as a function of E_{T}^{γ} for the $\ell\nu\gamma$ and $\ell^+\ell^-\gamma$ processes.

The normalized cross sections measured in bins of jet

FIG. 6. Measured E_T^γ differential cross sections of (a) the $pp \to \ell\nu\gamma$ process and of (b) the $pp \to \ell^+\ell^-\gamma$ process, using combined electron and muon measurements in the inclusive ($N_{\mathrm{jet}} \geq 0$) and exclusive ($N_{\mathrm{jet}} = 0$) extended fiducial regions. The lower plots show the ratio of the data to the predictions by different generators. The Monte Carlo uncertainties are shown only in the ratio plots. The cross-section predictions of the SHERPA and ALPGEN generators have been scaled by a global factor to match the total number of events observed in data. The global factor is 1.5 for the ALPGEN $\ell\nu\gamma$ signal sample and 1.0 for the SHERPA $\ell^+\ell^-\gamma$ signal sample. No global factor is applied for MCFM predictions.

multiplicity in $V\gamma$ events is presented in Fig. 7 and Table IX. The measurements are performed in the extended fiducial phase spaces defined in Table IV, with $E_T^\gamma > 15$ GeV for the low-E_T^γ region, and with $E_T^\gamma > 60$ GeV for the high-E_T^γ region. The systematic uncertainties on the jet multiplicity measurement are dominated by the uncertainties on the jet energy scale, the jet energy resolution and the background shape.

The transverse mass $m_T^{W\gamma}$ spectrum and the invariant mass $m^{Z\gamma}$ spectrum are also measured in the $\ell\nu\gamma$ and in the $\ell^+\ell^-\gamma$ processes, respectively. The transverse mass is defined in Eq. (6), where $m_{\ell\gamma}$ is the invariant mass of the lepton–photon system:

$$(m_T^{W\gamma})^2 = (\sqrt{m_{\ell\gamma}^2 + |\vec{p}_T(\gamma) + \vec{p}_T(\ell)|^2} + E_T^{\mathrm{miss}})^2$$
$$- |\vec{p}_T(\gamma) + \vec{p}_T(\ell) + \vec{E}_T^{\mathrm{miss}}|^2. \tag{6}$$

These measurements are performed in the extended fiducial phase space defined in Table IV, with $E_T^\gamma > 40$ GeV. The distribution of $m_T^{W\gamma}$ for the $\ell\nu\gamma$ candidates is shown in Fig. 3(d); the expected numbers of signal and background events are also shown. The unfolded $m_T^{W\gamma}$ spectrum is presented in Fig. 8(a) and Table X. The systematic uncertainties of $m_T^{W\gamma}$ spectrum measurements are dominated by the uncertainties on the EM energy scale, the jet energy scale, the E_T^{miss} energy scale and the background shape.

The distribution of $m^{Z\gamma}$ for the $\ell^+\ell^-\gamma$ candidates is presented in Fig. 4(c), together with the expected $m^{Z\gamma}$ distributions of the signal and background events. The unfolded $m^{Z\gamma}$ spectrum is presented in Fig. 8(b) and Table XI. The uncertainties in the $m^{Z\gamma}$ spectrum measurement arise predominantly from the uncertainties on the EM energy scale.

VIII. COMPARISON TO THEORETICAL PREDICTIONS

To test the predictions of the SM, the cross-section measurements of $pp \to \ell\nu\gamma + X$, $pp \to \ell^+\ell^-\gamma + X$ and $pp \to \nu\bar{\nu}\gamma + X$ production are compared to NLO and LO calculations using the MCFM [47] program. Version 6.3 of MCFM includes cross-section predictions for the production of $W\gamma$ + zero partons at NLO and for $W\gamma$ + one parton at LO. For $Z\gamma$ production the predictions are at NLO for both $Z\gamma$ + zero partons and $Z\gamma$ + one parton, and at LO for $Z\gamma$ + two partons. Finally, $\nu\bar{\nu}\gamma$ production is calculated at NLO for zero partons and LO for one parton.

Measurements of inclusive $\ell\nu\gamma$ production are compared to the NLO $W\gamma$ prediction with no restriction on the associated quark/gluon. Exclusive $\ell\nu\gamma$ production is compared to the same NLO prediction by requiring no parton with $|\eta| < 4.4$ and $p_T > 30$ GeV

in the final state. Similarly, measurements of inclusive $\ell^+\ell^-\gamma$ production are compared directly to the NLO $Z\gamma$ prediction while the exclusive $\ell\nu\gamma$ measurement is compared to the prediction with no additional parton with $|\eta| < 4.4$ and $p_T > 30$ GeV. The exclusive cross section for $\ell^+\ell^-\gamma$ production with exactly one jet with $|\eta| < 4.4$ and $p_T > 30$ GeV is compared to the NLO $Z\gamma$ + one-parton prediction with the same kinematic restriction on the single parton. Production of $l^+l^-\gamma$ with exactly two jets with $|\eta| < 4.4$ and $p_T > 30$ GeV is compared to the LO $Z\gamma$ + two-parton prediction. The cross sections for $\nu\bar{\nu}\gamma$ production are calculated in a similar manner using the MCFM NLO prediction for $\nu\bar{\nu}\gamma$ + zero partons.

All the MCFM predictions include W and Z boson production with photons from direct $W\gamma$ and $Z\gamma$ diboson production, from final-state radiation off the leptons in the W/Z decays and from quark/gluon radiation using the BFGSetII [48] photon fragmentation function. Event generation is done using the default electroweak parameters in the MCFM program and the parton distribution functions CT10 [30]. The renormalization, factorization and photon fragmentation scales are set equal to $\sqrt{M_V^2 + E_T^{\gamma\,2}}$. Photon isolation is defined using the fractional energy carried by partons in a cone $\Delta R_\gamma = 0.4$ about the photon direction. The fractional parton energy ϵ_h in the isolation cone (excluding the photon's energy) is required to be less than 0.5. The kinematic requirements for the parton-level generation are the same as those chosen at particle level for the extended fiducial cross-section measurements (see Table IV).

The parton-level cross-section uncertainties are evaluated by varying the PDFs and the renormalization and factorization scales, and by changing the definition of photon isolation. The PDF uncertainty is about 3%–4%. It is estimated using the CT10 error eigenvectors at their 68% CL limits, and varying the α_s values in the range 0.116 - 0.120. The variation of the renormalization and factorization scales from the nominal $\sqrt{M_V^2 + E_T^{\gamma\,2}}$ up and down by a common factor of two gives an uncertainty about 3%–7%. For the exclusive channels with no central jets with p_T greater than 30 GeV, the method suggested in Ref. [49] is used to estimate the uncertainty due to the energy scale of the process. The uncertainty due to the definition of photon isolation varies in the range 1%–5%. It is evaluated by varying the fractional parton energy ϵ_h^p from 0.0 to 1.0.

To compare these NLO SM predictions to the measured cross sections, they must be corrected for the differences between the parton-level and particle-level definitions of the jet and photon isolation, as done for data. The ALPGEN+HERWIG (for $W\gamma$) and SHERPA (for $Z\gamma$) MC samples are used to estimate the parton-to-particle scale factors. The scale factor ($S_{W\gamma}$ or $S_{Z\gamma}$) is defined as the number of simulated events passing the fiducial region selection cuts at the particle level divided by the number of simulated events passing the fiducial region selection cuts at the parton level. They increase the parton-level

E_T^γ [GeV]	[15,20]	[20,30]	[30,40]	[40,60]	[60,100]	[100,1000]
	$pp \to \ell\nu\gamma$, $N_{\mathrm{jet}} \geq 0$					
$d\sigma_{W\gamma}/dE_T^{W\gamma}$ [fb GeV^{-1}]	192 ± 32	84 ± 11	43.0 ± 5.0	13.9 ± 1.8	5.0 ± 0.5	0.090 ± 0.012
$1/\sigma_{W\gamma} \times d\sigma_{W\gamma}$	0.34	0.30	0.15	0.10	0.072	0.029
$1/\sigma_{W\gamma} \times d\sigma_{W\gamma}/dE_T^{W\gamma}$ [GeV^{-1}]	0.068	0.030	0.015	0.0050	0.0018	0.000032
Rel. Uncertainty	7.4%	5.4%	10%	6.6%	9.1%	10%
	$pp \to \ell\nu\gamma$, $N_{\mathrm{jet}} = 0$					
$d\sigma_{W\gamma}/dE_T^{W\gamma}$ [fb GeV^{-1}]	136 ± 22	54.5 ± 7.1	23.6 ± 3.3	6.9 ± 1.2	2.1 ± 0.3	0.030 ± 0.006
$1/\sigma_{W\gamma} \times d\sigma_{W\gamma}$	0.40	0.32	0.14	0.081	0.050	0.016
$1/\sigma_{W\gamma} \times d\sigma_{W\gamma}/dE_T^\gamma$ [GeV^{-1}]	0.080	0.032	0.014	0.0041	0.0013	0.000018
Rel. Uncertainty	8.8%	8.5%	11%	9.1%	11%	18%
	$pp \to \ell^+\ell^-\gamma$, $N_{\mathrm{jet}} \geq 0$					
$d\sigma_{Z\gamma}/dE_T^{Z\gamma}$ [fb GeV^{-1}]	120 ± 12	42.5 ± 4.2	13.0 ± 1.4	4.94 ± 0.61	1.40 ± 0.19	0.018 ± 0.007
$1/\sigma_{Z\gamma} \times d\sigma_{Z\gamma}$	0.45	0.32	0.098	0.075	0.042	0.012
$1/\sigma_{Z\gamma} \times d\sigma_{Z\gamma}/dE_T^\gamma$ [GeV^{-1}]	0.09	0.032	0.0098	0.0038	0.0011	0.000013
Rel. Uncertainty	5.9%	6.2%	10%	12%	12%	36%
	$pp \to \ell^+\ell^-\gamma$, $N_{\mathrm{jet}} = 0$					
$d\sigma_{Z\gamma}/dE_T^{Z\gamma}$ [fb GeV^{-1}]	106 ± 11	34.3 ± 4.1	9.3 ± 1.1	3.24 ± 0.47	1.01 ± 0.16	0.007 ± 0.004
$1/\sigma_{Z\gamma} \times d\sigma_{Z\gamma}$	0.49	0.32	0.087	0.060	0.038	0.0059
$1/\sigma_{Z\gamma} \times d\sigma_{Z\gamma}/dE_T^\gamma$ [GeV^{-1}]	0.098	0.032	0.0087	0.0030	0.00095	0.0000066
Rel. Uncertainty	6.5%	11%	12%	14%	15%	54%

TABLE VIII. The measured differential fiducial cross sections and normalized differential fiducial cross sections as a function of E_T^γ for the $\ell\nu\gamma$ and $\ell^+\ell^-\gamma$ processes using combined electron and muon measurements in the extended fiducial region defined in Table IV: inclusive with $N_{\mathrm{jet}} \geq 0$ and exclusive with $N_{\mathrm{jet}} = 0$. The uncertainties given here are the combination of the systematic and statistical uncertainties. Absolute uncertainties are presented for the measured differential fiducial cross sections, and relative uncertainties are presented for the measured normalized differential fiducial cross sections.

N_{jet}	0	1	2	3
	$pp \to \ell\nu\gamma$, $E_T^\gamma \geq 15$ GeV			
$1/\sigma_{W\gamma} \times d\sigma_{W\gamma}/dN_{\mathrm{jet}}$	0.58	0.27	0.12	0.037
Rel. Uncertainty	5.2%	11%	11%	22%
	$pp \to \ell\nu\gamma$, $E_T^\gamma \geq 60$ GeV			
$1/\sigma_{W\gamma} \times d\sigma_{W\gamma}/dN_{\mathrm{jet}}$	0.33	0.40	0.16	0.11
Rel. Uncertainty	10%	6.4%	11%	22%
	$pp \to \ell^+\ell^-\gamma$, $E_T^\gamma \geq 15$ GeV			
$1/\sigma_{Z\gamma} \times d\sigma_{Z\gamma}/dN_{\mathrm{jet}}$	0.80	0.15	0.052	-
Rel. Uncertainty	3.4%	11%	22%	-
	$pp \to \ell^+\ell^-\gamma$, $E_T^\gamma \geq 60$ GeV			
$1/\sigma_{Z\gamma} \times d\sigma_{Z\gamma}/dN_{\mathrm{jet}}$	0.60	0.28	0.12	-
Rel. Uncertainty	6.4%	9.4%	16%	-

TABLE IX. The measured differential fiducial cross sections as a function of jet multiplicity for $\ell\nu\gamma$ and $\ell^+\ell^-\gamma$ processes. The measurements are performed in the extended fiducial phase spaces defined in Table IV, with $E_T^\gamma > 15$ GeV and with $E_T^\gamma > 60$ GeV. The relative uncertainty is computed from the combination of cross sections from the electron and muon channels.

$m_T^{W\gamma}$ [GeV]	[50,100]	[100,150]	[150,200]	[200,300]	[300,400]	[400,1000]
$1/\sigma_{W\gamma} \times d\sigma_{W\gamma}$	0.037	0.27	0.32	0.24	0.079	0.050
$1/\sigma_{W\gamma} \times d\sigma_{W\gamma}/dm_T^{W\gamma}$ [GeV^{-1}]	0.00074	0.0054	0.0064	0.0024	0.00079	0.000083
Rel. Uncertainty	27%	8.0%	7.4%	6.4%	11%	17%

TABLE X. The measured differential fiducial cross sections as a function of $m_T^{W\gamma}$ for inclusive $\ell\nu\gamma$ process. The relative uncertainty is computed from the combination of cross sections from the electron and muon channels.

$m^{Z\gamma}$ [GeV]	[50,150]	[150,200]	[200,300]	[300,1000]
$1/\sigma_{Z\gamma} \times d\sigma_{Z\gamma}$	0.14	0.44	0.32	0.11
$1/\sigma_{Z\gamma} \times d\sigma_{Z\gamma}/dm^{Z\gamma}$ [GeV^{-1}]	0.0014	0.0088	0.0032	0.00016
Rel. Uncertainty	13%	5.5%	6.9%	14%

TABLE XI. The measured differential fiducial cross sections as a function of $m^{Z\gamma}$ for inclusive $\ell^+\ell^-\gamma$ process. The relative uncertainty is computed from the combination of cross sections from the electron and muon channels.
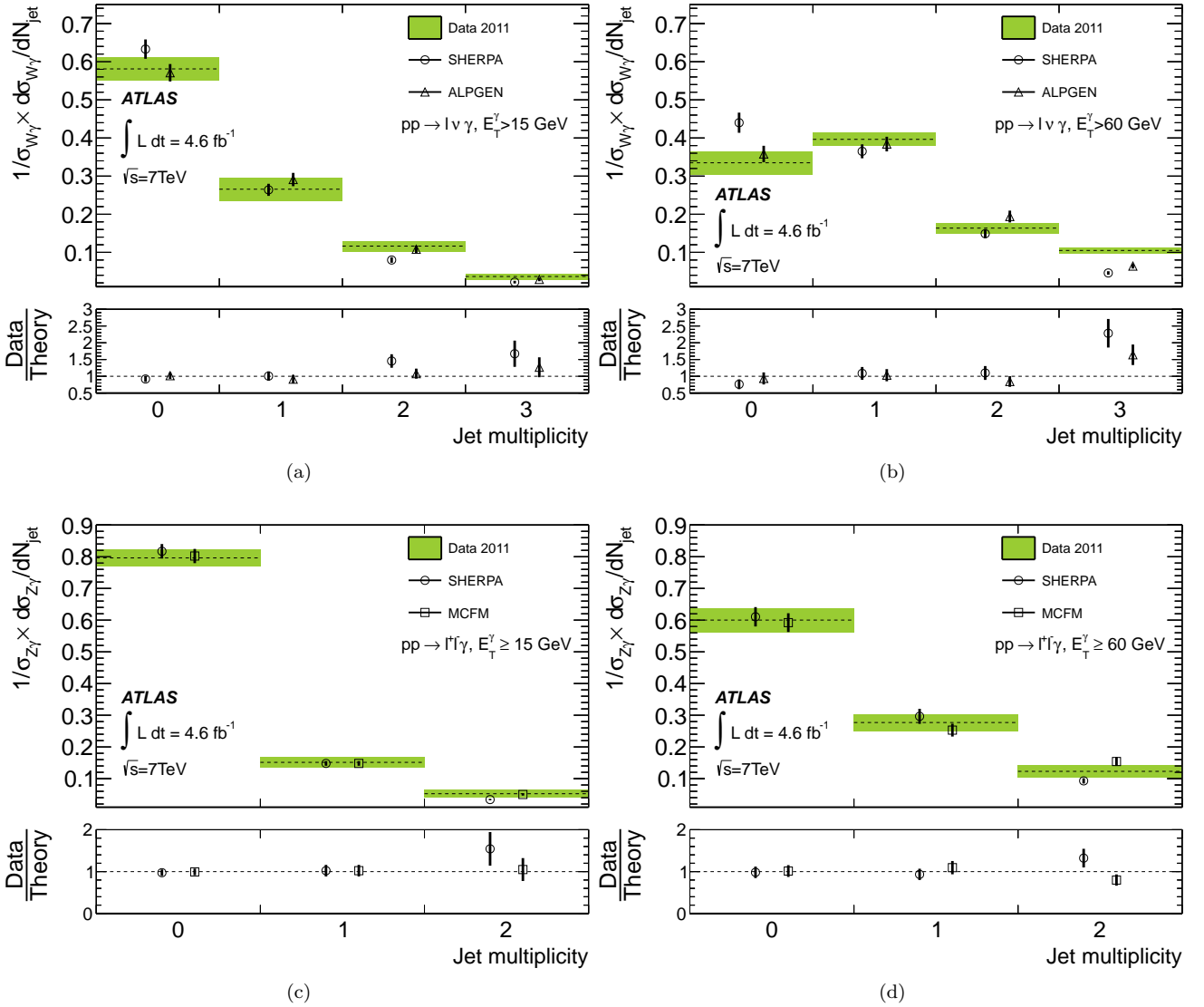
FIG. 7. The differential cross-section measurements as a function of the jet multiplicity for the $pp \to \ell\nu\gamma$ and $pp \to \ell^+\ell^-\gamma$ processes, for (a) $E_T^\gamma > 15$ GeV, $pp \to \ell\nu\gamma$, (b) $E_T^\gamma > 60$ GeV, $pp \to \ell\nu\gamma$, (c) $E_T^\gamma > 15$ GeV, $pp \to \ell^+\ell^-\gamma$ and (d) $E_T^\gamma > 60$ GeV, $pp \to \ell^+\ell^-\gamma$. The lower plots show the ratio of the data to the predictions by different generators. The MCFM prediction for inclusive (exclusive) $\ell\nu\gamma$ cross section with $p_T^\gamma > 60$ GeV is 171 ± 23 fb (80 ± 22 fb). The corresponding predictions for $p_T^\gamma > 15$ GeV are given in Table VII. MCFM does not provide the predictions for two and three jet bins for the $pp \to \ell\nu\gamma$ process, therefore only ALPGEN and SHERPA predictions are shown in (a) and (b).

cross sections by up to 13% with uncertainties that vary from 3% to 7% depending on the channel. A typical value of the scale factor predicted for the $W\gamma$ inclusive phase space by the ALGPEN (SHERPA) generator is 1.05 (1.00). The uncertainties for $W\gamma$ events are evaluated by comparing the differences in predictions made using ALPGEN and SHERPA. The uncertainties for $Z\gamma$ events are evaluated by comparing two signal samples: the nominal sample uses the SHERPA generator, the alternative sample is obtained from the MADGRAPH [50] generator interfaced to PYTHIA for parton shower and fragmentation processes. A typical value of the scale factor predicted

for the $Z\gamma$ inclusive phase space by the SHERPA (MAD-GRAPH) generator is 1.02 (1.03).

A. Integrated cross-section predictions

The inclusive and exclusive production cross sections in the extended fiducial regions defined in Table IV for the $\ell\nu\gamma$, $\ell^+\ell^-\gamma$ and $\nu\bar{\nu}\gamma$ final states are compared as described above to the NLO predictions made by the MCFM generator. The parton-level predictions corrected to the particle level are listed in Table VII together with the
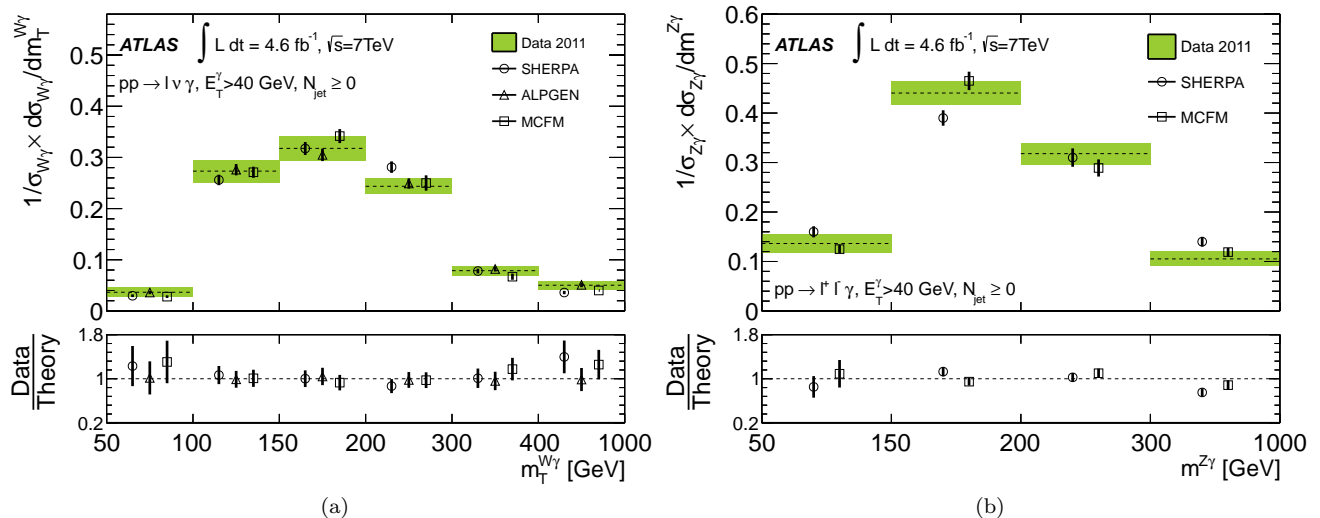
FIG. 8. The inclusive normalized differential cross section of (a) the $pp \to \ell\nu\gamma$ process as a function of $m_{\mathrm{T}}^{W\gamma}$ and (b) the $pp \to \ell^+\ell^-\gamma$ process as a function of $m^{Z\gamma}$. The lower plots show the ratio of the data to the prediction by different generators.

measured cross sections for events with $E_{\mathrm{T}}^{\gamma} >15$ GeV. The MCFM NLO predictions agree well with the measured $\ell^+\ell^-\gamma$ and $\nu\bar{\nu}\gamma$ cross sections. For the $\ell\nu\gamma + X$ channel the measured exclusive ($N_{\mathrm{jet}} =0$) cross section is slightly higher and the inclusive ($N_{\mathrm{jet}} \geq 0$) cross section significantly higher than the MCFM predictions. The discrepancy between the NLO prediction and data in the $\ell\nu\gamma + X$ channel is due to significant contributions from multi-jet production that are not observed in $\ell^+\ell^-\gamma$ as discussed in more detail below. In $W\gamma$ production there are contributions from processes with direct photon emission from the W boson which are absent in $Z\gamma$ production (see Fig. 1d). These additional $W\gamma$ production processes tend to have a higher jet multiplicity, and these contributions are not included in the current NLO calculations.

B. Differential cross sections for $pp \to \ell^+\ell^-\gamma$

The differential cross sections for $\ell^+\ell^-\gamma$ production can be compared to the NLO MCFM predictions and to those of the LO SHERPA generator scaled with an overall normalization factor obtained from data. The E_{T}^{γ} spectra from the inclusive and exclusive $\ell^+\ell^-\gamma$ channel are shown in Fig. 6(b). There is good agreement between the data and the SHERPA and MCFM predictions over the full E_{T}^{γ} range. The normalized differential spectrum for the $m^{Z\gamma}$ is compared to SHERPA and MCFM in Fig. 8(b). The NLO MCFM prediction reproduces the measured $m^{Z\gamma}$ somewhat better than the LO SHERPA MC. The normalized jet multiplicity spectrum from the $\ell^+\ell^-\gamma + X$ events is shown in Figs. 7(c) and (d). This can be compared to the LO SHERPA generator with up to three partons, as well as to the MCFM generator with NLO predictions for zero and one parton, and a LO prediction for two partons. As

shown in Figs. 7(c) and (d), both the MCFM and SHERPA generators are in good agreement with data.

C. Differential cross sections for $pp \to \ell\nu\gamma$

The background-subtracted, unfolded differential cross sections for $\ell\nu\gamma$ production can be compared to the NLO MCFM prediction and to both the ALPGEN and SHERPA MC generators. The predictions from MCFM are absolute cross sections, while those from both ALPGEN and SHERPA are scaled by an overall normalization factor obtained from data. The measured E_{T}^{γ} spectrum is shown in Fig. 6(a) for both inclusive and exclusive event selections. The MCFM prediction agrees with the data in the lowest photon E_{T}^{γ} bin but there are significant discrepancies in all higher E_{T}^{γ} bins, the effect being more enhanced for the inclusive event selection. The MC generators (ALPGEN and SHERPA) reproduce the shape of the E_{T}^{γ} spectrum reasonably well over the full E_{T}^{γ} range. The normalized differential cross section for $\ell\nu\gamma$ as a function of $m_{\mathrm{T}}^{W\gamma}$ is shown in Fig. 8(a). The MCFM, ALPGEN and SHERPA generators all provide a good description of the data.

The better description of ALPGEN and SHERPA compared to the MCFM prediction for the E_{T}^{γ} spectrum from $\ell\nu\gamma$ production, can be attributed to processes with large parton multiplicities, which correspond to tree-level diagrams of higher order in the strong coupling constant. A comparison of the jet multiplicities in the low-E_{T}^{γ} region (Fig. 7(a)) and in the high-E_{T}^{γ} region (Fig. 7(b)), shows that those processes with more than one parton (jet) contribute more in higher E_{T}^{γ} regions. The MCFM NLO cross-section prediction for $\ell\nu\gamma$ production includes real parton emission processes only up to one radiated

quark or gluon. The lack of higher-order QCD contributions results in an underestimate of the predicted cross sections. For the same reason, the improvement of the description by ALPGEN compared to SHERPA for the predictions of the jet multiplicity spectrum can be attributed to the fact that there are more additional hard partons included in the matrix element calculation with the ALPGEN generator.

IX. LIMITS ON ANOMALOUS TRIPLE-GAUGE-BOSON COUPLINGS

The reconstructed E_T^γ distributions from $V\gamma$ events with the exclusive zero-jet selection are used to set limits on $WW\gamma$, $ZZ\gamma$ and $Z\gamma\gamma$ anomalous triple-gauge-boson coupling parameters. Assuming C and P conservation separately, the aTGCs are generally chosen as λ_γ and $\Delta\kappa_\gamma$ ($\Delta\kappa_\gamma = \kappa_\gamma - 1$) for the $WW\gamma$ vertex [43, 44], and h_3^V and h_4^V for the $ZV\gamma$ vertices [51].

Form factors are introduced to avoid unitarity violation at very high energy. Typical choices of these form factors for the $WW\gamma$ aTGCs are: $\Delta\kappa_\gamma(s) = \Delta\kappa_\gamma/(1 + \hat{s}/\Lambda^2)^2$ and $\lambda_\gamma(s) = \lambda_\gamma/(1 + \hat{s}/\Lambda^2)^2$ [44]. For the $ZV\gamma$ aTGCs, conventional choices of form factors are $h_3^V(s) = h_3^V/(1+\hat{s}/\Lambda^2)^3$ and $h_4^V(s) = h_4^V/(1+\hat{s}/\Lambda^2)^4$ [51]. Here $\sqrt{\hat{s}}$ is the $W\gamma$ or $Z\gamma$ invariant mass and Λ is the new-physics energy scale. To conserve unitarity, Λ is chosen as 6 TeV in the $W\gamma$ analysis and 3 TeV in the $Z\gamma$ analysis. The results with energy cut-off $\Lambda = \infty$ are also presented as a comparison in the unitarity violation scheme.

Deviations of the aTGC parameters from the SM predictions would nearly all lead to an excess of high-energy photons associated with the W and Z bosons. Thus, measurements of the exclusive extended fiducial cross sections for $W\gamma$ production with $E_T^\gamma > 100$ GeV are used to extract aTGC limits. The cross-section predictions with aTGCs ($\sigma_{W\gamma}^{\mathrm{aTGC}}$ and $\sigma_{Z\gamma}^{\mathrm{aTGC}}$) are obtained from the MCFM generator. The number of expected $W\gamma$ events in the exclusive extended fiducial region ($N_{W\gamma}^{\mathrm{aTGC}}(\Delta\kappa_\gamma, \lambda_\gamma)$) for a given aTGC strength is obtained using Eq. (7)

$$N_{W\gamma}^{\mathrm{aTGC}}(\Delta\kappa_\gamma, \lambda_\gamma) = \sigma_{W\gamma}^{\mathrm{aTGC}} \times C_{W\gamma} \times A_{W\gamma} \times S_{W\gamma} \times \int \mathcal{L}dt.$$
(7)

For the $Z\gamma$ case, $N_{Z\gamma}^{\mathrm{aTGC}}(h_3^\gamma, h_4^\gamma)$ or $N_{Z\gamma}^{\mathrm{aTGC}}(h_3^Z, h_4^Z)$ are obtained in a similar way. The anomalous couplings influence the kinematic properties of $W\gamma$ and $Z\gamma$ events and thus the corrections for event reconstruction ($C_{W\gamma}$ and $C_{Z\gamma}$). The maximum variations of $C_{W\gamma}$ and $C_{Z\gamma}$ within the measured aTGC limits are quoted as additional systematic uncertainties.

The limits on a given aTGC parameter are extracted from a Frequentist Profile Likelihood test, as explained in Sec. VII, given the extended fiducial measurements. The profile likelihood combines the observed number of exclusive $V\gamma$ candidate events with $E_T^\gamma > 100$ GeV, the

processes	Measured	Expected
	$pp \to \ell\nu\gamma$	
Λ	∞	∞
$\Delta\kappa_\gamma$	$(-0.41, 0.46)$	$(-0.38, 0.43)$
λ_γ	$(-0.065, 0.061)$	$(-0.060, 0.056)$
Λ	6 TeV	6 TeV
$\Delta\kappa_\gamma$	$(-0.41, 0.47)$	$(-0.38, 0.43)$
λ_γ	$(-0.068, 0.063)$	$(-0.063, 0.059)$
processes	$pp \to \nu\nu\gamma$ and $pp \to \ell^+\ell^-\gamma$	
Λ	∞	∞
h_3^γ	$(-0.015, 0.016)$	$(-0.017, 0.018)$
h_3^Z	$(-0.013, 0.014)$	$(-0.015, 0.016)$
h_4^γ	$(-0.000094, 0.000092)$	$(-0.00010, 0.00010)$
h_4^Z	$(-0.000087, 0.000087)$	$(-0.000097, 0.000097)$
Λ	3 TeV	3 TeV
h_3^γ	$(-0.023, 0.024)$	$(-0.027, 0.028)$
h_3^Z	$(-0.018, 0.020)$	$(-0.022, 0.024)$
h_4^γ	$(-0.00037, 0.00036)$	$(-0.00043, 0.00042)$
h_4^Z	$(-0.00031, 0.00031)$	$(-0.00037, 0.00036)$

TABLE XII. The measured and expected 95% CL intervals on the charged ($\Delta\kappa_\gamma$, λ_γ) and neutral (h_3^γ, h_3^Z, h_4^γ, h_4^Z) anomalous couplings. The results obtained using different Λ values are shown, all the other couplings are set to the SM values. The two numbers in each parenthesis denote the 95% CL interval.

expected signal as a function of the aTGC (Eq. (7)) and the estimated number of background events.

The systematic uncertainties are included in the likelihood function as nuisance parameters with correlated Gaussian constraints. A point in the aTGC space is accepted (rejected) at the 95% CL if less (more) than 95% of the randomly generated pseudo-experiments exhibit larger profile likelihood ratio values than those observed in data.

The limits are defined as the values of aTGCs that demarcate the central 95% of the integral of the likelihood distribution. The resulting allowed ranges for the anomalous couplings are shown in Table XII for $WW\gamma$ and $ZV\gamma$ ($V = Z, \gamma$). These results are also compared in Fig. 9 with the results from LEP [11] and the Tevatron [4–6].

The limits on each aTGC parameter are obtained with the other aTGC parameters set to their SM values using a one-dimensional profile likelihood fit. The limits on each pair of aTGC are also evaluated by the same method. The 95% CL regions in two-dimensional aTGC space are shown as contours on the $(\Delta\kappa_\gamma, \lambda_\gamma)$, (h_3^γ, h_4^γ) and (h_3^Z, h_4^Z) planes in Fig. 10. Since all sensitivity of the measurement is contained in a single measurement of the $V\gamma$ cross sections in the high-E_T^γ regions, the likelihood ratio used to obtain the two-dimensional limits has one effective degree of freedom. Therefore the results of the aTGC frequentist limits found in the one-dimensional fit are identical to the corresponding limits obtained from the two-dimensional fits at the points where the other

aTGC is zero as shown in Fig. 10.

X. SEARCH FOR NARROW RESONANCES

Models such as Technicolor (TC) predict spin-1 mesons that have significant branching ratios to $W\gamma$ and $Z\gamma$. The discovery of a particle compatible with the SM Higgs [56, 57] does not exclude the full phase space of the TC models [58–60]. Therefore, they are used here as a benchmark for new physics processes that would appear as new resonant $W\gamma$ and $Z\gamma$ states.

Exotic resonance signals and SM backgrounds are modeled using probability density functions as described below. The model is then fit to the data to test for the presence of new physics. The electron ($e^+e^-\gamma$ and $e\nu\gamma$) and muon ($\mu^+\mu^-\gamma$ and $\mu\nu\gamma$) channels are evaluated independently in the search for $W\gamma$ and $Z\gamma$ resonances.

A. Generation and event selection

The Technicolor Strawman [61] model implemented in PYTHIA [24] is used to describe the production and decay of neutral and charged techni-mesons: $\omega_T \to Z\gamma$ and $a_T \to W\gamma$. The following parameters are used in the event generation: number of technicolors $N_{TC} = 4$; techniquark charges $Q_U = 1$ and $Q_D = 0$ for the $Z\gamma$ final state and $Q_U = 1/2$ and $Q_D = -1/2$ for the $W\gamma$ final state[5]; mixing angle between the techni-pions and electroweak gauge boson longitudinal component $\sin\chi = 1/3$. In addition, the mass splittings between the techni-mesons are set to be as follows: $m_{\rho_T} = m_{\omega_T}$, $m_{a_T} \approx 1.1 \times m_{\rho_T}$ and $m_{\rho_T} - m_{\pi_T} = m_W$.

This set of parameters follows those introduced for previous Low Scale Technicolor (LSTC) [62, 63] searches in the WZ and dilepton final states at the Tevatron and at the LHC. Using these parameters, the intrinsic widths of the resonances are of order 1 GeV, which is less than the measurement resolution. The results obtained in this study are therefore generic, as long as the resonances studied are narrow. The best limits on techni-meson production have been set at the LHC. Studying dilepton final states [64] in 4.9 fb^{-1} of $\sqrt{s} = 7$ TeV data, the ATLAS experiment excluded at the 95% CL the production of ω_T and ρ_T with masses $m_{\rho_T/\omega_T} < 855$ GeV. In the WZ final state [65], the CMS collaboration obtained an exclusion $m_{\rho_T/\omega_T} < 938$ GeV based on 5.0 fb^{-1} of $\sqrt{s} = 7$ TeV data.

The searches for narrow resonances in the $W\gamma$ and $Z\gamma$ final states are performed using the event selections de-

---

[5] This parameterization of the techni-quark charges is used in order to keep only the dominant a_T contribution in the $W\gamma$ final state to avoid the model dependence that could result from having two nearby peaks in the signal. In this way the ρ_T contribution is removed.

fined in Sec. IV but with the photon transverse energy E_T^γ required to be greater than 40 GeV. This choice is made to optimize the signal over SM background ratio since the decay products of a heavy resonance would be boosted. In order to keep the results as generic as possible, there is no further optimization of the cuts.

This study uses five mass points for m_{ω_T} ranging from 200 GeV to 650 GeV for the $Z\gamma$ channel, and seven mass points for m_{a_T} ranging from 275 GeV to 800 GeV for the $W\gamma$ channel. The signal samples are produced using the PYTHIA [24] generator interfaced to the full ATLAS GEANT4 [15] simulation [14] with events reconstructed as for the data. Table XIII summarizes the expected number of events at each mass point after all selection cuts.

m_{ω_T} [GeV]	m_{a_T} [GeV]	$W\gamma$ events	$Z\gamma$ events
200	225	-	47.8 ± 4.8
250	275	85.2 ± 8.4	-
300	330	58.2 ± 5.8	16.4 ± 1.3
350	385	39.3 ± 4.1	-
400	440	27.1 ± 2.2	6.9 ± 0.4
450	490	18.9 ± 1.6	-
500	550	13.6 ± 1.2	3.4 ± 0.2
650	720	-	1.4 ± 0.1
725	800	3.4 ± 0.3	-

TABLE XIII. Expected number of events after all selection cuts for the generated signal mass values. The quoted uncertainties are the combined statistical and systematic uncertainties. The number of expected events is indicated only for points used in the analysis.

B. Signal modeling

For the $\omega_T \to Z\gamma$ channel, the $m^{Z\gamma}$ distribution is fit by the sum of a Crystal-Ball function (CB) [66–68], which simulates the core mass resolution plus a non-Gaussian tail for low mass values, and a small wider Gaussian component that takes into account outliers in the mass distribution. The mean values of the CB and Gaussian functions are fixed to be equal. For simulated events, the mean fitted mass is found to be within 0.6 GeV of the generated resonance mass for both the $\mu^+\mu^-\gamma$ and $e^+e^-\gamma$ channels. At the reconstruction level, the full width at half maximum of the signal grows linearly from 9 GeV at $m_{\omega_T} = 200$ GeV to 30 GeV at $m_{\omega_T} = 650$ GeV. In order to scan for resonance signals in the data, $m^{Z\gamma}$ mass distributions are constructed in 5 GeV steps from 200 to 650 GeV by linearly interpolating the signal lineshape fit parameters for the $m^{Z\gamma}$ distributions.

For the $a_T \to W\gamma$ channel, the $m_T^{W\gamma}$ distribution is fit by a CB function. The mean value of the distribution is measured to be lower than the generated mass of the resonance as expected for the transverse mass. The signal resolution grows linearly from 20 GeV at $m_{a_T} = 275$ GeV
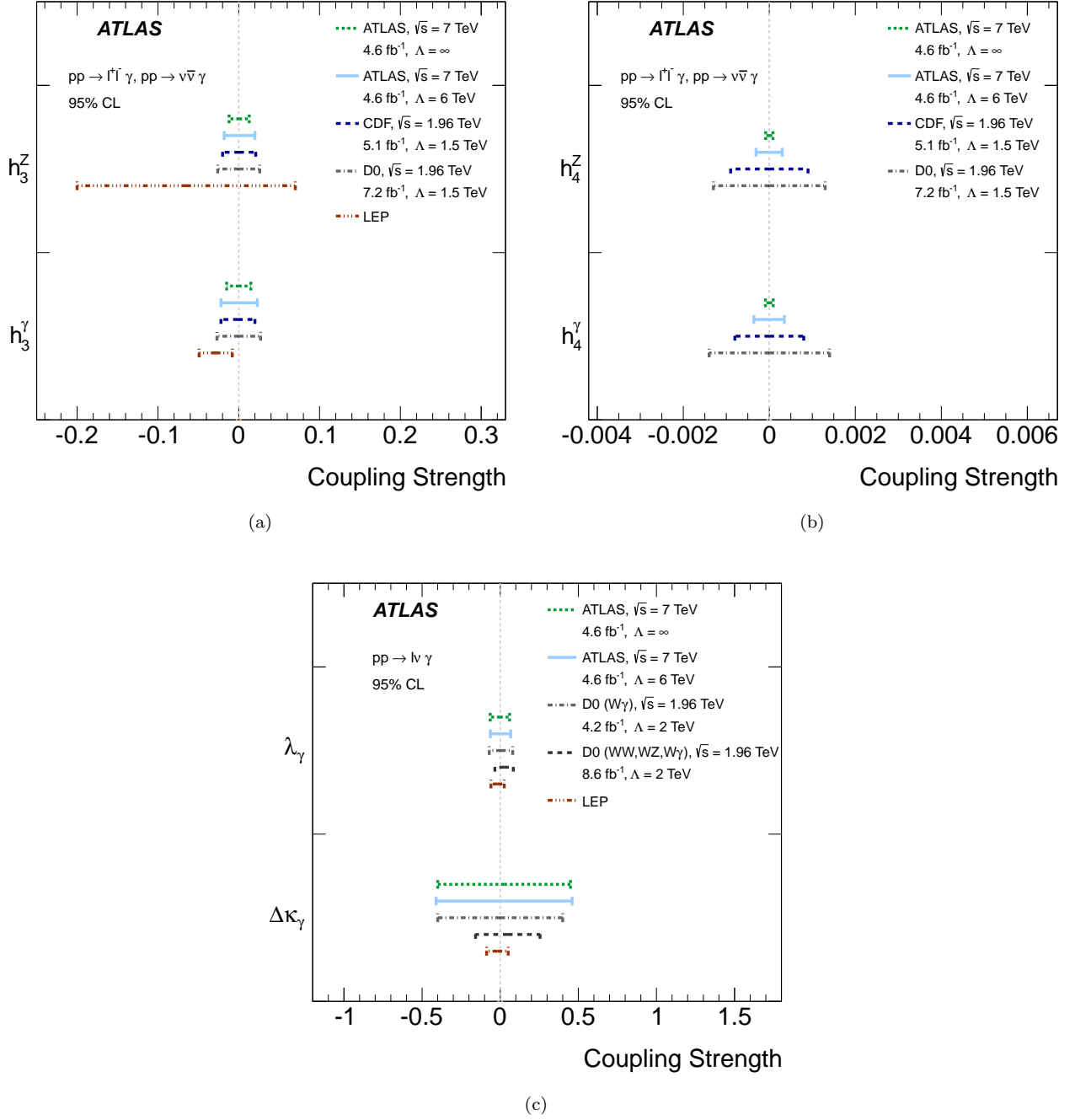
FIG. 9. The 95% CL intervals for anomalous couplings from ATLAS, D0 [5, 6], CDF [4] and LEP [11] for (a),(b) the neutral aTGC h_3^γ, h_3^Z, h_4^γ, h_4^Z as obtained from $Z\gamma$ events, and (c) the charged aTGCs $\Delta\kappa_\gamma$, λ_γ. The integrated luminosities and new-physics scale parameter Λ are shown. The ATLAS and D0 results for the charged aTGCs measured from $W\gamma$ production are shown. Except for the coupling under study, all other anomalous couplings are set to zero. The LEP charged aTGCs results were obtained from WW production, which is also sensitive to the WWZ couplings and therefore required some assumptions ($\lambda_Z = \lambda_\gamma$, $\Delta\kappa_\gamma = (cos^2\theta_W/sin^2\theta_W)(\Delta g^Z - \Delta\kappa_Z)$) about the relations between the $WW\gamma$ and WWZ aTGCs [11, 52–54], but did not require assumptions about the scale Λ. The combined aTGC results from the D0 experiment are obtained from $WW + WZ \to \ell\nu jj$, $WW + WZ \to l\nu l^+l^-$, $W\gamma \to l\nu\gamma$, and $WW \to l\nu l\nu$ events [55]. The LEP limits on neutral aTGC's are much larger than those from hadron colliders and are not included in (b).
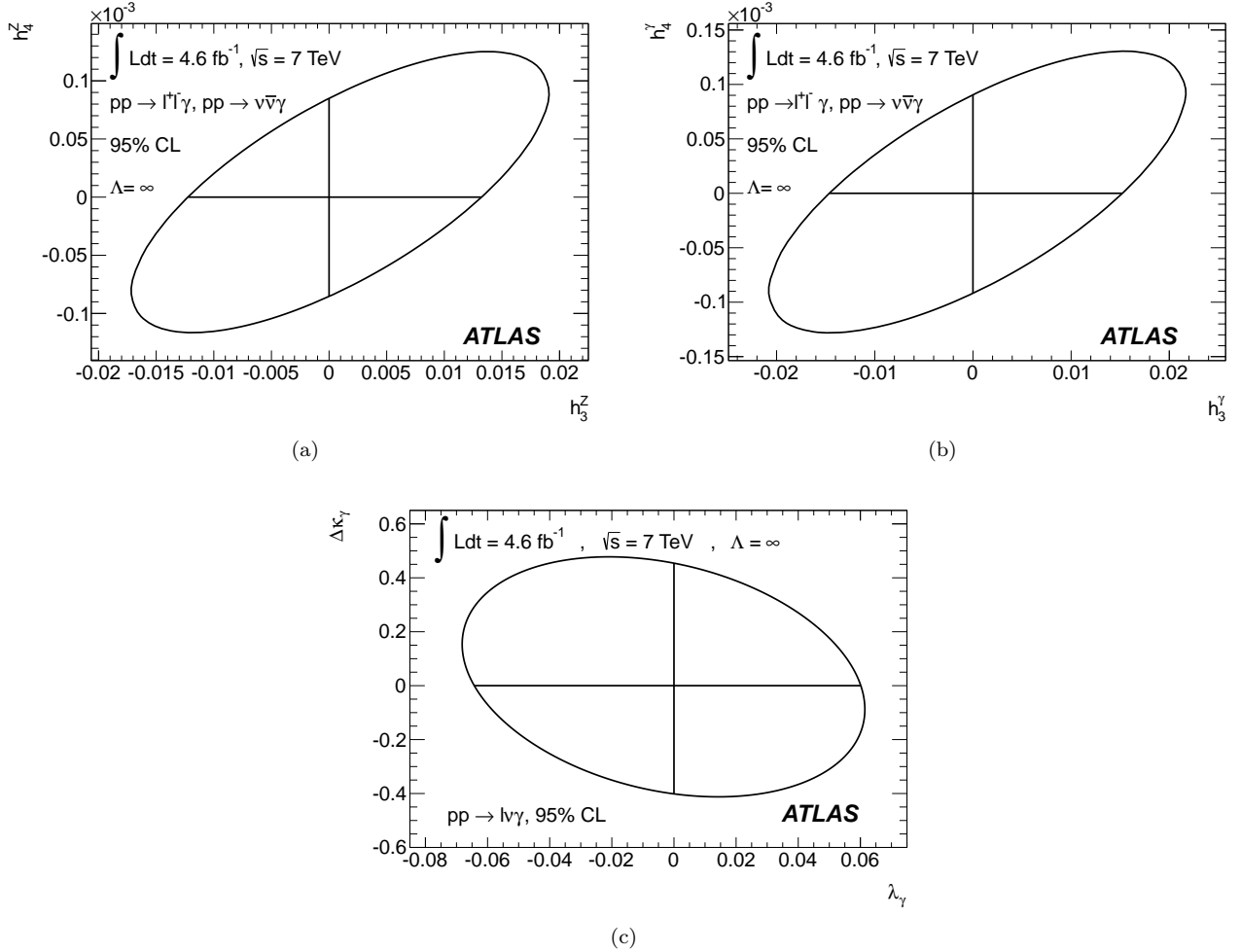
(a)

(b)

(c)

FIG. 10. Observed 95% CL limits shown in the two-parameter planes for pairs of anomalous couplings (a) h_3^Z and h_4^Z, (b) h_3^γ and h_4^γ, and (c) Δk_γ and λ_γ, corresponding to an infinite cut-off scale. The horizontal and vertical lines inside each contour correspond to the limits found in the one-parameter fit procedure, and the ellipses indicate the correlations between the one-parameter fits. Since all sensitivity of the measurement is contained in a single measurement of the $V\gamma$ cross sections in the high-E_T^γ regions, the likelihood ratio used to obtain the two-dimensional limits has one effective degree of freedom.

to about 35 GeV at $m_{a_T} = 800$ GeV. The data are scanned for $a_T \to W\gamma$ resonance signals using $m_T^{W\gamma}$ mass distributions constructed in 10 GeV steps from 275 to 800 GeV by linearly interpolating the signal lineshape fit parameters for the $m_T^{W\gamma}$ distributions.

C. Background modeling

The background estimations for the $V\gamma$ resonance searches use the techniques described in Sec.VI. The distributions of the SM predictions and the data after the event selection cuts are shown in Figs. 11(a) and (b) for $m_T^{e\nu\gamma}$ and $m_T^{\mu\nu\gamma}$, and in Figs. 12(a) and (b) for $m^{e^+e^-\gamma}$ and $m^{\mu^+\mu^-\gamma}$. All the mass distributions have a broad maximum at about 150 GeV. Since the search for a resonant structure on top of a peaking background is more

complex than on a falling distribution, the search is conducted only on the tails of the $m^{Z\gamma}$ and $m_T^{W\gamma}$ mass distributions for masses larger than 180 GeV.

A blinded search is conducted in the signal region. Agreement between the data and the Monte Carlo modeling is checked in two control regions for each final state. One control region is obtained by reversing the cut on the photon transverse energy ($E_T^\gamma < 40$ GeV), and the other one by reversing the cut (< 170 GeV) on the discriminating variable (i.e.: $m^{Z\gamma}$ for the $Z\gamma$ channel and $m_T^{W\gamma}$ for the $W\gamma$ channel). Good agreement is found between data and Monte Carlo samples in these control regions.

A probability density function is created to describe the SM background in the signal region. This approach has two advantages. The shape of the SM background is taken directly from the sidebands of the fit. The probability density function obtained is also less sensitive to statistical fluctuations in the tail than techniques rely-
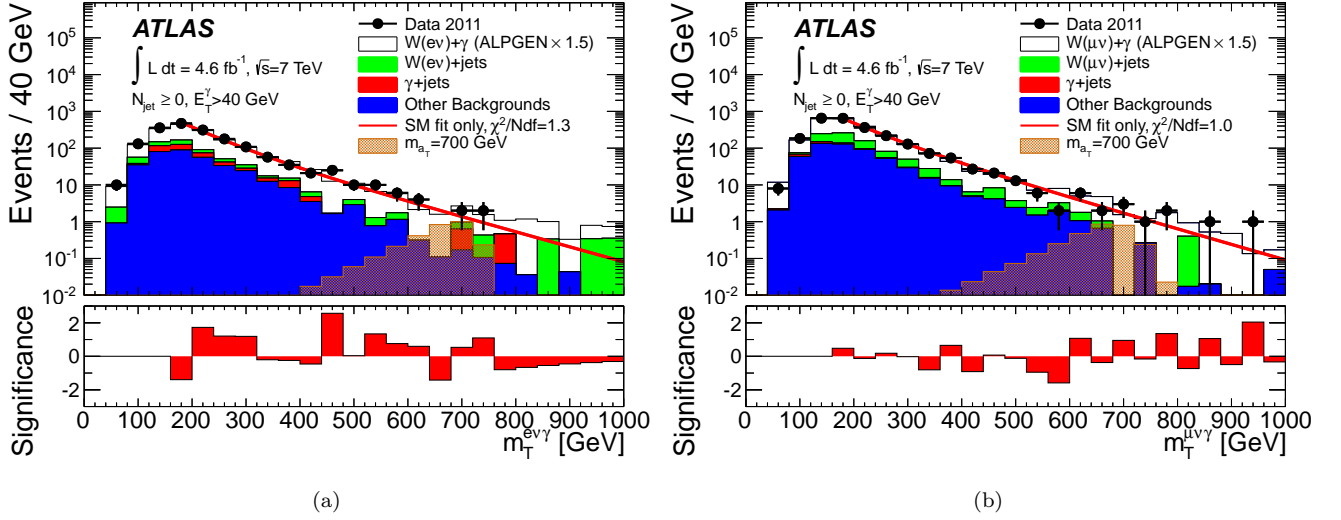
(a)

(b)

FIG. 11. Three-body transverse mass for (a) the $e\nu\gamma$ and (b) $\mu\nu\gamma$ final states. The background-only fit to the data is shown. The significance quoted is defined as $\frac{(D-B)}{\sqrt{B}}$, where D is the number of data events and B the number of predicted events by the fit in the bin considered. The background distributions for the expected $\ell\nu\gamma$ events are taken from the MC simulation (generated with ALPGEN) and normalized to the extracted number of $\ell\nu\gamma$ events. The signal near the limit at $m_{a_\mathrm{T}} = 700$ GeV is also shown.
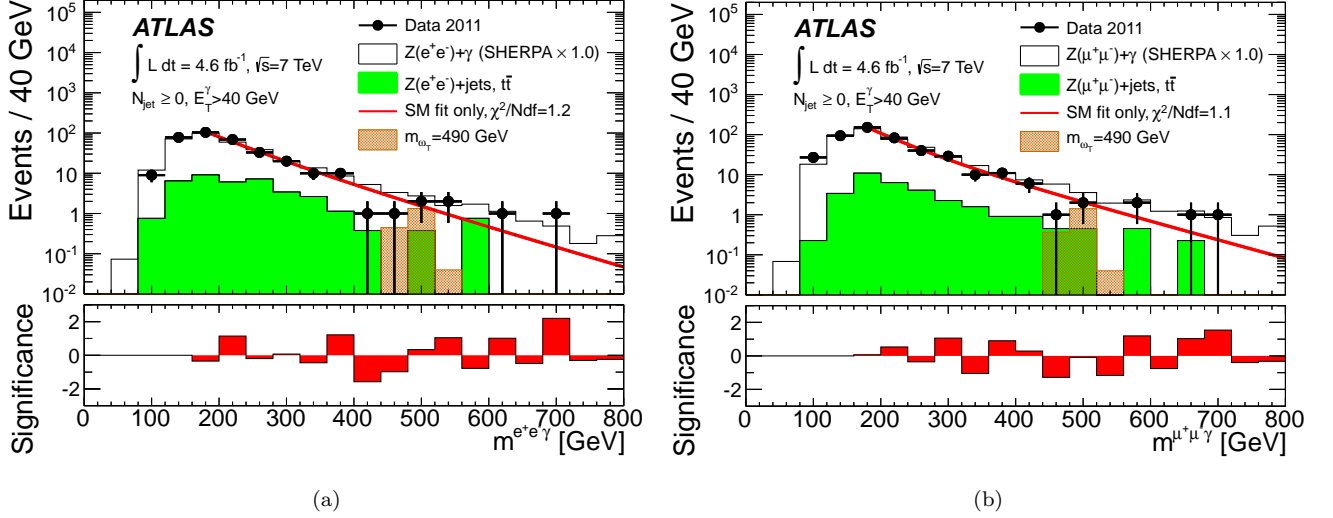

(a)

(b)

FIG. 12. Three-body invariant mass for (a) the $e^+e^-\gamma$ and (b) $\mu^+\mu^-\gamma$ final states. The background-only fit to the data is shown. The significance quoted is defined as $\frac{(D-B)}{\sqrt{B}}$, where D is the number of data events and B the number of predicted events by the fit in the bin considered. The background distributions for the expected $\ell^+\ell^-\gamma$ events are taken from the MC simulation (generated with SHERPA) and normalized to the extracted number of $\ell^+\ell^-\gamma$ events. The signal near the limit at $m_{\omega_\mathrm{T}} = 490$ GeV is also shown.

ing on Monte Carlo templates. For both the $W\gamma$ and $Z\gamma$ channels, the overall shape of the SM background in the signal region is due to the sum of components with different shapes. A double-exponential function provides the best model in the signal region:

$$f_{bkg} = N_{\mathrm{bkg}} \times (e^{\alpha_1 \cdot m} + e^{\alpha_2 \cdot m}). \qquad (8)$$

The background model is tested against a 1 fb^{-1} data sample that has been previously analyzed [8]. In addition it is tested with the nominal Monte Carlo distribution and the shape of the Monte Carlo distribution obtained by varying the background composition within systematic uncertainties. The double-exponential function is found to reproduce the shapes of all these distributions

properly, and is therefore used for the SM background estimation. The results of the unbinned fit to the data can be seen as the solid curve on each of the mass spectra in Figs. 11 and 12. The χ^2 per degree of freedom obtained for the background-only fit is close to unity for all the distributions.

D. Fit model and statistical methods

The normalization, N_{bkg}, and the two exponential coefficients, α_1 and α_2, in the SM background probability density function (Eq.(8)) are all free to vary. Another term takes into account a systematic uncertainty on the background shape. In order to ensure there are enough events in the sidebands on each side of the distribution, the SM background fit is performed in the range $[180, 800]$ GeV for the $m^{Z\gamma}$ distribution and the range $[180, 1000]$ GeV for the $m_{\text{T}}^{W\gamma}$ distribution. For both the data and the pseudo-data experiments, a maximum log-likelihood method is used to fit the SM background probability density function to the observed event distribution.

The parameters of the signal probability density functions are all fixed to their nominal values, except the normalization of the signal and two nuisance terms that account for systematic uncertainty on the signal event rate and resolution as explained below. The search is conducted by scanning the $m^{Z\gamma}$ and $m_{\text{T}}^{W\gamma}$ distributions every 5 GeV for the $Z\gamma$ channel and every 10 GeV for the $W\gamma$ channel using the signal template. The normalization of the signal is fit according to the equation

$$N_S = \sigma_{\text{Fid}} \times \epsilon_{\text{Reco}} \times \int \mathcal{L}dt \qquad (9)$$

where the factor σ_{Fid}, the signal fiducial cross section, is the only free parameter in this equation. The factor ϵ_{Reco} is the signal reconstruction efficiency[6], defined as the number of signal events passing the detector simulation and the full event selection divided by the number of events generated in the extended fiducial volume defined in Table IV but applying $E_{\text{T}}^{\gamma} > 40$ GeV. The factor ϵ_{Reco} accounts for the selection efficiency for signal events generated within the fiducial region. It includes, for example, effects due to the detector resolution on the lepton and photon transverse momentum and energies, and on the missing transverse energy. The normalization of the signal is determined simultaneously in the electron and muon samples for the combination. The results obtained are therefore less sensitive to statistical fluctuations in a given channel.

---

[6] ϵ_{Reco} contains both the acceptance $A_{W\gamma(Z\gamma)}$ and the correction factor $C_{W\gamma(Z\gamma)}$ in Eq.(1).

The parameter of interest used in this analysis is the fiducial cross section of an eventual new physics signal. σ_{Fid} is scanned to check the compatibility of the data with a background only or a signal plus background hypothesis.

The statistical test used is based on the Profile Likelihood Ratio [70] $L(\sigma_{\text{Fid}})$, to test different hypothesized values of σ_{Fid}. $L(\sigma_{\text{Fid}})$ is built from the likelihood function describing the probability density function of $m^{Z\gamma}$ and $m_T^{W\gamma}$ under a signal plus background hypothesis and the systematic uncertainties. It combines both electron and muon final states. The statistical tests are then performed on the $m_{\text{T}}^{W\gamma}$ and $m^{Z\gamma}$ distributions.

The data are interpreted using a modified frequentist approach (CL_s) [69] for setting limits. A fiducial cross section is claimed to be excluded at 95% CL when CL_s is less than 0.05. The probability of the background-only hypothesis, or p_0-value, is obtained using a frequentist approach. The latter gives the probability that the background fluctuates to the observed number of events or above.

E. Systematic uncertainties

Systematic uncertainties on the signal resonances are taken into account as nuisance parameters in the likelihood function used for the signal+background model. Two different effects are evaluated for each source of systematic uncertainty, one for the signal event rate and one for the resolution of the signal. Each systematic effect is investigated by propagating the corresponding uncertainty to the signal sample. These are computed separately for each of the simulated resonance mass points. The four categories of systematic uncertainties and their impacts on the resonant signals are summarized below for $m_{\omega_{\text{T}}} = 300$ GeV in the $Z\gamma$ channel and $m_{a_{\text{T}}} = 330$ GeV in the $W\gamma$ channel.

The systematic effects due to the photon isolation, identification, energy resolution and energy scale are considered. The impact of the photon geometric position in the detector on the peak resolution is also investigated to account for differences that could arise from changes of the photon pseudorapidity distribution in different theoretical models. The impact of this effect is minor and found to be about 0.2 GeV. The systematic uncertainties due to the photon reconstruction and identification contribute most to the systematic uncertainties on the signal. The total effect on the event rate is measured to be 5.7% in all the channels, and contributes about 0.5 GeV to the systematic uncertainty on the resolution of the central mass of the resonance.

The systematic effects due to the electron energy resolution and electron energy scale are treated as fully correlated with the photon energy scale and resolution in the final states containing electrons ($e^+e^-\gamma$ and $e\nu\gamma$). The effects of the muon energy scale and muon energy resolu-

tion, lepton identification and trigger efficiency are also investigated. The total effect of the lepton reconstruction and identification on the signal event rate is about 1.8% in the muon channels, and about 1.2% in the electron channels. The effect on the peak resolution is only about 0.2 GeV.

Systematic effects due to the jet energy scale and resolution and the calibration of the missing transverse energy impact only the $W\gamma$ channel. These are found to cause uncertainties in the event rate of about 1% and on the peak resolution of about 1 GeV.

Finally there is a systematic uncertainty on the resonance production rate due to the 3.9% uncertainty on the integrated luminosity [12].

The effects of all the systematic uncertainties are combined in quadrature. The total systematic uncertainty on the event rate is found to be approximately 7% for all the mass points in the two channels. The systematic uncertainty on the peak resolution is found to be approximately 1(2) GeV for the $Z\gamma$ channel at $m_{\omega_T} = 300(650)$ GeV and 1.5(3) GeV at $m_{a_T} = 330(800)$ GeV in the $W\gamma$ channel.

Since the SM backgrounds are determined using a sideband fit to the data, uncertainties in the detector resolution and physics object reconstruction or identification have a negligible effect on the background in this analysis. However, a systematic effect from the background modeling is investigated. The method considered consists of generating background-only pseudo-experiments, and fitting each pseudo-dataset with the signal+background model to measure a residual signal strength. For each final state, one thousand background-only pseudo-experiment samples are generated with the expected number of SM background events. For each pseudo-experiment, the signal+background model is fit in steps of $\Delta m_{\omega_T} = 1$ GeV for the $Z\gamma$ channel and $\Delta m_{a_T} = 1$ GeV for the $W\gamma$ channel to measure a residual signal strength. For each mass point the mean value of the fitted strength is measured. If there is no bias in the fit model, this distribution should be centered exactly at 0. Since this is not the case, the systematic uncertainty on the background shape is taken to be the difference between 0 and the most discrepant fitted strength obtained anywhere in the mass range, augmented by the 1σ uncertainty on that fitted strength. The size of this effect is measured to be 0.2 fb for the $Z\gamma$ analysis. This represents about 5% on the limit at low masses and up to 20% at high masses. It is measured to be 1.2 fb for the $W\gamma$ analysis, which represents about 6% on the limit at low masses and up to 25% at high masses. This dominant systematic effect is taken into account in the fit model, by allowing the backgrounds to fluctuate like the signal, but constrained by these values.

Finally, systematic effects are evaluated on the signal theoretical cross sections due to the limited knowledge of the proton PDFs and the energy scale of the process. These are computed by comparing predictions of the nominal LO PDF set MRST2007 [25] to the 68%

CL error set of the MSTW2008 [71] PDF sets using the LHAPDF framework [72]. The deviation of the predictions from the central value are added in quadrature and taken to be the size of the uncertainty. The magnitude of the PDF uncertainties on the cross sections is about 3% for the $Z\gamma$ channel and 5% for the $W\gamma$ channel.

F. Results

The reconstruction efficiencies, ϵ_{Reco}, and the expected and observed limits on the fiducial cross section times branching ratio for the $\omega_T \to Z\gamma$ and $a_T \to W\gamma$ resonance signals are summarized in Table XIV and Table XV, respectively. The efficiencies are relatively flat versus the mass of the resonances.

The search is used to set 95% CL limits on the production of techni-mesons. Figure 13 (a) shows the expected and observed limits obtained for $\omega_T \to Z\gamma$. The two largest deviations are observed at $m_{\omega_T} = 465$ GeV where a downward fluctuation is seen with a p-value of $p_0 \approx 0.01$ or a local significance of 2.7σ and at $m_{\omega_T} = 205$ GeV where an upward fluctuation is seen with a p-value of $p_0 \approx 0.02$ or a local significance of 2.4σ. In the $Z\gamma$ channel the expected mass limit on the LSTC production of ω_T is $m_{\omega_T} = 483$ GeV, while the observed limit is $m_{\omega_T} = 494$ GeV.

Figure 13 (b) shows the expected and observed limits obtained for $a_T \to W\gamma$. The largest deviation is observed at $m_{a_T} = 285$ GeV where an upward fluctuation is recorded with a p-value of $p_0 \approx 0.05$ or a local significance of 2.0σ. In the $W\gamma$ channel the expected mass limit on the LSTC production of a_T is $m_{a_T} = 619$ GeV, while the observed limit is $m_{a_T} = 703$ GeV.

These results are similar to those from previous searches for LSTC [64, 65] in other channels. They are more stringent than previous limits from vector resonance searches [10] in the $Z\gamma$ final state and they are the first limits to be set from single resonance searches in the $W\gamma$ channel.

m_{ω_T} [GeV]	ϵ_{Reco}	Expected (fb)	Observed (fb)
200	0.52 ± 0.05	$4.3^{+1.9}_{-1.3}$	8.3
300	0.54 ± 0.05	$2.6^{+1.2}_{-0.8}$	2.2
400	0.54 ± 0.05	$1.8^{+0.9}_{-0.6}$	2.2
500	0.55 ± 0.05	$1.4^{+0.7}_{-0.5}$	1.5
650	0.57 ± 0.05	$1.0^{+0.6}_{-0.3}$	0.9

TABLE XIV. Reconstruction efficiency in the extended fiducial volume as defined in Table IV but for $E_T^\gamma > 40$ GeV. The expected and observed 95% CL upper limits for the different signal points in the $Z\gamma$ final states are given.
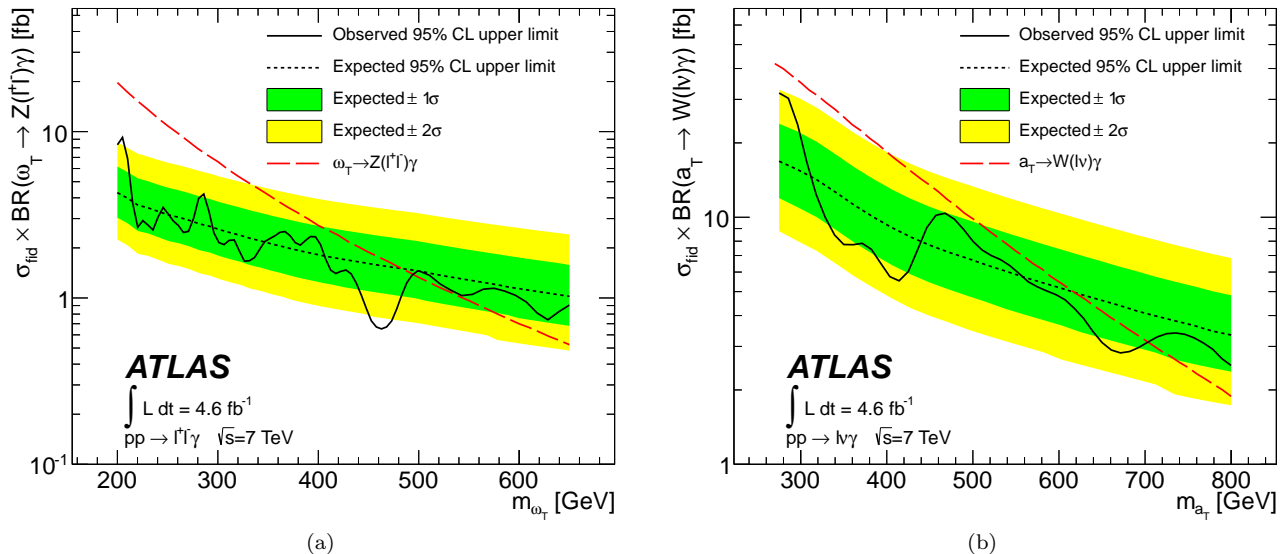
FIG. 13. 95% CL limits on narrow vector resonance production obtained using $\mathcal{L} = 4.6$ fb^{-1} of data for (a) the $pp \to \ell^+\ell^-\gamma$ final state and for (b) the $pp \to \ell\nu\gamma$ final state. The parameterization of LSTC [62, 63] used to benchmark the observed limit is obtained using $m_{\rho_{\mathrm{T}}} = m_W - m_{\pi_{\mathrm{T}}}$.

$m_{a_{\mathrm{T}}}$ [GeV]	ϵ_{Reco}	Expected (fb)	Observed (fb)
275	0.45 ± 0.04	$16.8^{+7.1}_{-4.9}$	31.9
330	0.43 ± 0.04	$13.4^{+5.7}_{-3.9}$	9.8
385	0.42 ± 0.04	$10.0^{+4.3}_{-2.9}$	7.2
440	0.41 ± 0.04	$8.0^{+3.4}_{-2.3}$	8.1
490	0.41 ± 0.04	$6.9^{+3.0}_{-2.0}$	8.9
550	0.40 ± 0.04	$5.9^{+2.5}_{-1.7}$	6.1
800	0.39 ± 0.04	$3.3^{+1.5}_{-0.9}$	2.5

TABLE XV. Reconstruction efficiency in the extended fiducial volume as defined in Table IV, but for $E_{\mathrm{T}}^{\gamma} > 40$ GeV. The expected and observed 95% CL upper limits are given for the different signal points in the $W\gamma$ final states.

XI. SUMMARY

The production of $W\gamma$ and $Z\gamma$ boson pairs in 7 TeV pp collisions is studied using 4.6 fb^{-1} of data collected with the ATLAS detector. The measurements are made using the leptonic decays of the W and Z bosons ($W(e\nu, \mu\nu)$ and $Z(e^+e^-, \mu^+\mu^-, \nu\bar{\nu})$) with associated high-energy isolated photons.

The results are compared to SM predictions using the NLO parton-level generator MCFM. In general, the NLO SM predictions for the exclusive $W\gamma$ and $Z\gamma$ production cross sections agree with measurements. However, as the photon E_{T}^{γ} threshold is raised for inclusive $pp \to \ell\nu\gamma$ production, the associated jet multiplicity increases and there are disagreements with the NLO predictions, which do not include multiple quark/gluon emission. The measurements are also compared to LO MC generators (AL-PGEN or SHERPA) with multiple quark/gluon emission in the matrix element calculations. These LO MC predictions reproduce the shape of the photon E_{T}^{γ} spectrum and the kinematic properties of the leptons and jets in the $W\gamma$ and $Z\gamma$ measurements.

The measurements of exclusive $W\gamma$ and $Z\gamma$ production with $E_{\mathrm{T}}^{\gamma} > 100$ GeV are used to constrain anomalous triple-gauge-boson couplings (λ_γ, $\Delta\kappa_\gamma$, h_3^V and h_4^V). They are also used to search for narrow resonances in the $V+\gamma$ final state with $E_{\mathrm{T}}^{\gamma} > 40$ GeV and compared to Low Scale Technicolor models. No evidence for physics beyond the SM is observed. The limits obtained from this study of anomalous triple-gauge-boson couplings are more stringent than previous LHC and Tevatron results. The results of the vector resonance search are the first ones reported for the study of the $W\gamma$ final state and the most stringent in the $Z\gamma$ final state. Using the LSTC benchmark model, the production of a_{T} is excluded up to $m_{a_{\mathrm{T}}} = 703$ GeV in the $W\gamma$ mode and the production of ω_{T} is excluded up to $m_{\omega_{\mathrm{T}}} = 494$ GeV in the $Z\gamma$ channel.

XII. ACKNOWLEDGEMENTS

[1] S. Weinberg, Phys. Rev. D **19**, 1277 (1979).
[2] L. Susskind, Phys. Rev. D **20**, 2619 (1979).
[3] ATLAS Collaboration, JINST **3**, S08003 (2008).
[4] F. Abe *et al.*, CDF Collaboration, Phys. Rev. D **107**, 051802 (2011).
[5] V. Abazov *et al.*, D0 Collaboration, Phys. Rev. Lett. **100**, 241805 (2008) .
[6] V. Abazov *et al.*, D0 Collaboration, Phys. Rev. D **85**, 052001 (2012).
[7] ATLAS Collaboration, JHEP **09**, 072 (2011).
[8] ATLAS Collaboration, Phys. Lett. B **717**, 49 (2012).
[9] CMS Collaboration, Phys. Lett. B **701**, 535 (2011).
[10] V. Abazov *et al.*, D0 Collaboration, Phys. Lett. B **671**, 349 (2009).
[11] The LEP Collaborations: ALEPH, DELPHI, L3, OPAL, and the LEP Electroweak Working Group. `arXiv:0612034`.
[12] ATLAS Collaboration, Eur. Phys. J. C **71**, 1630 (2011).
[13] ATLAS Collaboration, ATLAS-CONF-2011-116, (2011). http://cdsweb.cern.ch/record/1376384.
[14] ATLAS Collaboration, Eur. Phys. J. C **70**, 823 (2010).
[15] S. Agostinelli *et al.*, Nucl. Instrum. Meth. A **506**, 250 (2003).
[16] M. L. Mangano *et al.*, JHEP **0307**, 001 (2003).
[17] G. Corcella *et al.*, JHEP **0101**, 010 (2001).
[18] J. M. Butterworth, J. R. Forshaw, and M. H. Seymour, Z. Phys. C **72**, 637 (1996).
[19] T. Gleisberg *et al.*, JHEP **0402**, 056 (2004).
[20] J. Pumplin *et al.*, JHEP **0207**, 012 (2002).
[21] P. M. Nadolsky *et al.*, Phys. Rev. D **78**, 013004 (2008).
[22] P. Golonka and Z. Was, Eur. Phys. J. C **45**, 97 (2006).
[23] M. Schonherr and F. Krauss, JHEP **0812**, 018 (2008). P. Golonka and Z. Was, Eur. Phys. J. C **45**, 97 (2006).
[24] T. Sjöstrand, S. Mrenna, and P. Z. Skands, JHEP **05**, 026 (2006).
[25] A. Sherstnev and R.S. Thorne, Eur. Phys. J. C **55**, 553 (2008).
[26] N. Davidson, G. Nanava, T. Przedzinski, E. Richter-Was, and Z. Was, (2010) `arXiv:1002.0543`.
[27] S. Frixione, P. Nason, and C. Oleari, JHEP **11**, 070 (2007).
[28] S. Frixione and B. R. Webber, JHEP **06**, 029 (2002).
[29] S. Frixione, F. Stoeckli, P. Torrielli, and B. R. Webber, JHEP **01**, 053 (2011).
[30] H. -L. Lai, M. Guzzi, J. Huston, Z. Li, P. M. Nadolsky, J. Pumplin and C. -P. Yuan, Phys. Rev. D **82**, 074024 (2010).
[31] R. Hamberg, W. L. van Neerven, and T. Matsuura, Nucl. Phys. B **359**, 343 (1991); Erratum-ibid. B**644**, 403 (2002).
[32] C. Anastasiou, L. J. Dixon, K. Melnikov, and F. Petriello, Phys. Rev. D **69**, 094008 (2004).
[33] R. Bonciani, S. Catani, M. L. Mangano, and P. Nason, Nucl. Phys. B**529**, 424 (1998).
[34] S. Moch and P. Uwer, Phys. Rev. D **78**, 034003 (2008).
[35] ATLAS Collaboration, Eur. Phys. J. C. **72**, 1909 (2012).
[36] ATLAS Collaboration, Phys. Rev. D **83**, 052005 (2011).
[37] ATLAS Collaboration, ATLAS-CONF-2012-123, (2012). http://cdsweb.cern.ch/record/1473426
[38] ATLAS Collaboration, JHEP **1012**, 060 (2010).
[39] M. Cacciari, G. P. Salam, and G. Soyez, JHEP **04**, 063 (2008).
[40] ATLAS Collaboration, Eur. Phys. J. C. **72**, 1844 (2012).
[41] ATLAS Collaboration, Phys. Rev. D**85**, 092014 (2012).
[42] ATLAS Collaboration, Phys. Lett. B, **706**, 150 (2011).
[43] U. Baur and E. L. Berger, Phys. Rev. D **41**, 1476 (1990).
[44] U. Baur, T. Han, and J. Ohnemus, Phys. Rev. D **48**, 5140 (1993).
[45] ATLAS Collaboration, Phys. Lett. B **698**, 325 (2011).
[46] G. D'Agostini, Nucl. Instrum. Methods Phys. Res., Sect. A **362**, 487 (1995).
[47] J. M. Campbell, R. Ellis and C. Williams, JHEP **1107**, 018 (2011).
[48] L. Bourhis, M. Fontannaz. and J. P. Guillet, Eur. Phys. J. C **2**, 529 (1998).
[49] I. W. Stewart and F. J. Tackmann, Phys. Rev. D **85**, 034011 (2012).
[50] J. Alwall, M. Herquet, F. Maltoni, O. Mattalaer and T. Stelzer, JHEP **06**, 128 (2011).
[51] U. Baur and E. L. Berger, Phys. Rev. D **47**, 4889 (1993).
[52] K. Hagiwara, S. Ishihara, R. Szalapski, and D. Zeppenfeld, Phys. Lett. B **283**, 353 (1992).
[53] K. Hagiwara, S. Ishihara, R. Szalapski, and D. Zeppenfeld, Phys. Rev. D **48**, 2182 (1993).
[54] G. Gounaris *et al.*, Physics at LEP2, vol. 1, 525-576, CERN-96-01-V-1 `arXiv:hep-ph/9601233`.

[55] V. Abazov *et al.*, D0 Collaboration, Phys. Lett. B **718**, 451 (2012).

[56] ATLAS Collaboration, Phys. Lett. B **716**, 1 (2012).

[57] CMS Collaboration, Phys. Lett. B **716**, 30 (2012).

[58] E. Eichten, K. Lane, and A. Martin, `arXiv:hep-ph/1210.5462`.

[59] D. D. Dietrich, F. Sannino, and K. Tuominen, Phys. Rev. D **72**, 055001 (2005).

[60] R. Foadi, M. T. Frandsen, and F. Sannino, `arXiv:hep-ph/1211.1083`.

[61] K. Lane and S. Mrenna, Phys. Rev. D **67**, 115011 (2003).

[62] K. D. Lane, Phys. Rev. D **60**, 075007 (1999).

[63] E. Eichten and K. Lane, Phys. Lett. B **669**, 235 (2008).

[64] ATLAS Collaboration, (2012) `arXiv:1209.2535`.

[65] CMS Collaboration, (2012) `arXiv:1206.0433`.

[66] M. J. Oreglia, Ph.D. Thesis, SLAC-R-236 (1980), Appendix D., SLAC.

[67] J. E. Gaiser, Ph.D. Thesis, SLAC-R-255 (1982), Appendix F., SLAC.

[68] T. Skwarnickia, Ph.D. Thesis, F31-86-02 (1986), Appendix E., DESY.

[69] A. L. Read, J. Phys. G **28**, 26932704 (2002).

[70] G. Cowan, K. Cranmer, E. Gross, and O. Vitells, Eur. Phys. J. C **71**, 1554 (2011).

[71] A. D. Martin, W. J. Stirling, R. S. Thorne, and G. Watt, Eur. Phys. J. C **63**, 189 (2009).

[72] M. R. Whalley, D. Bourilkov and R. C. Group, `arXiv:hep-ph/0508110`.

The ATLAS Collaboration

G. Aad[48], T. Abajyan[21], B. Abbott[111], J. Abdallah[12], S. Abdel Khalek[115], A.A. Abdelalim[49], O. Abdinov[11], R. Aben[105], B. Abi[112], M. Abolins[88], O.S. AbouZeid[158], H. Abramowicz[153], H. Abreu[136], B.S. Acharya[164a,164b,a], L. Adamczyk[38], D.L. Adams[25], T.N. Addy[56], J. Adelman[176], S. Adomeit[98], P. Adragna[75], T. Adye[129], S. Aefsky[23], J.A. Aguilar-Saavedra[124b,b], M. Agustoni[17], S.P. Ahlen[22], F. Ahles[48], A. Ahmad[148], M. Ahsan[41], G. Aielli[133a,133b], T.P.A. Åkesson[79], G. Akimoto[155], A.V. Akimov[94], M.A. Alam[76], J. Albert[169], S. Albrand[55], M. Aleksa[30], I.N. Aleksandrov[64], F. Alessandria[89a], C. Alexa[26a], G. Alexander[153], G. Alexandre[49], T. Alexopoulos[10], M. Alhroob[164a,164c], M. Aliev[16], G. Alimonti[89a], J. Alison[120], B.M.M. Allbrooke[18], L.J. Allison[71], P.P. Allport[73], S.E. Allwood-Spiers[53], J. Almond[82], A. Aloisio[102a,102b], R. Alon[172], A. Alonso[36], F. Alonso[70], A. Altheimer[35], B. Alvarez Gonzalez[88], M.G. Alviggi[102a,102b], K. Amako[65], C. Amelung[23], V.V. Ammosov[128,∗], S.P. Amor Dos Santos[124a], A. Amorim[124a,c], S. Amoroso[48], N. Amram[153], C. Anastopoulos[30], L.S. Ancu[17], N. Andari[115], T. Andeen[35], C.F. Anders[58b], G. Anders[58a], K.J. Anderson[31], A. Andreazza[89a,89b], V. Andrei[58a], M-L. Andrieux[55], X.S. Anduaga[70], S. Angelidakis[9], P. Anger[44], A. Angerami[35], F. Anghinolfi[30], A. Anisenkov[107], N. Anjos[124a], A. Annovi[47], A. Antonaki[9], M. Antonelli[47], A. Antonov[96], J. Antos[144b], F. Anulli[132a], M. Aoki[101], S. Aoun[83], L. Aperio Bella[5], R. Apolle[118,d], G. Arabidze[88], I. Aracena[143], Y. Arai[65], A.T.H. Arce[45], S. Arfaoui[148], J-F. Arguin[93], S. Argyropoulos[42], E. Arik[19a,∗], M. Arik[19a], A.J. Armbruster[87], O. Arnaez[81], V. Arnal[80], A. Artamonov[95], G. Artoni[132a,132b], D. Arutinov[21], S. Asai[155], S. Ask[28], B. Åsman[146a,146b], D. Asner[29], L. Asquith[6], K. Assamagan[25], A. Astbury[169], M. Atkinson[165], B. Aubert[5], B. Auerbach[6], E. Auge[115], K. Augsten[126], M. Aurousseau[145a], G. Avolio[30], D. Axen[168], G. Azuelos[93,e], Y. Azuma[155], M.A. Baak[30], G. Baccaglioni[89a], C. Bacci[134a,134b], A.M. Bach[15], H. Bachacou[136], K. Bachas[154], M. Backes[49], M. Backhaus[21], J. Backus Mayes[143], E. Badescu[26a], P. Bagnaia[132a,132b], Y. Bai[33a], D.C. Bailey[158], T. Bain[35], J.T. Baines[129], O.K. Baker[176], S. Baker[77], P. Balek[127], F. Balli[136], E. Banas[39], P. Banerjee[93], Sw. Banerjee[173], D. Banfi[30], A. Bangert[150], V. Bansal[169], H.S. Bansil[18], L. Barak[172], S.P. Baranov[94], T. Barber[48], E.L. Barberio[86], D. Barberis[50a,50b], M. Barbero[83], D.Y. Bardin[64], T. Barillari[99], M. Barisonzi[175], T. Barklow[143], N. Barlow[28], B.M. Barnett[129], R.M. Barnett[15], A. Baroncelli[134a], G. Barone[49], A.J. Barr[118], F. Barreiro[80], J. Barreiro Guimarães da Costa[57], R. Bartoldus[143], A.E. Barton[71], V. Bartsch[149], A. Basye[165], R.L. Bates[53], L. Batkova[144a], J.R. Batley[28], A. Battaglia[17], M. Battistin[30], F. Bauer[136], H.S. Bawa[143,f], S. Beale[98], T. Beau[78], P.H. Beauchemin[161], R. Beccherle[50a], P. Bechtle[21], H.P. Beck[17], K. Becker[175], S. Becker[98], M. Beckingham[138], K.H. Becks[175], A.J. Beddall[19c], A. Beddall[19c], S. Bedikian[176], V.A. Bednyakov[64], C.P. Bee[83], L.J. Beemster[105], M. Begel[25], S. Behar Harpaz[152], P.K. Behera[62], M. Beimforde[99], C. Belanger-Champagne[85], P.J. Bell[49], W.H. Bell[49], G. Bella[153], L. Bellagamba[20a], M. Bellomo[30], A. Belloni[57], O. Beloborodova[107,g], K. Belotskiy[96], O. Beltramello[30], O. Benary[153], D. Benchekroun[135a], K. Bendtz[146a,146b], N. Benekos[165], Y. Benhammou[153], E. Benhar Noccioli[49], J.A. Benitez Garcia[159b], D.P. Benjamin[45], M. Benoit[115], J.R. Bensinger[23], K. Benslama[130], S. Bentvelsen[105], D. Berge[30], E. Bergeaas Kuutmann[42], N. Berger[5], F. Berghaus[169], E. Berglund[105], J. Beringer[15], P. Bernat[77], R. Bernhard[48], C. Bernius[25], T. Berry[76], C. Bertella[83], A. Bertin[20a,20b], F. Bertolucci[122a,122b], M.I. Besana[89a,89b], G.J. Besjes[104], N. Besson[136], S. Bethke[99], W. Bhimji[46], R.M. Bianchi[30], L. Bianchini[23], M. Bianco[72a,72b], O. Biebel[98], S.P. Bieniek[77], K. Bierwagen[54], J. Biesiada[15], M. Biglietti[134a], H. Bilokon[47], M. Bindi[20a,20b], S. Binet[115], A. Bingul[19c], C. Bini[132a,132b], C. Biscarat[178], B. Bittner[99], C.W. Black[150], J.E. Black[143], K.M. Black[22], R.E. Blair[6], J.-B. Blanchard[136], T. Blazek[144a], I. Bloch[42], C. Blocker[23], J. Blocki[39], W. Blum[81], U. Blumenschein[54], G.J. Bobbink[105], V.S. Bobrovnikov[107], S.S. Bocchetta[79], A. Bocci[45], C.R. Boddy[118], M. Boehler[48], J. Boek[175], T.T. Boek[175], N. Boelaert[36], J.A. Bogaerts[30], A. Bogdanchikov[107], A. Bogouch[90,∗], C. Bohm[146a], J. Bohm[125], V. Boisvert[76], T. Bold[38], V. Boldea[26a], N.M. Bolnet[136], M. Bomben[78], M. Bona[75], M. Boonekamp[136], S. Bordoni[78], C. Borer[17], A. Borisov[128], G. Borissov[71], I. Borjanovic[13a], M. Borri[82], S. Borroni[42], J. Bortfeldt[98], V. Bortolotto[134a,134b], K. Bos[105], D. Boscherini[20a], M. Bosman[12], H. Boterenbrood[105], J. Bouchami[93], J. Boudreau[123], E.V. Bouhova-Thacker[71], D. Boumediene[34], C. Bourdarios[115], N. Bousson[83], A. Boveia[31], J. Boyd[30], I.R. Boyko[64], I. Bozovic-Jelisavcic[13b], J. Bracinik[18], P. Branchini[134a], A. Brandt[8], G. Brandt[118], O. Brandt[54], U. Bratzler[156], B. Brau[84], J.E. Brau[114], H.M. Braun[175,∗], S.F. Brazzale[164a,164c], B. Brelier[158], J. Bremer[30], K. Brendlinger[120], R. Brenner[166], S. Bressler[172], T.M. Bristow[145b], D. Britton[53], F.M. Brochu[28], I. Brock[21], R. Brock[88], F. Broggi[89a], C. Bromberg[88], J. Bronner[99], G. Brooijmans[35], T. Brooks[76], W.K. Brooks[32b], G. Brown[82], P.A. Bruckman de Renstrom[39], D. Bruncko[144b], R. Bruneliere[48], S. Brunet[60], A. Bruni[20a], G. Bruni[20a], M. Bruschi[20a], L. Bryngemark[79], T. Buanes[14], Q. Buat[55], F. Bucci[49], J. Buchanan[118], P. Buchholz[141], R.M. Buckingham[118], A.G. Buckley[46], S.I. Buda[26a], I.A. Budagov[64], B. Budick[108], L. Bugge[117], O. Bulekov[96], A.C. Bundock[73], M. Bunse[43], T. Buran[117,∗], H. Burckhart[30], S. Burdin[73], T. Burgess[14], S. Burke[129], E. Busato[34], V. Büscher[81], P. Bussey[53], C.P. Buszello[166], B. Butler[143], J.M. Butler[22], C.M. Buttar[53], J.M. Butterworth[77], W. Buttinger[28], M. Byszewski[30], S. Cabrera Urbán[167], D. Caforio[20a,20b], O. Cakir[4a], P. Calafiura[15], G. Calderini[78], P. Calfayan[98], R. Calkins[106], L.P. Caloba[24a], R. Caloi[132a,132b], D. Calvet[34], S. Calvet[34], R. Camacho Toro[34], P. Camarri[133a,133b], D. Cameron[117], L.M. Caminada[15], R. Caminal Armadans[12], S. Campana[30], M. Campanelli[77],

V. Canale[102a,102b], F. Canelli[31], A. Canepa[159a], J. Cantero[80], R. Cantrill[76], M.D.M. Capeans Garrido[30],
I. Caprini[26a], M. Caprini[26a], D. Capriotti[99], M. Capua[37a,37b], R. Caputo[81], R. Cardarelli[133a], T. Carli[30],
G. Carlino[102a], L. Carminati[89a,89b], S. Caron[104], E. Carquin[32b], G.D. Carrillo-Montoya[145b], A.A. Carter[75],
J.R. Carter[28], J. Carvalho[124a,h], D. Casadei[108], M.P. Casado[12], M. Cascella[122a,122b], C. Caso[50a,50b,*],
E. Castaneda-Miranda[173], V. Castillo Gimenez[167], N.F. Castro[124a], G. Cataldi[72a], P. Catastini[57], A. Catinaccio[30],
J.R. Catmore[30], A. Cattai[30], G. Cattani[133a,133b], S. Caughron[88], V. Cavaliere[165], P. Cavalleri[78], D. Cavalli[89a],
M. Cavalli-Sforza[12], V. Cavasinni[122a,122b], F. Ceradini[134a,134b], A.S. Cerqueira[24b], A. Cerri[15], L. Cerrito[75],
F. Cerutti[15], S.A. Cetin[19b], A. Chafaq[135a], D. Chakraborty[106], I. Chalupkova[127], K. Chan[3], P. Chang[165],
B. Chapleau[85], J.D. Chapman[28], J.W. Chapman[87], D.G. Charlton[18], V. Chavda[82], C.A. Chavez Barajas[30],
S. Cheatham[85], S. Chekanov[6], S.V. Chekulaev[159a], G.A. Chelkov[64], M.A. Chelstowska[104], C. Chen[63], H. Chen[25],
S. Chen[33c], X. Chen[173], Y. Chen[35], Y. Cheng[31], A. Cheplakov[64], R. Cherkaoui El Moursli[135e], V. Chernyatin[25],
E. Cheu[7], S.L. Cheung[158], L. Chevalier[136], G. Chiefari[102a,102b], L. Chikovani[51a,*], J.T. Childers[30], A. Chilingarov[71],
G. Chiodini[72a], A.S. Chisholm[18], R.T. Chislett[77], A. Chitan[26a], M.V. Chizhov[64], G. Choudalakis[31], S. Chouridou[9],
I.A. Christidi[77], A. Christov[48], D. Chromek-Burckhart[30], M.L. Chu[151], J. Chudoba[125], G. Ciapetti[132a,132b],
A.K. Ciftci[4a], R. Ciftci[4a], D. Cinca[34], V. Cindro[74], A. Ciocio[15], M. Cirilli[87], P. Cirkovic[13b], Z.H. Citron[172],
M. Citterio[89a], M. Ciubancan[26a], A. Clark[49], P.J. Clark[46], R.N. Clarke[15], W. Cleland[123], J.C. Clemens[83],
B. Clement[55], C. Clement[146a,146b], Y. Coadou[83], M. Cobal[164a,164c], A. Coccaro[138], J. Cochran[63], L. Coffey[23],
J.G. Cogan[143], J. Coggeshall[165], J. Colas[5], S. Cole[106], A.P. Colijn[105], N.J. Collins[18], C. Collins-Tooth[53], J. Collot[55],
T. Colombo[119a,119b], G. Colon[84], G. Compostella[99], P. Conde Muiño[124a], E. Coniavitis[166], M.C. Conidi[12],
S.M. Consonni[89a,89b], V. Consorti[48], S. Constantinescu[26a], C. Conta[119a,119b], G. Conti[57], F. Conventi[102a,i],
M. Cooke[15], B.D. Cooper[77], A.M. Cooper-Sarkar[118], K. Copic[15], T. Cornelissen[175], M. Corradi[20a], F. Corriveau[85,j],
A. Corso-Radu[163], A. Cortes-Gonzalez[165], G. Cortiana[99], G. Costa[89a], M.J. Costa[167], D. Costanzo[139], D. Côté[30],
G. Cottin[32a], L. Courneyea[169], G. Cowan[76], B.E. Cox[82], K. Cranmer[108], S. Crépé-Renaudin[55], F. Crescioli[78],
M. Cristinziani[21], G. Crosetti[37a,37b], C.-M. Cuciuc[26a], C. Cuenca Almenar[176], T. Cuhadar Donszelmann[139],
J. Cummings[176], M. Curatolo[47], C.J. Curtis[18], C. Cuthbert[150], P. Cwetanski[60], H. Czirr[141], P. Czodrowski[44],
Z. Czyczula[176], S. D'Auria[53], M. D'Onofrio[73], A. D'Orazio[132a,132b], M.J. Da Cunha Sargedas De Sousa[124a],
C. Da Via[82], W. Dabrowski[38], A. Dafinca[118], T. Dai[87], F. Dallaire[93], C. Dallapiccola[84], M. Dam[36],
D.S. Damiani[137], H.O. Danielsson[30], V. Dao[104], G. Darbo[50a], G.L. Darlea[26b], J.A. Dassoulas[42], W. Davey[21],
T. Davidek[127], N. Davidson[86], R. Davidson[71], E. Davies[118,d], M. Davies[93], O. Davignon[78], A.R. Davison[77],
Y. Davygora[58a], E. Dawe[142], I. Dawson[139], R.K. Daya-Ishmukhametova[23], K. De[8], R. de Asmundis[102a],
S. De Castro[20a,20b], S. De Cecco[78], J. de Graat[98], N. De Groot[104], P. de Jong[105], C. De La Taille[115],
H. De la Torre[80], F. De Lorenzi[63], L. De Nooij[105], D. De Pedis[132a], A. De Salvo[132a], U. De Sanctis[164a,164c],
A. De Santo[149], J.B. De Vivie De Regie[115], G. De Zorzi[132a,132b], W.J. Dearnaley[71], R. Debbe[25], C. Debenedetti[46],
B. Dechenaux[55], D.V. Dedovich[64], J. Degenhardt[120], J. Del Peso[80], T. Del Prete[122a,122b], T. Delemontex[55],
M. Deliyergiyev[74], A. Dell'Acqua[30], L. Dell'Asta[22], M. Della Pietra[102a,i], D. della Volpe[102a,102b], M. Delmastro[5],
P.A. Delsart[55], C. Deluca[105], S. Demers[176], M. Demichev[64], B. Demirkoz[12,k], S.P. Denisov[128], D. Derendarz[39],
J.E. Derkaoui[135d], F. Derue[78], P. Dervan[73], K. Desch[21], E. Devetak[148], P.O. Deviveiros[105], A. Dewhurst[129],
B. DeWilde[148], S. Dhaliwal[105], R. Dhullipudi[25,l], A. Di Ciaccio[133a,133b], L. Di Ciaccio[5], C. Di Donato[102a,102b],
A. Di Girolamo[30], B. Di Girolamo[30], S. Di Luise[134a,134b], A. Di Mattia[152], B. Di Micco[30], R. Di Nardo[47],
A. Di Simone[133a,133b], R. Di Sipio[20a,20b], M.A. Diaz[32a], E.B. Diehl[87], J. Dietrich[42], T.A. Dietzsch[58a], S. Diglio[86],
K. Dindar Yagci[40], J. Dingfelder[21], F. Dinut[26a], C. Dionisi[132a,132b], P. Dita[26a], S. Dita[26a], F. Dittus[30], F. Djama[83],
T. Djobava[51b], M.A.B. do Vale[24c], A. Do Valle Wemans[124a,m], T.K.O. Doan[5], M. Dobbs[85], D. Dobos[30],
E. Dobson[30,n], J. Dodd[35], C. Doglioni[49], T. Doherty[53], T. Dohmae[155], Y. Doi[65,*], J. Dolejsi[127], Z. Dolezal[127],
B.A. Dolgoshein[96,*], M. Donadelli[24d], J. Donini[34], J. Dopke[30], A. Doria[102a], A. Dos Anjos[173], A. Dotti[122a,122b],
M.T. Dova[70], A.D. Doxiadis[105], A.T. Doyle[53], N. Dressnandt[120], M. Dris[10], J. Dubbert[99], S. Dube[15], E. Dubreuil[34],
E. Duchovni[172], G. Duckeck[98], D. Duda[175], A. Dudarev[30], F. Dudziak[63], I.P. Duerdoth[82], L. Duflot[115],
M-A. Dufour[85], L. Duguid[76], M. Dührssen[30], M. Dunford[58a], H. Duran Yildiz[4a], M. Düren[52], R. Duxfield[139],
M. Dwuznik[38], W.L. Ebenstein[45], J. Ebke[98], S. Eckweiler[81], W. Edson[2], C.A. Edwards[76], N.C. Edwards[53],
W. Ehrenfeld[21], T. Eifert[143], G. Eigen[14], K. Einsweiler[15], E. Eisenhandler[75], T. Ekelof[166], M. El Kacimi[135c],
M. Ellert[166], S. Elles[5], F. Ellinghaus[81], K. Ellis[75], N. Ellis[30], J. Elmsheuser[98], M. Elsing[30], D. Emeliyanov[129],
R. Engelmann[148], A. Engl[98], B. Epp[61], J. Erdmann[176], A. Ereditato[17], D. Eriksson[146a], J. Ernst[2], M. Ernst[25],
J. Ernwein[136], D. Errede[165], S. Errede[165], E. Ertel[81], M. Escalier[115], H. Esch[43], C. Escobar[123], X. Espinal Curull[12],
B. Esposito[47], F. Etienne[83], A.I. Etienvre[136], E. Etzion[153], D. Evangelakou[54], H. Evans[60], L. Fabbri[20a,20b],
C. Fabre[30], R.M. Fakhrutdinov[128], S. Falciano[132a], Y. Fang[33a], M. Fanti[89a,89b], A. Farbin[8], A. Farilla[134a],
J. Farley[148], T. Farooque[158], S. Farrell[163], S.M. Farrington[170], P. Farthouat[30], F. Fassi[167], P. Fassnacht[30],
D. Fassouliotis[9], B. Fatholahzadeh[158], A. Favareto[89a,89b], L. Fayard[115], P. Federic[144a], O.L. Fedin[121],
W. Fedorko[168], M. Fehling-Kaschek[48], L. Feligioni[83], C. Feng[33d], E.J. Feng[6], A.B. Fenyuk[128], J. Ferencei[144b],
W. Fernando[6], S. Ferrag[53], J. Ferrando[53], V. Ferrara[42], A. Ferrari[166], P. Ferrari[105], R. Ferrari[119a],

D.E. Ferreira de Lima[53], A. Ferrer[167], D. Ferrere[49], C. Ferretti[87], A. Ferretto Parodi[50a,50b], M. Fiascaris[31],
F. Fiedler[81], A. Filipčič[74], F. Filthaut[104], M. Fincke-Keeler[169], M.C.N. Fiolhais[124a,h], L. Fiorini[167], A. Firan[40],
G. Fischer[42], M.J. Fisher[109], E.A. Fitzgerald[23], M. Flechl[48], I. Fleck[141], J. Fleckner[81], P. Fleischmann[174],
S. Fleischmann[175], G. Fletcher[75], T. Flick[175], A. Floderus[79], L.R. Flores Castillo[173], A.C. Florez Bustos[159b],
M.J. Flowerdew[99], T. Fonseca Martin[17], A. Formica[136], A. Forti[82], D. Fortin[159a], D. Fournier[115], A.J. Fowler[45],
H. Fox[71], P. Francavilla[12], M. Franchini[20a,20b], S. Franchino[119a,119b], D. Francis[30], T. Frank[172], M. Franklin[57],
S. Franz[30], M. Fraternali[119a,119b], S. Fratina[120], S.T. French[28], C. Friedrich[42], F. Friedrich[44], D. Froidevaux[30],
J.A. Frost[28], C. Fukunaga[156], E. Fullana Torregrosa[127], B.G. Fulsom[143], J. Fuster[167], C. Gabaldon[30],
O. Gabizon[172], S. Gadatsch[105], T. Gadfort[25], S. Gadomski[49], G. Gagliardi[50a,50b], P. Gagnon[60], C. Galea[98],
B. Galhardo[124a], E.J. Gallas[118], V. Gallo[17], B.J. Gallop[129], P. Gallus[126], K.K. Gan[109], Y.S. Gao[143,f],
A. Gaponenko[15], F. Garberson[176], C. García[167], J.E. García Navarro[167], M. Garcia-Sciveres[15], R.W. Gardner[31],
N. Garelli[143], V. Garonne[30], C. Gatti[47], G. Gaudio[119a], B. Gaur[141], L. Gauthier[93], P. Gauzzi[132a,132b],
I.L. Gavrilenko[94], C. Gay[168], G. Gaycken[21], E.N. Gazis[10], P. Ge[33d,o], Z. Gecse[168], C.N.P. Gee[129], D.A.A. Geerts[105],
Ch. Geich-Gimbel[21], K. Gellerstedt[146a,146b], C. Gemme[50a], A. Gemmell[53], M.H. Genest[55], S. Gentile[132a,132b],
M. George[54], S. George[76], D. Gerbaudo[12], P. Gerlach[175], A. Gershon[153], C. Geweniger[58a], H. Ghazlane[135b],
N. Ghodbane[34], B. Giacobbe[20a], S. Giagu[132a,132b], V. Giangiobbe[12], F. Gianotti[30], B. Gibbard[25], A. Gibson[158],
S.M. Gibson[30], M. Gilchriese[15], T.P.S. Gillam[28], D. Gillberg[30], A.R. Gillman[129], D.M. Gingrich[3,e], N. Giokaris[9],
M.P. Giordani[164c], R. Giordano[102a,102b], F.M. Giorgi[16], P. Giovannini[99], P.F. Giraud[136], D. Giugni[89a], M. Giunta[93],
B.K. Gjelsten[117], L.K. Gladilin[97], C. Glasman[80], J. Glatzer[21], A. Glazov[42], G.L. Glonti[64], J.R. Goddard[75],
J. Godfrey[142], J. Godlewski[30], M. Goebel[42], C. Goeringer[81], S. Goldfarb[87], T. Golling[176], D. Golubkov[128],
A. Gomes[124a,c], L.S. Gomez Fajardo[42], R. Gonçalo[76], J. Goncalves Pinto Firmino Da Costa[42], L. Gonella[21],
S. González de la Hoz[167], G. Gonzalez Parra[12], M.L. Gonzalez Silva[27], S. Gonzalez-Sevilla[49], J.J. Goodson[148],
L. Goossens[30], T. Göpfert[44], P.A. Gorbounov[95], H.A. Gordon[25], I. Gorelov[103], G. Gorfine[175], B. Gorini[30],
E. Gorini[72a,72b], A. Gorišek[74], E. Gornicki[39], A.T. Goshaw[6], M. Gosselink[105], C. Gössling[43], M.I. Gostkin[64],
I. Gough Eschrich[163], M. Gouighri[135a], D. Goujdami[135c], M.P. Goulette[49], A.G. Goussiou[138], C. Goy[5],
S. Gozpinar[23], I. Grabowska-Bold[38], P. Grafström[20a,20b], K-J. Grahn[42], E. Gramstad[117], F. Grancagnolo[72a],
S. Grancagnolo[16], V. Grassi[148], V. Gratchev[121], H.M. Gray[30], J.A. Gray[148], E. Graziani[134a], O.G. Grebenyuk[121],
T. Greenshaw[73], Z.D. Greenwood[25,l], K. Gregersen[36], I.M. Gregor[42], P. Grenier[143], J. Griffiths[8], N. Grigalashvili[64],
A.A. Grillo[137], K. Grimm[71], S. Grinstein[12], Ph. Gris[34], Y.V. Grishkevich[97], J.-F. Grivaz[115], A. Grohsjean[42],
E. Gross[172], J. Grosse-Knetter[54], J. Groth-Jensen[172], K. Grybel[141], D. Guest[176], O. Gueta[153], C. Guicheney[34],
E. Guido[50a,50b], T. Guillemin[115], S. Guindon[54], U. Gul[53], J. Gunther[125], B. Guo[158], J. Guo[35], P. Gutierrez[111],
N. Guttman[153], O. Gutzwiller[173], C. Guyot[136], C. Gwenlan[118], C.B. Gwilliam[73], A. Haas[108], S. Haas[30], C. Haber[15],
H.K. Hadavand[8], D.R. Hadley[18], P. Haefner[21], Z. Hajduk[39], H. Hakobyan[177], D. Hall[118], G. Halladjian[62],
K. Hamacher[175], P. Hamal[113], K. Hamano[86], M. Hamer[54], A. Hamilton[145b,p], S. Hamilton[161], L. Han[33b],
K. Hanagaki[116], K. Hanawa[160], M. Hance[15], C. Handel[81], P. Hanke[58a], J.R. Hansen[36], J.B. Hansen[36],
J.D. Hansen[36], P.H. Hansen[36], P. Hansson[143], K. Hara[160], T. Harenberg[175], S. Harkusha[90], D. Harper[87],
R.D. Harrington[46], O.M. Harris[138], J. Hartert[48], F. Hartjes[105], T. Haruyama[65], A. Harvey[56], S. Hasegawa[101],
Y. Hasegawa[140], S. Hassani[136], S. Haug[17], M. Hauschild[30], R. Hauser[88], M. Havranek[21], C.M. Hawkes[18],
R.J. Hawkings[30], A.D. Hawkins[79], T. Hayakawa[66], T. Hayashi[160], D. Hayden[76], C.P. Hays[118], H.S. Hayward[73],
S.J. Haywood[129], S.J. Head[18], V. Hedberg[79], L. Heelan[8], S. Heim[120], B. Heinemann[15], S. Heisterkamp[36],
L. Helary[22], C. Heller[98], M. Heller[30], S. Hellman[146a,146b], D. Hellmich[21], C. Helsens[12], R.C.W. Henderson[71],
M. Henke[58a], A. Henrichs[176], A.M. Henriques Correia[30], S. Henrot-Versille[115], C. Hensel[54], C.M. Hernandez[8],
Y. Hernández Jiménez[167], R. Herrberg[16], G. Herten[48], R. Hertenberger[98], L. Hervas[30], G.G. Hesketh[77],
N.P. Hessey[105], R. Hickling[75], E. Higón-Rodriguez[167], J.C. Hill[28], K.H. Hiller[42], S. Hillert[21], S.J. Hillier[18],
I. Hinchliffe[15], E. Hines[120], M. Hirose[116], F. Hirsch[43], D. Hirschbuehl[175], J. Hobbs[148], N. Hod[153],
M.C. Hodgkinson[139], P. Hodgson[139], A. Hoecker[30], M.R. Hoeferkamp[103], J. Hoffman[40], D. Hoffmann[83],
M. Hohlfeld[81], S.O. Holmgren[146a], T. Holy[126], J.L. Holzbauer[88], T.M. Hong[120], L. Hooft van Huysduynen[108],
S. Horner[48], J-Y. Hostachy[55], S. Hou[151], A. Hoummada[135a], J. Howard[118], J. Howarth[82], M. Hrabovsky[113],
I. Hristova[16], J. Hrivnac[115], T. Hryn'ova[5], P.J. Hsu[81], S.-C. Hsu[138], D. Hu[35], Z. Hubacek[30], F. Hubaut[83],
F. Huegging[21], A. Huettmann[42], T.B. Huffman[118], E.W. Hughes[35], G. Hughes[71], M. Huhtinen[30], M. Hurwitz[15],
N. Huseynov[64,q], J. Huston[88], J. Huth[57], G. Iacobucci[49], G. Iakovidis[10], M. Ibbotson[82], I. Ibragimov[141],
L. Iconomidou-Fayard[115], J. Idarraga[115], P. Iengo[102a], O. Igonkina[105], Y. Ikegami[65], K. Ikematsu[141], M. Ikeno[65],
D. Iliadis[154], N. Ilic[158], T. Ince[99], P. Ioannou[9], M. Iodice[134a], K. Iordanidou[9], V. Ippolito[132a,132b], A. Irles Quiles[167],
C. Isaksson[166], M. Ishino[67], M. Ishitsuka[157], R. Ishmukhametov[109], C. Issever[118], S. Istin[19a], A.V. Ivashin[128],
W. Iwanski[39], H. Iwasaki[65], J.M. Izen[41], V. Izzo[102a], B. Jackson[120], J.N. Jackson[73], P. Jackson[1], M.R. Jaekel[30],
V. Jain[2], K. Jakobs[48], S. Jakobsen[36], T. Jakoubek[125], J. Jakubek[126], D.O. Jamin[151], D.K. Jana[111], E. Jansen[77],
H. Jansen[30], J. Janssen[21], A. Jantsch[99], M. Janus[48], R.C. Jared[173], G. Jarlskog[79], L. Jeanty[57], G.-Y. Jeng[150],
I. Jen-La Plante[31], D. Jennens[86], P. Jenni[30], P. Jež[36], S. Jézéquel[5], M.K. Jha[20a], H. Ji[173], W. Ji[81], J. Jia[148],

Y. Jiang[33b], M. Jimenez Belenguer[42], S. Jin[33a], O. Jinnouchi[157], M.D. Joergensen[36], D. Joffe[40],
M. Johansen[146a,146b], K.E. Johansson[146a], P. Johansson[139], S. Johnert[42], K.A. Johns[7], K. Jon-And[146a,146b],
G. Jones[170], R.W.L. Jones[71], T.J. Jones[73], C. Joram[30], P.M. Jorge[124a], K.D. Joshi[82], J. Jovicevic[147], T. Jovin[13b],
X. Ju[173], C.A. Jung[43], R.M. Jungst[30], V. Juranek[125], P. Jussel[61], A. Juste Rozas[12], S. Kabana[17], M. Kaci[167],
A. Kaczmarska[39], P. Kadlecik[36], M. Kado[115], H. Kagan[109], M. Kagan[57], E. Kajomovitz[152], S. Kalinin[175],
L.V. Kalinovskaya[64], S. Kama[40], N. Kanaya[155], M. Kaneda[30], S. Kaneti[28], T. Kanno[157], V.A. Kantserov[96],
J. Kanzaki[65], B. Kaplan[108], A. Kapliy[31], D. Kar[53], M. Karagounis[21], K. Karakostas[10], M. Karnevskiy[58b],
V. Kartvelishvili[71], A.N. Karyukhin[128], L. Kashif[173], G. Kasieczka[58b], R.D. Kass[109], A. Kastanas[14], Y. Kataoka[155],
J. Katzy[42], V. Kaushik[7], K. Kawagoe[69], T. Kawamoto[155], G. Kawamura[81], S. Kazama[155], V.F. Kazanin[107],
M.Y. Kazarinov[64], R. Keeler[169], P.T. Keener[120], R. Kehoe[40], M. Keil[54], G.D. Kekelidze[64], J.S. Keller[138],
M. Kenyon[53], H. Keoshkerian[5], O. Kepka[125], N. Kerschen[30], B.P. Kerševan[74], S. Kersten[175], K. Kessoku[155],
J. Keung[158], F. Khalil-zada[11], H. Khandanyan[146a,146b], A. Khanov[112], D. Kharchenko[64], A. Khodinov[96],
A. Khomich[58a], T.J. Khoo[28], G. Khoriauli[21], A. Khoroshilov[175], V. Khovanskiy[95], E. Khramov[64], J. Khubua[51b],
H. Kim[146a,146b], S.H. Kim[160], N. Kimura[171], O. Kind[16], B.T. King[73], M. King[66], R.S.B. King[118], J. Kirk[129],
A.E. Kiryunin[99], T. Kishimoto[66], D. Kisielewska[38], T. Kitamura[66], T. Kittelmann[123], K. Kiuchi[160], E. Kladiva[144b],
M. Klein[73], U. Klein[73], K. Kleinknecht[81], M. Klemetti[85], A. Klier[172], P. Klimek[146a,146b], A. Klimentov[25],
R. Klingenberg[43], J.A. Klinger[82], E.B. Klinkby[36], T. Klioutchnikova[30], P.F. Klok[104], S. Klous[105], E.-E. Kluge[58a],
T. Kluge[73], P. Kluit[105], S. Kluth[99], E. Kneringer[61], E.B.F.G. Knoops[83], A. Knue[54], B.R. Ko[45], T. Kobayashi[155],
M. Kobel[44], M. Kocian[143], P. Kodys[127], S. Koenig[81], F. Koetsveld[104], P. Koevesarki[21], T. Koffas[29], E. Koffeman[105],
L.A. Kogan[118], S. Kohlmann[175], F. Kohn[54], Z. Kohout[126], T. Kohriki[65], T. Koi[143], G.M. Kolachev[107,*],
H. Kolanoski[16], I. Koletsou[89a], J. Koll[88], A.A. Komar[94], Y. Komori[155], T. Kondo[65], K. Köneke[30], A.C. König[104],
T. Kono[42,r], A.I. Kononov[48], R. Konoplich[108,s], N. Konstantinidis[77], R. Kopeliansky[152], S. Koperny[38], L. Köpke[81],
A.K. Kopp[48], K. Korcyl[39], K. Kordas[154], A. Korn[46], A. Korol[107], I. Korolkov[12], E.V. Korolkova[139],
V.A. Korotkov[128], O. Kortner[99], S. Kortner[99], V.V. Kostyukhin[21], S. Kotov[99], V.M. Kotov[64], A. Kotwal[45],
C. Kourkoumelis[9], V. Kouskoura[154], A. Koutsman[159a], R. Kowalewski[169], T.Z. Kowalski[38], W. Kozanecki[136],
A.S. Kozhin[128], V. Kral[126], V.A. Kramarenko[97], G. Kramberger[74], M.W. Krasny[78], A. Krasznahorkay[108],
J.K. Kraus[21], A. Kravchenko[25], S. Kreiss[108], F. Krejci[126], J. Kretzschmar[73], K. Kreutzfeldt[52], N. Krieger[54],
P. Krieger[158], K. Kroeninger[54], H. Kroha[99], J. Kroll[120], J. Kroseberg[21], J. Krstic[13a], U. Kruchonak[64], H. Krüger[21],
T. Kruker[17], N. Krumnack[63], Z.V. Krumshteyn[64], M.K. Kruse[45], T. Kubota[86], S. Kuday[4a], S. Kuehn[48],
A. Kugel[58c], T. Kuhl[42], V. Kukhtin[64], Y. Kulchitsky[90], S. Kuleshov[32b], M. Kuna[78], J. Kunkle[120], A. Kupco[125],
H. Kurashige[66], M. Kurata[160], Y.A. Kurochkin[90], V. Kus[125], E.S. Kuwertz[147], M. Kuze[157], J. Kvita[142], R. Kwee[16],
A. La Rosa[49], L. La Rotonda[37a,37b], L. Labarga[80], S. Lablak[135a], C. Lacasta[167], F. Lacava[132a,132b], J. Lacey[29],
H. Lacker[16], D. Lacour[78], V.R. Lacuesta[167], E. Ladygin[64], R. Lafaye[5], B. Laforge[78], T. Lagouri[176], S. Lai[48],
E. Laisne[55], L. Lambourne[77], C.L. Lampen[7], W. Lampl[7], E. Lançon[136], U. Landgraf[48], M.P.J. Landon[75],
V.S. Lang[58a], C. Lange[42], A.J. Lankford[163], F. Lanni[25], K. Lantzsch[30], A. Lanza[119a], S. Laplace[78], C. Lapoire[21],
J.F. Laporte[136], T. Lari[89a], A. Larner[118], M. Lassnig[30], P. Laurelli[47], V. Lavorini[37a,37b], W. Lavrijsen[15],
P. Laycock[73], O. Le Dortz[78], E. Le Guirriec[83], E. Le Menedeu[12], T. LeCompte[6], F. Ledroit-Guillon[55], H. Lee[105],
J.S.H. Lee[116], S.C. Lee[151], L. Lee[176], M. Lefebvre[169], M. Legendre[136], F. Legger[98], C. Leggett[15], M. Lehmacher[21],
G. Lehmann Miotto[30], A.G. Leister[176], M.A.L. Leite[24d], R. Leitner[127], D. Lellouch[172], B. Lemmer[54],
V. Lendermann[58a], K.J.C. Leney[145b], T. Lenz[105], G. Lenzen[175], B. Lenzi[30], K. Leonhardt[44], S. Leontsinis[10],
F. Lepold[58a], C. Leroy[93], J-R. Lessard[169], C.G. Lester[28], C.M. Lester[120], J. Levêque[5], D. Levin[87], L.J. Levinson[172],
A. Lewis[118], G.H. Lewis[108], A.M. Leyko[21], M. Leyton[16], B. Li[33b], B. Li[83], H. Li[148], H.L. Li[31], S. Li[33b,t], X. Li[87],
Z. Liang[118,u], H. Liao[34], B. Liberti[133a], P. Lichard[30], K. Lie[165], W. Liebig[14], C. Limbach[21], A. Limosani[86],
M. Limper[62], S.C. Lin[151,v], F. Linde[105], J.T. Linnemann[88], E. Lipeles[120], A. Lipniacka[14], T.M. Liss[165],
D. Lissauer[25], A. Lister[168], A.M. Litke[137], D. Liu[151], J.B. Liu[33b], L. Liu[87], M. Liu[33b], Y. Liu[33b], M. Livan[119a,119b],
S.S.A. Livermore[118], A. Lleres[55], J. Llorente Merino[80], S.L. Lloyd[75], F. Lo Sterzo[132a,132b], E. Lobodzinska[42],
P. Loch[7], W.S. Lockman[137], T. Loddenkoetter[21], F.K. Loebinger[82], A.E. Loevschall-Jensen[36], A. Loginov[176],
C.W. Loh[168], T. Lohse[16], K. Lohwasser[48], M. Lokajicek[125], V.P. Lombardo[5], R.E. Long[71], L. Lopes[124a],
D. Lopez Mateos[57], J. Lorenz[98], N. Lorenzo Martinez[115], M. Losada[162], P. Loscutoff[15], M.J. Losty[159a,*], X. Lou[41],
A. Lounis[115], K.F. Loureiro[162], J. Love[6], P.A. Love[71], A.J. Lowe[143,f], F. Lu[33a], H.J. Lubatti[138], C. Luci[132a,132b],
A. Lucotte[55], D. Ludwig[42], I. Ludwig[48], J. Ludwig[48], F. Luehring[60], W. Lukas[61], L. Luminari[132a], E. Lund[117],
B. Lundberg[79], J. Lundberg[146a,146b], O. Lundberg[146a,146b], B. Lund-Jensen[147], J. Lundquist[36], M. Lungwitz[81],
D. Lynn[25], E. Lytken[79], H. Ma[25], L.L. Ma[173], G. Maccarrone[47], A. Macchiolo[99], B. Maček[74],
J. Machado Miguens[124a], D. Macina[30], R. Mackeprang[36], R. Madar[48], R.J. Madaras[15], H.J. Maddocks[71],
W.F. Mader[44], A. Madsen[166], M. Maeno[5], T. Maeno[25], L. Magnoni[163], E. Magradze[54], K. Mahboubi[48],
J. Mahlstedt[105], S. Mahmoud[73], G. Mahout[18], C. Maiani[136], C. Maidantchik[24a], A. Maio[124a,c], S. Majewski[25],
Y. Makida[65], N. Makovec[115], P. Mal[136,w], B. Malaescu[78], Pa. Malecki[39], P. Malecki[39], V.P. Maleev[121], F. Malek[55],
U. Mallik[62], D. Malon[6], C. Malone[143], S. Maltezos[10], V. Malyshev[107], S. Malyukov[30], J. Mamuzic[13b],

L. Mandelli[89a], I. Mandić[74], R. Mandrysch[62], J. Maneira[124a], A. Manfredini[99], L. Manhaes de Andrade Filho[24b],
J.A. Manjarres Ramos[136], A. Mann[98], P.M. Manning[137], A. Manousakis-Katsikakis[9], B. Mansoulie[136],
R. Mantifel[85], A. Mapelli[30], L. Mapelli[30], L. March[167], J.F. Marchand[29], F. Marchese[133a,133b], G. Marchiori[78],
M. Marcisovsky[125], C.P. Marino[169], F. Marroquim[24a], Z. Marshall[30], L.F. Marti[17], S. Marti-Garcia[167], B. Martin[30],
B. Martin[88], J.P. Martin[93], T.A. Martin[18], V.J. Martin[46], B. Martin dit Latour[49], H. Martinez[136], M. Martinez[12],
V. Martinez Outschoorn[57], S. Martin-Haugh[149], A.C. Martyniuk[169], M. Marx[82], F. Marzano[132a], A. Marzin[111],
L. Masetti[81], T. Mashimo[155], R. Mashinistov[94], J. Masik[82], A.L. Maslennikov[107], I. Massa[20a,20b], N. Massol[5],
P. Mastrandrea[148], A. Mastroberardino[37a,37b], T. Masubuchi[155], H. Matsunaga[155], T. Matsushita[66], P. Mättig[175],
S. Mättig[42], C. Mattravers[118,d], J. Maurer[83], S.J. Maxfield[73], D.A. Maximov[107,g], R. Mazini[151], M. Mazur[21],
L. Mazzaferro[133a,133b], M. Mazzanti[89a], J. Mc Donald[85], S.P. Mc Kee[87], A. McCarn[165], R.L. McCarthy[148],
T.G. McCarthy[29], N.A. McCubbin[129], K.W. McFarlane[56,*], J.A. Mcfayden[139], G. Mchedlidze[51b], T. Mclaughlan[18],
S.J. McMahon[129], R.A. McPherson[169,j], A. Meade[84], J. Mechnich[105], M. Mechtel[175], M. Medinnis[42], S. Meehan[31],
R. Meera-Lebbai[111], T. Meguro[116], S. Mehlhase[36], A. Mehta[73], K. Meier[58a], B. Meirose[79], C. Melachrinos[31],
B.R. Mellado Garcia[173], F. Meloni[89a,89b], L. Mendoza Navas[162], Z. Meng[151,x], A. Mengarelli[20a,20b], S. Menke[99],
E. Meoni[161], K.M. Mercurio[57], P. Mermod[49], L. Merola[102a,102b], C. Meroni[89a], F.S. Merritt[31], H. Merritt[109],
A. Messina[30,y], J. Metcalfe[25], A.S. Mete[163], C. Meyer[81], C. Meyer[31], J-P. Meyer[136], J. Meyer[174], J. Meyer[54],
S. Michal[30], R.P. Middleton[129], S. Migas[73], L. Mijović[136], G. Mikenberg[172], M. Mikestikova[125], M. Mikuž[74],
D.W. Miller[31], R.J. Miller[88], W.J. Mills[168], C. Mills[57], A. Milov[172], D.A. Milstead[146a,146b], D. Milstein[172],
A.A. Minaenko[128], M. Miñano Moya[167], I.A. Minashvili[64], A.I. Mincer[108], B. Mindur[38], M. Mineev[64], Y. Ming[173],
L.M. Mir[12], G. Mirabelli[132a], J. Mitrevski[137], V.A. Mitsou[167], S. Mitsui[65], P.S. Miyagawa[139], J.U. Mjörnmark[79],
T. Moa[146a,146b], V. Moeller[28], S. Mohapatra[148], W. Mohr[48], R. Moles-Valls[167], A. Molfetas[30], K. Mönig[42],
J. Monk[77], E. Monnier[83], J. Montejo Berlingen[12], F. Monticelli[70], S. Monzani[20a,20b], R.W. Moore[3],
G.F. Moorhead[86], C. Mora Herrera[49], A. Moraes[53], N. Morange[136], J. Morel[54], G. Morello[37a,37b], D. Moreno[81],
M. Moreno Llácer[167], P. Morettini[50a], M. Morgenstern[44], M. Morii[57], A.K. Morley[30], G. Mornacchi[30],
J.D. Morris[75], L. Morvaj[101], N. Möser[21], H.G. Moser[99], M. Mosidze[51b], J. Moss[109], R. Mount[143], E. Mountricha[10,z],
S.V. Mouraviev[94,*], E.J.W. Moyse[84], F. Mueller[58a], J. Mueller[123], K. Mueller[21], T. Mueller[81], D. Muenstermann[30],
T.A. Müller[98], Y. Munwes[153], W.J. Murray[129], I. Mussche[105], E. Musto[152], A.G. Myagkov[128], M. Myska[125],
O. Nackenhorst[54], J. Nadal[12], K. Nagai[160], R. Nagai[157], Y. Nagai[83], K. Nagano[65], A. Nagarkar[109], Y. Nagasaka[59],
M. Nagel[99], A.M. Nairz[30], Y. Nakahama[30], K. Nakamura[65], T. Nakamura[155], I. Nakano[110], H. Namasivayam[41],
G. Nanava[21], A. Napier[161], R. Narayan[58b], M. Nash[77,d], T. Nattermann[21], T. Naumann[42], G. Navarro[162],
H.A. Neal[87], P.Yu. Nechaeva[94], T.J. Neep[82], A. Negri[119a,119b], G. Negri[30], M. Negrini[20a], S. Nektarijevic[49],
A. Nelson[163], T.K. Nelson[143], S. Nemecek[125], P. Nemethy[108], A.A. Nepomuceno[24a], M. Nessi[30,aa],
M.S. Neubauer[165], M. Neumann[175], A. Neusiedl[81], R.M. Neves[108], P. Nevski[25], F.M. Newcomer[120], P.R. Newman[18],
D.H. Nguyen[6], V. Nguyen Thi Hong[136], R.B. Nickerson[118], R. Nicolaidou[136], B. Nicquevert[30], F. Niedercorn[115],
J. Nielsen[137], N. Nikiforou[35], A. Nikiforov[16], V. Nikolaenko[128], I. Nikolic-Audit[78], K. Nikolics[49], K. Nikolopoulos[18],
H. Nilsen[48], P. Nilsson[8], Y. Ninomiya[155], A. Nisati[132a], R. Nisius[99], T. Nobe[157], L. Nodulman[6], M. Nomachi[116],
I. Nomidis[154], S. Norberg[111], M. Nordberg[30], J. Novakova[127], M. Nozaki[65], L. Nozka[113], A.-E. Nuncio-Quiroz[21],
G. Nunes Hanninger[86], T. Nunnemann[98], E. Nurse[77], B.J. O'Brien[46], D.C. O'Neil[142], V. O'Shea[53], L.B. Oakes[98],
F.G. Oakham[29,e], H. Oberlack[99], J. Ocariz[78], A. Ochi[66], M.I. Ochoa[77], S. Oda[69], S. Odaka[65], J. Odier[83],
H. Ogren[60], A. Oh[82], S.H. Oh[45], C.C. Ohm[30], T. Ohshima[101], W. Okamura[116], H. Okawa[25], Y. Okumura[31],
T. Okuyama[155], A. Olariu[26a], A.G. Olchevski[64], S.A. Olivares Pino[46], M. Oliveira[124a,h], D. Oliveira Damazio[25],
E. Oliver Garcia[167], D. Olivito[120], A. Olszewski[39], J. Olszowska[39], A. Onofre[124a,ab], P.U.E. Onyisi[31,ac],
C.J. Oram[159a], M.J. Oreglia[31], Y. Oren[153], D. Orestano[134a,134b], N. Orlando[72a,72b], C. Oropeza Barrera[53],
R.S. Orr[158], B. Osculati[50a,50b], R. Ospanov[120], C. Osuna[12], G. Otero y Garzon[27], J.P. Ottersbach[105],
M. Ouchrif[135d], E.A. Ouellette[169], F. Ould-Saada[117], A. Ouraou[136], Q. Ouyang[33a], A. Ovcharova[15], M. Owen[82],
S. Owen[139], V.E. Ozcan[19a], N. Ozturk[8], A. Pacheco Pages[12], C. Padilla Aranda[12], S. Pagan Griso[15], E. Paganis[139],
C. Pahl[99], F. Paige[25], P. Pais[84], K. Pajchel[117], G. Palacino[159b], C.P. Paleari[7], S. Palestini[30], D. Pallin[34],
A. Palma[124a], J.D. Palmer[18], Y.B. Pan[173], E. Panagiotopoulou[10], J.G. Panduro Vazquez[76], P. Pani[105],
N. Panikashvili[87], S. Panitkin[25], D. Pantea[26a], A. Papadelis[146a], Th.D. Papadopoulou[10], A. Paramonov[6],
D. Paredes Hernandez[34], W. Park[25,ad], M.A. Parker[28], F. Parodi[50a,50b], J.A. Parsons[35], U. Parzefall[48],
S. Pashapour[54], E. Pasqualucci[132a], S. Passaggio[50a], A. Passeri[134a], F. Pastore[134a,134b,*], Fr. Pastore[76],
G. Pásztor[49,ae], S. Pataraia[175], N.D. Patel[150], J.R. Pater[82], S. Patricelli[102a,102b], T. Pauly[30], J. Pearce[169],
S. Pedraza Lopez[167], M.I. Pedraza Morales[173], S.V. Peleganchuk[107], D. Pelikan[166], H. Peng[33b], B. Penning[31],
A. Penson[35], J. Penwell[60], M. Perantoni[24a], K. Perez[35,af], T. Perez Cavalcanti[42], E. Perez Codina[159a],
M.T. Pérez García-Estañ[167], V. Perez Reale[35], L. Perini[89a,89b], H. Pernegger[30], R. Perrino[72a], P. Perrodo[5],
V.D. Peshekhonov[64], K. Peters[30], B.A. Petersen[30], J. Petersen[30], T.C. Petersen[36], E. Petit[5], A. Petridis[154],
C. Petridou[154], E. Petrolo[132a], F. Petrucci[134a,134b], D. Petschull[42], M. Petteni[142], R. Pezoa[32b], A. Phan[86],
P.W. Phillips[129], G. Piacquadio[30], A. Picazio[49], E. Piccaro[75], M. Piccinini[20a,20b], S.M. Piec[42], R. Piegaia[27],

D.T. Pignotti[109], J.E. Pilcher[31], A.D. Pilkington[82], J. Pina[124a,c], M. Pinamonti[164a,164c,ag], A. Pinder[118], J.L. Pinfold[3], A. Pingel[36], B. Pinto[124a], C. Pizio[89a,89b], M.-A. Pleier[25], V. Pleskot[127], E. Plotnikova[64], P. Plucinski[146a,146b], A. Poblaguev[25], S. Poddar[58a], F. Podlyski[34], R. Poettgen[81], L. Poggioli[115], D. Pohl[21], M. Pohl[49], G. Polesello[119a], A. Policicchio[37a,37b], R. Polifka[158], A. Polini[20a], J. Poll[75], V. Polychronakos[25], D. Pomeroy[23], K. Pommès[30], L. Pontecorvo[132a], B.G. Pope[88], G.A. Popeneciu[26a], D.S. Popovic[13a], A. Poppleton[30], X. Portell Bueso[30], G.E. Pospelov[99], S. Pospisil[126], I.N. Potrap[99], C.J. Potter[149], C.T. Potter[114], G. Poulard[30], J. Poveda[60], V. Pozdnyakov[64], R. Prabhu[77], P. Pralavorio[83], A. Pranko[15], S. Prasad[30], R. Pravahan[25], S. Prell[63], K. Pretzl[17], D. Price[60], J. Price[73], L.E. Price[6], D. Prieur[123], M. Primavera[72a], K. Prokofiev[108], F. Prokoshin[32b], S. Protopopescu[25], J. Proudfoot[6], X. Prudent[44], M. Przybycien[38], H. Przysiezniak[5], S. Psoroulas[21], E. Ptacek[114], E. Pueschel[84], D. Puldon[148], J. Purdham[87], M. Purohit[25,ad], P. Puzo[115], Y. Pylypchenko[62], J. Qian[87], A. Quadt[54], D.R. Quarrie[15], W.B. Quayle[173], M. Raas[104], V. Radeka[25], V. Radescu[42], P. Radloff[114], F. Ragusa[89a,89b], G. Rahal[178], A.M. Rahimi[109], D. Rahm[25], S. Rajagopalan[25], M. Rammensee[48], M. Rammes[141], A.S. Randle-Conde[40], K. Randrianarivony[29], C. Rangel-Smith[78], K. Rao[163], F. Rauscher[98], T.C. Rave[48], T. Ravenscroft[53], M. Raymond[30], A.L. Read[117], D.M. Rebuzzi[119a,119b], A. Redelbach[174], G. Redlinger[25], R. Reece[120], K. Reeves[41], A. Reinsch[114], I. Reisinger[43], M. Relich[163], C. Rembser[30], Z.L. Ren[151], A. Renaud[115], M. Rescigno[132a], S. Resconi[89a], B. Resende[136], P. Reznicek[98], R. Rezvani[158], R. Richter[99], E. Richter-Was[5], M. Ridel[78], P. Rieck[16], M. Rijssenbeek[148], A. Rimoldi[119a,119b], L. Rinaldi[20a], R.R. Rios[40], E. Ritsch[61], I. Riu[12], G. Rivoltella[89a,89b], F. Rizatdinova[112], E. Rizvi[75], S.H. Robertson[85,j], A. Robichaud-Veronneau[118], D. Robinson[28], J.E.M. Robinson[82], A. Robson[53], J.G. Rocha de Lima[106], C. Roda[122a,122b], D. Roda Dos Santos[30], A. Roe[54], S. Roe[30], O. Røhne[117], S. Rolli[161], A. Romaniouk[96], M. Romano[20a,20b], G. Romeo[27], E. Romero Adam[167], N. Rompotis[138], L. Roos[78], E. Ros[167], S. Rosati[132a], K. Rosbach[49], A. Rose[149], M. Rose[76], G.A. Rosenbaum[158], P.L. Rosendahl[14], O. Rosenthal[141], L. Rosselet[49], V. Rossetti[12], E. Rossi[132a,132b], L.P. Rossi[50a], M. Rotaru[26a], I. Roth[172], J. Rothberg[138], D. Rousseau[115], C.R. Royon[136], A. Rozanov[83], Y. Rozen[152], X. Ruan[33a,ah], F. Rubbo[12], I. Rubinskiy[42], N. Ruckstuhl[105], V.I. Rud[97], C. Rudolph[44], M.S. Rudolph[158], F. Rühr[7], A. Ruiz-Martinez[63], L. Rumyantsev[64], Z. Rurikova[48], N.A. Rusakovich[64], A. Ruschke[98], J.P. Rutherfoord[7], N. Ruthmann[48], P. Ruzicka[125], Y.F. Ryabov[121], M. Rybar[127], G. Rybkin[115], N.C. Ryder[118], A.F. Saavedra[150], I. Sadeh[153], H.F-W. Sadrozinski[137], R. Sadykov[64], F. Safai Tehrani[132a], H. Sakamoto[155], G. Salamanna[75], A. Salamon[133a], M. Saleem[111], D. Salek[30], D. Salihagic[99], A. Salnikov[143], J. Salt[167], B.M. Salvachua Ferrando[6], D. Salvatore[37a,37b], F. Salvatore[149], A. Salvucci[104], A. Salzburger[30], D. Sampsonidis[154], B.H. Samset[117], A. Sanchez[102a,102b], J. Sánchez[167], V. Sanchez Martinez[167], H. Sandaker[14], H.G. Sander[81], M.P. Sanders[98], M. Sandhoff[175], T. Sandoval[28], C. Sandoval[162], R. Sandstroem[99], D.P.C. Sankey[129], A. Sansoni[47], C. Santamarina Rios[85], C. Santoni[34], R. Santonico[133a,133b], H. Santos[124a], I. Santoyo Castillo[149], K. Sapp[123], J.G. Saraiva[124a], T. Sarangi[173], E. Sarkisyan-Grinbaum[8], B. Sarrazin[21], F. Sarri[122a,122b], G. Sartisohn[175], O. Sasaki[65], Y. Sasaki[155], N. Sasao[67], I. Satsounkevitch[90], G. Sauvage[5,*], E. Sauvan[5], J.B. Sauvan[115], P. Savard[158,e], V. Savinov[123], D.O. Savu[30], L. Sawyer[25,l], D.H. Saxon[53], J. Saxon[120], C. Sbarra[20a], A. Sbrizzi[20a,20b], D.A. Scannicchio[163], M. Scarcella[150], J. Schaarschmidt[115], P. Schacht[99], D. Schaefer[120], A. Schaelicke[46], S. Schaepe[21], S. Schaetzel[58b], U. Schäfer[81], A.C. Schaffer[115], D. Schaile[98], R.D. Schamberger[148], V. Scharf[58a], V.A. Schegelsky[121], D. Scheirich[87], M. Schernau[163], M.I. Scherzer[35], C. Schiavi[50a,50b], J. Schieck[98], M. Schioppa[37a,37b], S. Schlenker[30], E. Schmidt[48], K. Schmieden[21], C. Schmitt[81], C. Schmitt[98], S. Schmitt[58b], B. Schneider[17], Y.J. Schnellbach[73], U. Schnoor[44], L. Schoeffel[136], A. Schoening[58b], A.L.S. Schorlemmer[54], M. Schott[81], D. Schouten[159a], J. Schovancova[125], M. Schram[85], C. Schroeder[81], N. Schroer[58c], M.J. Schultens[21], J. Schultes[175], H.-C. Schultz-Coulon[58a], H. Schulz[16], M. Schumacher[48], B.A. Schumm[137], Ph. Schune[136], A. Schwartzman[143], Ph. Schwegler[99], Ph. Schwemling[78], R. Schwienhorst[88], J. Schwindling[136], T. Schwindt[21], M. Schwoerer[5], F.G. Sciacca[17], E. Scifo[115], G. Sciolla[23], W.G. Scott[129], J. Searcy[87], G. Sedov[42], E. Sedykh[121], S.C. Seidel[103], A. Seiden[137], F. Seifert[44], J.M. Seixas[24a], G. Sekhniaidze[102a], S.J. Sekula[40], K.E. Selbach[46], D.M. Seliverstov[121], B. Sellden[146a], G. Sellers[73], M. Seman[144b], N. Semprini-Cesari[20a,20b], C. Serfon[30], L. Serin[115], L. Serkin[54], T. Serre[83], R. Seuster[159a], H. Severini[111], A. Sfyrla[30], E. Shabalina[54], M. Shamim[114], L.Y. Shan[33a], J.T. Shank[22], Q.T. Shao[86], M. Shapiro[15], P.B. Shatalov[95], K. Shaw[164a,164c], D. Sherman[176], P. Sherwood[77], S. Shimizu[101], M. Shimojima[100], T. Shin[56], M. Shiyakova[64], A. Shmeleva[94], M.J. Shochet[31], D. Short[118], S. Shrestha[63], E. Shulga[96], M.A. Shupe[7], P. Sicho[125], A. Sidoti[132a], F. Siegert[48], Dj. Sijacki[13a], O. Silbert[172], J. Silva[124a], Y. Silver[153], D. Silverstein[143], S.B. Silverstein[146a], V. Simak[126], O. Simard[136], Lj. Simic[13a], S. Simion[115], E. Simioni[81], B. Simmons[77], R. Simoniello[89a,89b], M. Simonyan[36], P. Sinervo[158], N.B. Sinev[114], V. Sipica[141], G. Siragusa[174], A. Sircar[25], A.N. Sisakyan[64,*], S.Yu. Sivoklokov[97], J. Sjölin[146a,146b], T.B. Sjursen[14], L.A. Skinnari[15], H.P. Skottowe[57], K. Skovpen[107], P. Skubic[111], M. Slater[18], T. Slavicek[126], K. Sliwa[161], V. Smakhtin[172], B.H. Smart[46], L. Smestad[117], S.Yu. Smirnov[96], Y. Smirnov[96], L.N. Smirnova[97,ai], O. Smirnova[79], B.C. Smith[57], K.M. Smith[53], M. Smizanska[71], K. Smolek[126], A.A. Snesarev[94], G. Snidero[75], S.W. Snow[82], J. Snow[111], S. Snyder[25], R. Sobie[169,j], J. Sodomka[126], A. Soffer[153], D.A. Soh[151,u], C.A. Solans[30], M. Solar[126], J. Solc[126], E.Yu. Soldatov[96], U. Soldevila[167], E. Solfaroli Camillocci[132a,132b], A.A. Solodkov[128], O.V. Solovyanov[128], V. Solovyev[121], N. Soni[1], A. Sood[15],

V. Sopko[126], B. Sopko[126], M. Sosebee[8], R. Soualah[164a,164c], P. Soueid[93], A. Soukharev[107], D. South[42],
S. Spagnolo[72a,72b], F. Spanò[76], R. Spighi[20a], G. Spigo[30], R. Spiwoks[30], M. Spousta[127,aj], T. Spreitzer[158],
B. Spurlock[8], R.D. St. Denis[53], J. Stahlman[120], R. Stamen[58a], E. Stanecka[39], R.W. Stanek[6], C. Stanescu[134a],
M. Stanescu-Bellu[42], M.M. Stanitzki[42], S. Stapnes[117], E.A. Starchenko[128], J. Stark[55], P. Staroba[125],
P. Starovoitov[42], R. Staszewski[39], A. Staude[98], P. Stavina[144a,*], G. Steele[53], P. Steinbach[44], P. Steinberg[25],
I. Stekl[126], B. Stelzer[142], H.J. Stelzer[88], O. Stelzer-Chilton[159a], H. Stenzel[52], S. Stern[99], G.A. Stewart[30],
J.A. Stillings[21], M.C. Stockton[85], M. Stoebe[85], K. Stoerig[48], G. Stoicea[26a], S. Stonjek[99], P. Strachota[127],
A.R. Stradling[8], A. Straessner[44], J. Strandberg[147], S. Strandberg[146a,146b], A. Strandlie[117], M. Strang[109],
E. Strauss[143], M. Strauss[111], P. Strizenec[144b], R. Ströhmer[174], D.M. Strom[114], J.A. Strong[76,*], R. Stroynowski[40],
B. Stugu[14], I. Stumer[25,*], J. Stupak[148], P. Sturm[175], N.A. Styles[42], D. Su[143], HS. Subramania[3], R. Subramaniam[25],
A. Succurro[12], Y. Sugaya[116], C. Suhr[106], M. Suk[127], V.V. Sulin[94], S. Sultansoy[4c], T. Sumida[67], X. Sun[55],
J.E. Sundermann[48], K. Suruliz[139], G. Susinno[37a,37b], M.R. Sutton[149], Y. Suzuki[65], Y. Suzuki[66], M. Svatos[125],
S. Swedish[168], M. Swiatlowski[143], I. Sykora[144a], T. Sykora[127], D. Ta[105], K. Tackmann[42], A. Taffard[163],
R. Tafirout[159a], N. Taiblum[153], Y. Takahashi[101], H. Takai[25], R. Takashima[68], H. Takeda[66], T. Takeshita[140],
Y. Takubo[65], M. Talby[83], A. Talyshev[107,g], J.Y.C. Tam[174], M.C. Tamsett[25], K.G. Tan[86], J. Tanaka[155],
R. Tanaka[115], S. Tanaka[131], S. Tanaka[65], A.J. Tanasijczuk[142], K. Tani[66], N. Tannoury[83], S. Tapprogge[81],
D. Tardif[158], S. Tarem[152], F. Tarrade[29], G.F. Tartarelli[89a], P. Tas[127], M. Tasevsky[125], E. Tassi[37a,37b],
Y. Tayalati[135d], C. Taylor[77], F.E. Taylor[92], G.N. Taylor[86], W. Taylor[159b], M. Teinturier[115], F.A. Teischinger[30],
M. Teixeira Dias Castanheira[75], P. Teixeira-Dias[76], K.K. Temming[48], H. Ten Kate[30], P.K. Teng[151], S. Terada[65],
K. Terashi[155], J. Terron[80], M. Testa[47], R.J. Teuscher[158,j], J. Therhaag[21], T. Theveneaux-Pelzer[78], S. Thoma[48],
J.P. Thomas[18], E.N. Thompson[35], P.D. Thompson[18], P.D. Thompson[158], A.S. Thompson[53], L.A. Thomsen[36],
E. Thomson[120], M. Thomson[28], W.M. Thong[86], R.P. Thun[87,*], F. Tian[35], M.J. Tibbetts[15], T. Tic[125],
V.O. Tikhomirov[94], Y.A. Tikhonov[107,g], S. Timoshenko[96], E. Tiouchichine[83], P. Tipton[176], S. Tisserant[83],
T. Todorov[5], S. Todorova-Nova[161], B. Toggerson[163], J. Tojo[69], S. Tokár[144a], K. Tokushuku[65], K. Tollefson[88],
M. Tomoto[101], L. Tompkins[31], K. Toms[103], A. Tonoyan[14], C. Topfel[17], N.D. Topilin[64], E. Torrence[114], H. Torres[78],
E. Torró Pastor[167], J. Toth[83,ae], F. Touchard[83], D.R. Tovey[139], T. Trefzger[174], L. Tremblet[30], A. Tricoli[30],
I.M. Trigger[159a], S. Trincaz-Duvoid[78], M.F. Tripiana[70], N. Triplett[25], W. Trischuk[158], B. Trocmé[55], C. Troncon[89a],
M. Trottier-McDonald[142], P. True[88], M. Trzebinski[39], A. Trzupek[39], C. Tsarouchas[30], J.C-L. Tseng[118],
M. Tsiakiris[105], P.V. Tsiareshka[90], D. Tsionou[136], G. Tsipolitis[10], S. Tsiskaridze[12], V. Tsiskaridze[48],
E.G. Tskhadadze[51a], I.I. Tsukerman[95], V. Tsulaia[15], J.-W. Tsung[21], S. Tsuno[65], D. Tsybychev[148], A. Tua[139],
A. Tudorache[26a], V. Tudorache[26a], J.M. Tuggle[31], M. Turala[39], D. Turecek[126], I. Turk Cakir[4d], R. Turra[89a,89b],
P.M. Tuts[35], A. Tykhonov[74], M. Tylmad[146a,146b], M. Tyndel[129], G. Tzanakos[9], K. Uchida[21], I. Ueda[155], R. Ueno[29],
M. Ughetto[83], M. Ugland[14], M. Uhlenbrock[21], F. Ukegawa[160], G. Unal[30], A. Undrus[25], G. Unel[163], F.C. Ungaro[48],
Y. Unno[65], D. Urbaniec[35], P. Urquijo[21], G. Usai[8], L. Vacavant[83], V. Vacek[126], B. Vachon[85], S. Vahsen[15],
N. Valencic[105], S. Valentinetti[20a,20b], A. Valero[167], L. Valery[34], S. Valkar[127], E. Valladolid Gallego[167],
S. Vallecorsa[152], J.A. Valls Ferrer[167], R. Van Berg[120], P.C. Van Der Deijl[105], R. van der Geer[105],
H. van der Graaf[105], R. Van Der Leeuw[105], E. van der Poel[105], D. van der Ster[30], N. van Eldik[30], P. van Gemmeren[6],
J. Van Nieuwkoop[142], I. van Vulpen[105], M. Vanadia[99], W. Vandelli[30], A. Vaniachine[6], P. Vankov[42], F. Vannucci[78],
R. Vari[132a], E.W. Varnes[7], T. Varol[84], D. Varouchas[15], A. Vartapetian[8], K.E. Varvell[150], V.I. Vassilakopoulos[56],
F. Vazeille[34], T. Vazquez Schroeder[54], F. Veloso[124a], S. Veneziano[132a], A. Ventura[72a,72b], D. Ventura[84],
M. Venturi[48], N. Venturi[158], V. Vercesi[119a], M. Verducci[138], W. Verkerke[105], J.C. Vermeulen[105], A. Vest[44],
M.C. Vetterli[142,e], I. Vichou[165], T. Vickey[145b,ak], O.E. Vickey Boeriu[145b], G.H.A. Viehhauser[118], S. Viel[168],
M. Villa[20a,20b], M. Villaplana Perez[167], E. Vilucchi[47], M.G. Vincter[29], E. Vinek[30], V.B. Vinogradov[64], J. Virzi[15],
O. Vitells[172], M. Viti[42], I. Vivarelli[48], F. Vives Vaque[3], S. Vlachos[10], D. Vladoiu[98], M. Vlasak[126], A. Vogel[21],
P. Vokac[126], G. Volpi[47], M. Volpi[86], G. Volpini[89a], H. von der Schmitt[99], H. von Radziewski[48], E. von Toerne[21],
V. Vorobel[127], V. Vorwerk[12], M. Vos[167], R. Voss[30], J.H. Vossebeld[73], N. Vranjes[136], M. Vranjes Milosavljevic[105],
V. Vrba[125], M. Vreeswijk[105], T. Vu Anh[48], R. Vuillermet[30], I. Vukotic[31], W. Wagner[175], P. Wagner[21], H. Wahlen[175],
S. Wahrmund[44], J. Wakabayashi[101], S. Walch[87], J. Walder[71], R. Walker[98], W. Walkowiak[141], R. Wall[176],
P. Waller[73], B. Walsh[176], C. Wang[45], H. Wang[173], H. Wang[40], J. Wang[151], J. Wang[33a], R. Wang[103], S.M. Wang[151],
T. Wang[21], A. Warburton[85], C.P. Ward[28], D.R. Wardrope[77], M. Warsinsky[48], A. Washbrook[46], C. Wasicki[42],
I. Watanabe[66], P.M. Watkins[18], A.T. Watson[18], I.J. Watson[150], M.F. Watson[18], G. Watts[138], S. Watts[82],
A.T. Waugh[150], B.M. Waugh[77], M.S. Weber[17], J.S. Webster[31], A.R. Weidberg[118], P. Weigell[99], J. Weingarten[54],
C. Weiser[48], P.S. Wells[30], T. Wenaus[25], D. Wendland[16], Z. Weng[151,u], T. Wengler[30], S. Wenig[30], N. Wermes[21],
M. Werner[48], P. Werner[30], M. Werth[163], M. Wessels[58a], J. Wetter[161], C. Weydert[55], K. Whalen[29], A. White[8],
M.J. White[86], S. White[122a,122b], S.R. Whitehead[118], D. Whiteson[163], D. Whittington[60], D. Wicke[175],
F.J. Wickens[129], W. Wiedenmann[173], M. Wielers[129], P. Wienemann[21], C. Wiglesworth[75], L.A.M. Wiik-Fuchs[21],
P.A. Wijeratne[77], A. Wildauer[99], M.A. Wildt[42,r], I. Wilhelm[127], H.G. Wilkens[30], J.Z. Will[98], E. Williams[35],
H.H. Williams[120], S. Williams[28], W. Willis[35], S. Willocq[84], J.A. Wilson[18], M.G. Wilson[143], A. Wilson[87],

I. Wingerter-Seez[5], S. Winkelmann[48], F. Winklmeier[30], M. Wittgen[143], S.J. Wollstadt[81], M.W. Wolter[39], H. Wolters[124a,h], W.C. Wong[41], G. Wooden[87], B.K. Wosiek[39], J. Wotschack[30], M.J. Woudstra[82], K.W. Wozniak[39], K. Wraight[53], M. Wright[53], B. Wrona[73], S.L. Wu[173], X. Wu[49], Y. Wu[33b,al], E. Wulf[35], B.M. Wynne[46], S. Xella[36], M. Xiao[136], S. Xie[48], C. Xu[33b,z], D. Xu[33a], L. Xu[33b], B. Yabsley[150], S. Yacoob[145a,am], M. Yamada[65], H. Yamaguchi[155], A. Yamamoto[65], K. Yamamoto[63], S. Yamamoto[155], T. Yamamura[155], T. Yamanaka[155], K. Yamauchi[101], T. Yamazaki[155], Y. Yamazaki[66], Z. Yan[22], H. Yang[33e], H. Yang[173], U.K. Yang[82], Y. Yang[109], Z. Yang[146a,146b], S. Yanush[91], L. Yao[33a], Y. Yasu[65], E. Yatsenko[42], J. Ye[40], S. Ye[25], A.L. Yen[57], M. Yilmaz[4b], R. Yoosoofmiya[123], K. Yorita[171], R. Yoshida[6], K. Yoshihara[155], C. Young[143], C.J.S. Young[118], S. Youssef[22], D. Yu[25], D.R. Yu[15], J. Yu[8], J. Yu[112], L. Yuan[66], A. Yurkewicz[106], B. Zabinski[39], R. Zaidan[62], A.M. Zaitsev[128], L. Zanello[132a,132b], D. Zanzi[99], A. Zaytsev[25], C. Zeitnitz[175], M. Zeman[126], A. Zemla[39], O. Zenin[128], T. Ženiš[144a], D. Zerwas[115], G. Zevi della Porta[57], D. Zhang[87], H. Zhang[88], J. Zhang[6], X. Zhang[33d], Z. Zhang[115], L. Zhao[108], Z. Zhao[33b], A. Zhemchugov[64], J. Zhong[118], B. Zhou[87], N. Zhou[163], Y. Zhou[151], C.G. Zhu[33d], H. Zhu[42], J. Zhu[87], Y. Zhu[33b], X. Zhuang[33a], V. Zhuravlov[99], A. Zibell[98], D. Zieminska[60], N.I. Zimin[64], R. Zimmermann[21], S. Zimmermann[21], S. Zimmermann[48], Z. Zinonos[122a,122b], M. Ziolkowski[141], R. Zitoun[5], L. Živković[35], V.V. Zmouchko[128,*], G. Zobernig[173], A. Zoccoli[20a,20b], M. zur Nedden[16], V. Zutshi[106], L. Zwalinski[30].

[1] School of Chemistry and Physics, University of Adelaide, Adelaide, Australia
[2] Physics Department, SUNY Albany, Albany NY, United States of America
[3] Department of Physics, University of Alberta, Edmonton AB, Canada
[4] [(a)] Department of Physics, Ankara University, Ankara; [(b)] Department of Physics, Gazi University, Ankara; [(c)] Division of Physics, TOBB University of Economics and Technology, Ankara; [(d)] Turkish Atomic Energy Authority, Ankara, Turkey
[5] LAPP, CNRS/IN2P3 and Université de Savoie, Annecy-le-Vieux, France
[6] High Energy Physics Division, Argonne National Laboratory, Argonne IL, United States of America
[7] Department of Physics, University of Arizona, Tucson AZ, United States of America
[8] Department of Physics, The University of Texas at Arlington, Arlington TX, United States of America
[9] Physics Department, University of Athens, Athens, Greece
[10] Physics Department, National Technical University of Athens, Zografou, Greece
[11] Institute of Physics, Azerbaijan Academy of Sciences, Baku, Azerbaijan
[12] Institut de Física d'Altes Energies and Departament de Física de la Universitat Autònoma de Barcelona and ICREA, Barcelona, Spain
[13] [(a)] Institute of Physics, University of Belgrade, Belgrade; [(b)] Vinca Institute of Nuclear Sciences, University of Belgrade, Belgrade, Serbia
[14] Department for Physics and Technology, University of Bergen, Bergen, Norway
[15] Physics Division, Lawrence Berkeley National Laboratory and University of California, Berkeley CA, United States of America
[16] Department of Physics, Humboldt University, Berlin, Germany
[17] Albert Einstein Center for Fundamental Physics and Laboratory for High Energy Physics, University of Bern, Bern, Switzerland
[18] School of Physics and Astronomy, University of Birmingham, Birmingham, United Kingdom
[19] [(a)] Department of Physics, Bogazici University, Istanbul; [(b)] Division of Physics, Dogus University, Istanbul; [(c)] Department of Physics Engineering, Gaziantep University, Gaziantep, Turkey
[20] [(a)] INFN Sezione di Bologna; [(b)] Dipartimento di Fisica, Università di Bologna, Bologna, Italy
[21] Physikalisches Institut, University of Bonn, Bonn, Germany
[22] Department of Physics, Boston University, Boston MA, United States of America
[23] Department of Physics, Brandeis University, Waltham MA, United States of America
[24] [(a)] Universidade Federal do Rio De Janeiro COPPE/EE/IF, Rio de Janeiro; [(b)] Federal University of Juiz de Fora (UFJF), Juiz de Fora; [(c)] Federal University of Sao Joao del Rei (UFSJ), Sao Joao del Rei; [(d)] Instituto de Fisica, Universidade de Sao Paulo, Sao Paulo, Brazil
[25] Physics Department, Brookhaven National Laboratory, Upton NY, United States of America
[26] [(a)] National Institute of Physics and Nuclear Engineering, Bucharest; [(b)] University Politehnica Bucharest, Bucharest; [(c)] West University in Timisoara, Timisoara, Romania
[27] Departamento de Física, Universidad de Buenos Aires, Buenos Aires, Argentina
[28] Cavendish Laboratory, University of Cambridge, Cambridge, United Kingdom
[29] Department of Physics, Carleton University, Ottawa ON, Canada
[30] CERN, Geneva, Switzerland
[31] Enrico Fermi Institute, University of Chicago, Chicago IL, United States of America
[32] [(a)] Departamento de Física, Pontificia Universidad Católica de Chile, Santiago; [(b)] Departamento de Física,

Universidad Técnica Federico Santa María, Valparaíso, Chile

[33] [a] Institute of High Energy Physics, Chinese Academy of Sciences, Beijing; [b] Department of Modern Physics, University of Science and Technology of China, Anhui; [c] Department of Physics, Nanjing University, Jiangsu; [d] School of Physics, Shandong University, Shandong; [e] Physics Department, Shanghai Jiao Tong University, Shanghai, China

[34] Laboratoire de Physique Corpusculaire, Clermont Université and Université Blaise Pascal and CNRS/IN2P3, Clermont-Ferrand, France

[35] Nevis Laboratory, Columbia University, Irvington NY, United States of America

[36] Niels Bohr Institute, University of Copenhagen, Kobenhavn, Denmark

[37] [a] INFN Gruppo Collegato di Cosenza; [b] Dipartimento di Fisica, Università della Calabria, Rende, Italy

[38] AGH University of Science and Technology, Faculty of Physics and Applied Computer Science, Krakow, Poland

[39] The Henryk Niewodniczanski Institute of Nuclear Physics, Polish Academy of Sciences, Krakow, Poland

[40] Physics Department, Southern Methodist University, Dallas TX, United States of America

[41] Physics Department, University of Texas at Dallas, Richardson TX, United States of America

[42] DESY, Hamburg and Zeuthen, Germany

[43] Institut für Experimentelle Physik IV, Technische Universität Dortmund, Dortmund, Germany

[44] Institut für Kern- und Teilchenphysik, Technical University Dresden, Dresden, Germany

[45] Department of Physics, Duke University, Durham NC, United States of America

[46] SUPA - School of Physics and Astronomy, University of Edinburgh, Edinburgh, United Kingdom

[47] INFN Laboratori Nazionali di Frascati, Frascati, Italy

[48] Fakultät für Mathematik und Physik, Albert-Ludwigs-Universität, Freiburg, Germany

[49] Section de Physique, Université de Genève, Geneva, Switzerland

[50] [a] INFN Sezione di Genova; [b] Dipartimento di Fisica, Università di Genova, Genova, Italy

[51] [a] E. Andronikashvili Institute of Physics, Iv. Javakhishvili Tbilisi State University, Tbilisi; [b] High Energy Physics Institute, Tbilisi State University, Tbilisi, Georgia

[52] II Physikalisches Institut, Justus-Liebig-Universität Giessen, Giessen, Germany

[53] SUPA - School of Physics and Astronomy, University of Glasgow, Glasgow, United Kingdom

[54] II Physikalisches Institut, Georg-August-Universität, Göttingen, Germany

[55] Laboratoire de Physique Subatomique et de Cosmologie, Université Joseph Fourier and CNRS/IN2P3 and Institut National Polytechnique de Grenoble, Grenoble, France

[56] Department of Physics, Hampton University, Hampton VA, United States of America

[57] Laboratory for Particle Physics and Cosmology, Harvard University, Cambridge MA, United States of America

[58] [a] Kirchhoff-Institut für Physik, Ruprecht-Karls-Universität Heidelberg, Heidelberg; [b] Physikalisches Institut, Ruprecht-Karls-Universität Heidelberg, Heidelberg; [c] ZITI Institut für technische Informatik, Ruprecht-Karls-Universität Heidelberg, Mannheim, Germany

[59] Faculty of Applied Information Science, Hiroshima Institute of Technology, Hiroshima, Japan

[60] Department of Physics, Indiana University, Bloomington IN, United States of America

[61] Institut für Astro- und Teilchenphysik, Leopold-Franzens-Universität, Innsbruck, Austria

[62] University of Iowa, Iowa City IA, United States of America

[63] Department of Physics and Astronomy, Iowa State University, Ames IA, United States of America

[64] Joint Institute for Nuclear Research, JINR Dubna, Dubna, Russia

[65] KEK, High Energy Accelerator Research Organization, Tsukuba, Japan

[66] Graduate School of Science, Kobe University, Kobe, Japan

[67] Faculty of Science, Kyoto University, Kyoto, Japan

[68] Kyoto University of Education, Kyoto, Japan

[69] Department of Physics, Kyushu University, Fukuoka, Japan

[70] Instituto de Física La Plata, Universidad Nacional de La Plata and CONICET, La Plata, Argentina

[71] Physics Department, Lancaster University, Lancaster, United Kingdom

[72] [a] INFN Sezione di Lecce; [b] Dipartimento di Matematica e Fisica, Università del Salento, Lecce, Italy

[73] Oliver Lodge Laboratory, University of Liverpool, Liverpool, United Kingdom

[74] Department of Physics, Jožef Stefan Institute and University of Ljubljana, Ljubljana, Slovenia

[75] School of Physics and Astronomy, Queen Mary University of London, London, United Kingdom

[76] Department of Physics, Royal Holloway University of London, Surrey, United Kingdom

[77] Department of Physics and Astronomy, University College London, London, United Kingdom

[78] Laboratoire de Physique Nucléaire et de Hautes Energies, UPMC and Université Paris-Diderot and CNRS/IN2P3, Paris, France

[79] Fysiska institutionen, Lunds universitet, Lund, Sweden

[80] Departamento de Fisica Teorica C-15, Universidad Autonoma de Madrid, Madrid, Spain

[81] Institut für Physik, Universität Mainz, Mainz, Germany
[82] School of Physics and Astronomy, University of Manchester, Manchester, United Kingdom
[83] CPPM, Aix-Marseille Université and CNRS/IN2P3, Marseille, France
[84] Department of Physics, University of Massachusetts, Amherst MA, United States of America
[85] Department of Physics, McGill University, Montreal QC, Canada
[86] School of Physics, University of Melbourne, Victoria, Australia
[87] Department of Physics, The University of Michigan, Ann Arbor MI, United States of America
[88] Department of Physics and Astronomy, Michigan State University, East Lansing MI, United States of America
[89] [a] INFN Sezione di Milano; [b] Dipartimento di Fisica, Università di Milano, Milano, Italy
[90] B.I. Stepanov Institute of Physics, National Academy of Sciences of Belarus, Minsk, Republic of Belarus
[91] National Scientific and Educational Centre for Particle and High Energy Physics, Minsk, Republic of Belarus
[92] Department of Physics, Massachusetts Institute of Technology, Cambridge MA, United States of America
[93] Group of Particle Physics, University of Montreal, Montreal QC, Canada
[94] P.N. Lebedev Institute of Physics, Academy of Sciences, Moscow, Russia
[95] Institute for Theoretical and Experimental Physics (ITEP), Moscow, Russia
[96] Moscow Engineering and Physics Institute (MEPhI), Moscow, Russia
[97] D.V.Skobeltsyn Institute of Nuclear Physics, M.V.Lomonosov Moscow State University, Moscow, Russia
[98] Fakultät für Physik, Ludwig-Maximilians-Universität München, München, Germany
[99] Max-Planck-Institut für Physik (Werner-Heisenberg-Institut), München, Germany
[100] Nagasaki Institute of Applied Science, Nagasaki, Japan
[101] Graduate School of Science and Kobayashi-Maskawa Institute, Nagoya University, Nagoya, Japan
[102] [a] INFN Sezione di Napoli; [b] Dipartimento di Scienze Fisiche, Università di Napoli, Napoli, Italy
[103] Department of Physics and Astronomy, University of New Mexico, Albuquerque NM, United States of America
[104] Institute for Mathematics, Astrophysics and Particle Physics, Radboud University Nijmegen/Nikhef, Nijmegen, Netherlands
[105] Nikhef National Institute for Subatomic Physics and University of Amsterdam, Amsterdam, Netherlands
[106] Department of Physics, Northern Illinois University, DeKalb IL, United States of America
[107] Budker Institute of Nuclear Physics, SB RAS, Novosibirsk, Russia
[108] Department of Physics, New York University, New York NY, United States of America
[109] Ohio State University, Columbus OH, United States of America
[110] Faculty of Science, Okayama University, Okayama, Japan
[111] Homer L. Dodge Department of Physics and Astronomy, University of Oklahoma, Norman OK, United States of America
[112] Department of Physics, Oklahoma State University, Stillwater OK, United States of America
[113] Palacký University, RCPTM, Olomouc, Czech Republic
[114] Center for High Energy Physics, University of Oregon, Eugene OR, United States of America
[115] LAL, Université Paris-Sud and CNRS/IN2P3, Orsay, France
[116] Graduate School of Science, Osaka University, Osaka, Japan
[117] Department of Physics, University of Oslo, Oslo, Norway
[118] Department of Physics, Oxford University, Oxford, United Kingdom
[119] [a] INFN Sezione di Pavia; [b] Dipartimento di Fisica, Università di Pavia, Pavia, Italy
[120] Department of Physics, University of Pennsylvania, Philadelphia PA, United States of America
[121] Petersburg Nuclear Physics Institute, Gatchina, Russia
[122] [a] INFN Sezione di Pisa; [b] Dipartimento di Fisica E. Fermi, Università di Pisa, Pisa, Italy
[123] Department of Physics and Astronomy, University of Pittsburgh, Pittsburgh PA, United States of America
[124] [a] Laboratorio de Instrumentacao e Fisica Experimental de Particulas - LIP, Lisboa, Portugal; [b] Departamento de Fisica Teorica y del Cosmos and CAFPE, Universidad de Granada, Granada, Spain
[125] Institute of Physics, Academy of Sciences of the Czech Republic, Praha, Czech Republic
[126] Czech Technical University in Prague, Praha, Czech Republic
[127] Faculty of Mathematics and Physics, Charles University in Prague, Praha, Czech Republic
[128] State Research Center Institute for High Energy Physics, Protvino, Russia
[129] Particle Physics Department, Rutherford Appleton Laboratory, Didcot, United Kingdom
[130] Physics Department, University of Regina, Regina SK, Canada
[131] Ritsumeikan University, Kusatsu, Shiga, Japan
[132] [a] INFN Sezione di Roma I; [b] Dipartimento di Fisica, Università La Sapienza, Roma, Italy
[133] [a] INFN Sezione di Roma Tor Vergata; [b] Dipartimento di Fisica, Università di Roma Tor Vergata, Roma, Italy
[134] [a] INFN Sezione di Roma Tre; [b] Dipartimento di Matematica e Fisica, Università Roma Tre, Roma, Italy
[135] [a] Faculté des Sciences Ain Chock, Réseau Universitaire de Physique des Hautes Energies - Université Hassan

II, Casablanca; [b] Centre National de l'Energie des Sciences Techniques Nucleaires, Rabat; [c] Faculté des Sciences Semlalia, Université Cadi Ayyad, LPHEA-Marrakech; [d] Faculté des Sciences, Université Mohamed Premier and LPTPM, Oujda; [e] Faculté des sciences, Université Mohammed V-Agdal, Rabat, Morocco

136 DSM/IRFU (Institut de Recherches sur les Lois Fondamentales de l'Univers), CEA Saclay (Commissariat à l'Energie Atomique et aux Energies Alternatives), Gif-sur-Yvette, France

137 Santa Cruz Institute for Particle Physics, University of California Santa Cruz, Santa Cruz CA, United States of America

138 Department of Physics, University of Washington, Seattle WA, United States of America

139 Department of Physics and Astronomy, University of Sheffield, Sheffield, United Kingdom

140 Department of Physics, Shinshu University, Nagano, Japan

141 Fachbereich Physik, Universität Siegen, Siegen, Germany

142 Department of Physics, Simon Fraser University, Burnaby BC, Canada

143 SLAC National Accelerator Laboratory, Stanford CA, United States of America

144 [a] Faculty of Mathematics, Physics & Informatics, Comenius University, Bratislava; [b] Department of Subnuclear Physics, Institute of Experimental Physics of the Slovak Academy of Sciences, Kosice, Slovak Republic

145 [a] Department of Physics, University of Johannesburg, Johannesburg; [b] School of Physics, University of the Witwatersrand, Johannesburg, South Africa

146 [a] Department of Physics, Stockholm University; [b] The Oskar Klein Centre, Stockholm, Sweden

147 Physics Department, Royal Institute of Technology, Stockholm, Sweden

148 Departments of Physics & Astronomy and Chemistry, Stony Brook University, Stony Brook NY, United States of America

149 Department of Physics and Astronomy, University of Sussex, Brighton, United Kingdom

150 School of Physics, University of Sydney, Sydney, Australia

151 Institute of Physics, Academia Sinica, Taipei, Taiwan

152 Department of Physics, Technion: Israel Institute of Technology, Haifa, Israel

153 Raymond and Beverly Sackler School of Physics and Astronomy, Tel Aviv University, Tel Aviv, Israel

154 Department of Physics, Aristotle University of Thessaloniki, Thessaloniki, Greece

155 International Center for Elementary Particle Physics and Department of Physics, The University of Tokyo, Tokyo, Japan

156 Graduate School of Science and Technology, Tokyo Metropolitan University, Tokyo, Japan

157 Department of Physics, Tokyo Institute of Technology, Tokyo, Japan

158 Department of Physics, University of Toronto, Toronto ON, Canada

159 [a] TRIUMF, Vancouver BC; [b] Department of Physics and Astronomy, York University, Toronto ON, Canada

160 Faculty of Pure and Applied Sciences, University of Tsukuba, Tsukuba, Japan

161 Department of Physics and Astronomy, Tufts University, Medford MA, United States of America

162 Centro de Investigaciones, Universidad Antonio Narino, Bogota, Colombia

163 Department of Physics and Astronomy, University of California Irvine, Irvine CA, United States of America

164 [a] INFN Gruppo Collegato di Udine; [b] ICTP, Trieste; [c] Dipartimento di Chimica, Fisica e Ambiente, Università di Udine, Udine, Italy

165 Department of Physics, University of Illinois, Urbana IL, United States of America

166 Department of Physics and Astronomy, University of Uppsala, Uppsala, Sweden

167 Instituto de Física Corpuscular (IFIC) and Departamento de Física Atómica, Molecular y Nuclear and Departamento de Ingeniería Electrónica and Instituto de Microelectrónica de Barcelona (IMB-CNM), University of Valencia and CSIC, Valencia, Spain

168 Department of Physics, University of British Columbia, Vancouver BC, Canada

169 Department of Physics and Astronomy, University of Victoria, Victoria BC, Canada

170 Department of Physics, University of Warwick, Coventry, United Kingdom

171 Waseda University, Tokyo, Japan

172 Department of Particle Physics, The Weizmann Institute of Science, Rehovot, Israel

173 Department of Physics, University of Wisconsin, Madison WI, United States of America

174 Fakultät für Physik und Astronomie, Julius-Maximilians-Universität, Würzburg, Germany

175 Fachbereich C Physik, Bergische Universität Wuppertal, Wuppertal, Germany

176 Department of Physics, Yale University, New Haven CT, United States of America

177 Yerevan Physics Institute, Yerevan, Armenia

178 Centre de Calcul de l'Institut National de Physique Nucléaire et de Physique des Particules (IN2P3), Villeurbanne, France

[a] Also at Department of Physics, King's College London, London, United Kingdom

[b] Also at Laboratorio de Instrumentacao e Fisica Experimental de Particulas - LIP, Lisboa, Portugal

[c] Also at Faculdade de Ciencias and CFNUL, Universidade de Lisboa, Lisboa, Portugal

[d] Also at Particle Physics Department, Rutherford Appleton Laboratory, Didcot, United Kingdom

[e] Also at TRIUMF, Vancouver BC, Canada

[f] Also at Department of Physics, California State University, Fresno CA, United States of America

[g] Also at Novosibirsk State University, Novosibirsk, Russia

[h] Also at Department of Physics, University of Coimbra, Coimbra, Portugal

[i] Also at Università di Napoli Parthenope, Napoli, Italy

[j] Also at Institute of Particle Physics (IPP), Canada

[k] Also at Department of Physics, Middle East Technical University, Ankara, Turkey

[l] Also at Louisiana Tech University, Ruston LA, United States of America

[m] Also at Dep Fisica and CEFITEC of Faculdade de Ciencias e Tecnologia, Universidade Nova de Lisboa, Caparica, Portugal

[n] Also at Department of Physics and Astronomy, University College London, London, United Kingdom

[o] Also at Department of Physics and Astronomy, Michigan State University, East Lansing MI, United States of America

[p] Also at Department of Physics, University of Cape Town, Cape Town, South Africa

[q] Also at Institute of Physics, Azerbaijan Academy of Sciences, Baku, Azerbaijan

[r] Also at Institut für Experimentalphysik, Universität Hamburg, Hamburg, Germany

[s] Also at Manhattan College, New York NY, United States of America

[t] Also at CPPM, Aix-Marseille Université and CNRS/IN2P3, Marseille, France

[u] Also at School of Physics and Engineering, Sun Yat-sen University, Guanzhou, China

[v] Also at Academia Sinica Grid Computing, Institute of Physics, Academia Sinica, Taipei, Taiwan

[w] Also at School of Physical Sciences, National Institute of Science Education and Research, Bhubaneswar, India

[x] Also at School of Physics, Shandong University, Shandong, China

[y] Also at Dipartimento di Fisica, Università La Sapienza, Roma, Italy

[z] Also at DSM/IRFU (Institut de Recherches sur les Lois Fondamentales de l'Univers), CEA Saclay (Commissariat à l'Energie Atomique et aux Energies Alternatives), Gif-sur-Yvette, France

[aa] Also at Section de Physique, Université de Genève, Geneva, Switzerland

[ab] Also at Departamento de Fisica, Universidade de Minho, Braga, Portugal

[ac] Also at Department of Physics, The University of Texas at Austin, Austin TX, United States of America

[ad] Also at Department of Physics and Astronomy, University of South Carolina, Columbia SC, United States of America

[ae] Also at Institute for Particle and Nuclear Physics, Wigner Research Centre for Physics, Budapest, Hungary

[af] Also at California Institute of Technology, Pasadena CA, United States of America

[ag] Also at International School for Advanced Studies (SISSA), Trieste, Italy

[ah] Also at LAL, Université Paris-Sud and CNRS/IN2P3, Orsay, France

[ai] Also at Faculty of Physics, M.V.Lomonosov Moscow State University, Moscow, Russia

[aj] Also at Nevis Laboratory, Columbia University, Irvington NY, United States of America

[ak] Also at Department of Physics, Oxford University, Oxford, United Kingdom

[al] Also at Department of Physics, The University of Michigan, Ann Arbor MI, United States of America

[am] Also at Discipline of Physics, University of KwaZulu-Natal, Durban, South Africa

* Deceased